Vertical Control of Unmanned Helicopter During Payload Drop

By

Divyarajsinh Raol

A Thesis submitted to the Faculty of Graduate Studies of

The University of Manitoba

In partial fulfillment of the requirements of the degree of

MASTER OF SCIENCE

Department of Mechanical Engineering

University of Manitoba

Winnipeg, Manitoba, Canada

Abstract

Unmanned helicopters in recent years have gained much attention due to their potential in both civil as well as military applications. Helicopter is an inherently unstable system. As a result there is a growing need of developing a control structure that allows the helicopter to perform various applications while remaining stable throughout the flight.

This thesis presents developments of a robust controller for the vertical channel of an unmanned helicopter while carrying and dropping a payload. In addition, a simulation platform is developed in Simulink that uses a nonlinear six degree of freedom helicopter model.

Quantitative Feedback Theory, a frequency domain technique, is used to design a controller that meets specific performance criteria when uncertainties associated with different payload weights exist in the system. The controller performance is examined in simulation for an Xcell 60 helicopter for effective lifting and dropping of up to 10 lb payload. The performance is then compared with a traditional Proportional-Integral-Derivative controller. Further, the effect of actuator dynamics on the controller performance is also evaluated. Finally, a controller that is robust in minimizing the effect of actuator dynamics and the payload drop while keeping the helicopter stable in flight is designed.

Acknowledgements

Table of Contents

List of Figures

List of Tables

Nomenclature

Symbol	Definition	Units
a	Slope of lift curve	1/rad,1/deg
a_{1s}	First harmonic coefficient of longitudinal blade flapping	rad, deg
b	Number of blades	
b_{1s}	First harmonic coefficient of lateral blade flapping	rad, deg
c	Chord of blade	ft
c_d	Drag coefficient	
g	Gravitational acceleration	ft/s^2
p	Roll rate	rad/s, deg/s
q	Pitch rate	rad/s, deg/s
r	Yaw rate	rad/s, deg/s
r_b	Radius of blade	ft
r_{be}	Radius of blade element	ft
A_1	First lateral harmonic of blade feathering	rad, deg
B_1	First longitudinal harmonic of blade feathering	rad, deg
I_b	Moment of inertia of blade	slug ft^2
M_H	Mass of helicopter	lb
W_H	Gross weight of helicopter	lb
W_p	Weight of payload	lb
Q	Torque	ft lbf
T	Thrust	lbf
α	Angle of attack	rad, deg
β	Blade flapping angle	rad, deg
θ	Blade pitch	rad, deg
θ_T	Blade twist	rad, deg
v_i	Induced velocity	ft/s
ρ	Air density	slug/ft^3

φ	Inflow angle	rad, deg
ψ_b	Azimuth position of blade	rad, deg
θ	Helicopter pitch angle	rad, deg
Φ	Helicopter roll angle	rad, deg
Ψ	Helicopter yaw angle	rad, deg
Ω	Rotational speed of rotor	rad/s, deg/s
Subscripts		
c	Climb	
f	Forward	
i	Induced	
P	Perpendicular	
T	Tangential	
W	Weight	
MR	Main rotor	
TR	Tail rotor	

Definitions

Airfoil	Structure that makes the flight possible by creating the necessary lift force.
Angle of attack	Angle between the airfoil chord and its direction of motion relative to the air.
Blade twist	Blade twist allows an airfoil section near the blade root to have a larger pitch angle than a section near the tip.
Chord line	Straight line connecting leading and trailing edges of airfoil.
Chord	Length of chord line from tip of leading edge to trailing edge.
Drag	Resistance or force that opposes the motion of airfoil through the air.
Induced velocity	Velocity induced at the wake of the rotor due to generation of lift.
Lateral motion	Left and right motions of helicopter
Lift	Force acting on the airfoil in direction perpendicular to relative wind.
Longitudinal motion	Forward/backward motion of helicopter
North-East-Down (N.E.D) frame	Coordinate frame attached to the helicopter center of mass aligned with the earth's north, east orientation and down directed towards the center of earth.
Tip-Path-Plane (TPP)	A plane on which the tips of the blades lie.

1. Introduction

1.1 Motivation

Unmanned Arial Vehicles (UAVs), also known as drones, are vehicles without a pilot on-board. There are of two types of UAVs: autonomous or remotely controlled by a pilot on ground. Earliest attempts to develop an UAV dates back to 1916 and their original purpose was target practice to train military. After the world wars, UAVs came into spotlight as concerns on losing pilots over hostile territories increased. Over the years, much research has focused on making UAVs light and autonomous.

UAVs are now available in a wide variety of sizes and configurations. One of these configuration types is an unmanned helicopter. Due to its takeoff/landing, and hovering capabilities, unmanned helicopter have considerable advantages over unmanned aircraft. For example, in filmmaking and the inspection of buildings the use of unmanned helicopters have an advantage over fixed wing aircraft as these applications require the aerial vehicle to hover over a location to gather detailed information.

Similar to unmanned aircraft, unmanned helicopters also have uses in aerial surveillance, including forest fire monitoring, pipeline security monitoring, and terrain mapping. The advantage of using helicopters is that they can hover over a location making them easier to improve the task of terrain mapping or precisely dropping supplies to disaster struck areas, which are not accessible by road. These tasks require the helicopter to remain stable throughout the flight as payload mass is added or dropped.

In spite of their advantages, helicopters are difficult to fly, as they are inherently unstable and require constant pilot input. Hence, the current focus of research is on developing a reliable autonomous control technology or autopilots that allow a computer to control the helicopter. These autopilots require control algorithms that allow the unmanned helicopter to perform the payload drop application while remaining stable throughout the flight.

1.2 Objective of this Research

The objective of this research is to develop a simple, yet robust controller for the vertical channel of an unmanned helicopter while carrying and dropping of payloads. The controller has to minimize the change in altitude and velocity after the payload is dropped while remaining stable throughout the flight. The effects on the performance of a controller considering various details of helicopter dynamics have to be studied.

1.3 Scope of the Thesis

Chapter 2 provides background information on different components of a helicopter and the response of the helicopter during different flight conditions. It describes the current research work performed with unmanned helicopters. Different simulation models and controllers that have been developed prior to this work are briefly described.

Chapter 3 presents the nonlinear equations describing a helicopter model, starting with forces and torques acting on it. The helicopter forces are calculated using Blade Element Theory. The equations of motion are used in Simulink environment of MATLAB software. The simulation performance is verified by studying the response of the helicopter to different inputs.

Chapter 4 studies the vertical control loop of an unmanned helicopter. A number of controllers are designed for the vertical channel of the helicopter using Quantitative Feedback Theory (QFT). The response of the helicopter to the controllers is studied in the simulation platform. The performance is then compared to a Proportional-Integral-Derivative controller (PID). Additionally, the effect of adding actuator dynamics on the helicopter simulation is also studied for the different controllers. Controllers are designed by including the actuator dynamics in the design process to improve the performance of the controllers.

Chapter 5 presents the conclusions by outlining the contributions made as well as suggestions for any future work.

2. Background

2.1 Helicopter Functions and Operations

In order to understand the dynamics behind the helicopter flight it is important to know and understand the use of its different components. The different components of the Xcell 60 helicopter are displayed in Figure 2-1.
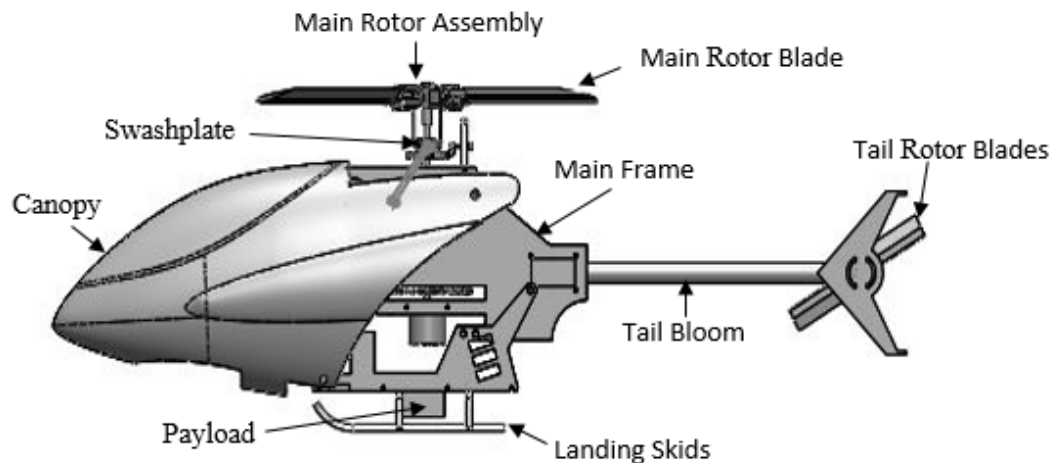
Figure 2-1: Typical unmanned helicopter

Main rotor provides the necessary lift force to fly the helicopter. It is one of the rotating components of a helicopter. It consists of rotor blades, rotor shaft and hub. The power necessary to rotate the blades is provided by an electric motor. The blades are rotated at a constant speed. Changing the orientation of the blade or the angle of attack similar to an airplane's wing varies the amount and direction of lift. The orientations of the blades are changed by Swash plate mechanism. The purpose of a swash plate is to convert the control inputs into rotating inputs. It consists of a stationary plate and a rotating plate. If the orientation of the stationary plate is altered, the pitch of the blade changes along the azimuth, which results in misaligning the rotor thrust force from the weight of the helicopter causing the changes in the motion of the helicopter.

The rotation of the main rotor also generates a moment on the helicopter body. In a conventional helicopter, a tail rotor is used to negate this moment. Typically, the tail rotor

assembly is connected to the main rotor assembly with a specific gear ratio. However, there are additional component that allows changing the pitch of the tail rotor blades that are used to change the orientation of helicopter in yaw direction while hovering.

To fly an unmanned helicopter autonomously three things are needed; an autopilot that performs the tasks of providing control inputs, a ground station that allows planning of missions and a receiver-transmitter setup that allows for communication between the ground station and the helicopter. A helicopter is primarily controlled by four inputs commands as shown in Figure 2-2. The longitudinal and lateral cyclic pitch for motions in the x-y direction of the helicopter by controlling the pitch and roll moments; main rotor collective pitch for vertical motion by changing the vertical force (thrust) and pedal collective pitch for yaw motion by changing the tail rotor thrust.
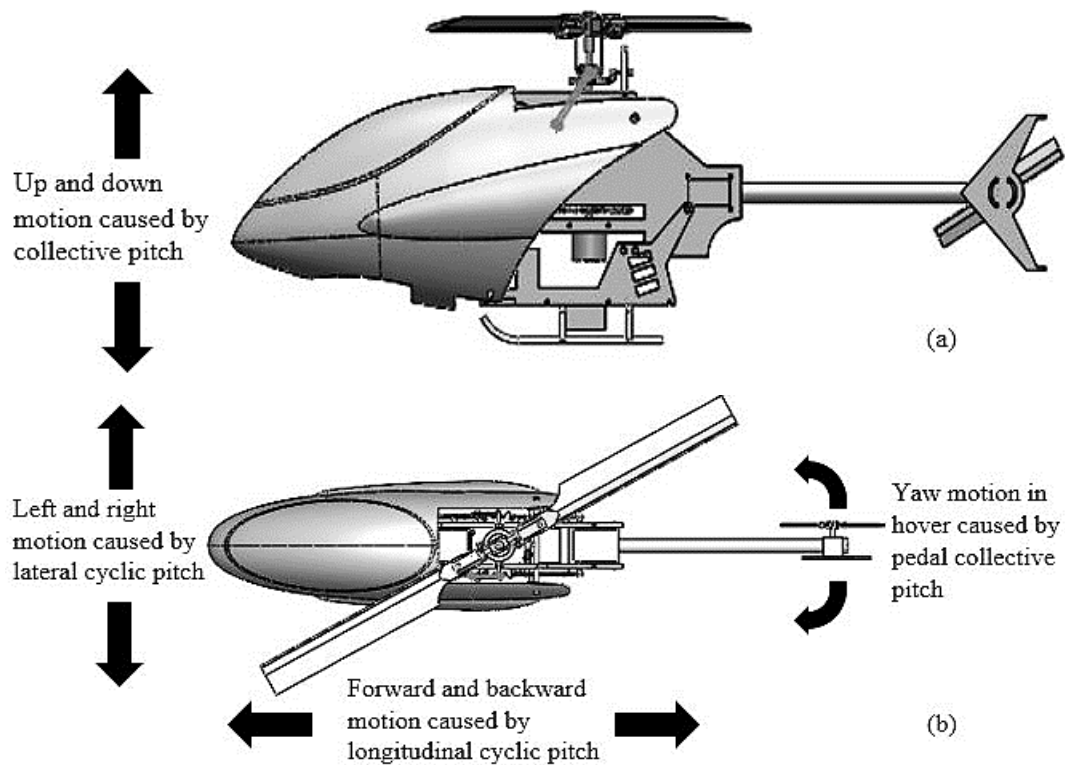
Figure 2-2: Helicopter motions; (a) side view; (b) top view

The response of the helicopter depends on the flight conditions and the flight plans. The response of the helicopter in hover greatly differs from that of cruise flight. Hence, it is important to understand how a helicopter behaves in different flight conditions such as hovering, vertical flight, forward flight, and flight with a payload.

(i) **Hovering**: When a helicopter maintains a constant position at a selected point at a particular altitude, the helicopter is considered to be in hovering mode. It is actually a special case of vertical flight. For a helicopter to hover, the main rotor must supply thrust force equal to the total weight of the helicopter as shown in Figure 2-3 (a).

(ii) **Vertical flight**: Assuming a no-wind condition, the tip-path plane (TPP) and the hub plane of the blades will remain horizontal. If the collective pitch of the blade is increased, it generates greater lift than the helicopter weight. Thus, by upsetting the vertical balance of forces and as a result the vertical velocity increases, helicopters will climb vertically.

(iii) **Forward flight**: If the cyclic pitch commands are changed, the tip-path plane is tipped from the original configuration that results in the lift and drag forces to be misaligned from the helicopter weight as shown in Figure 2-3 (b). If the resultant force is greater in the forward direction, the helicopter is pitched forward and the helicopter flies forward. Similarly, if the resultant force is greater in the positive y-direction, the helicopter moves in positive Y direction as shown in Figure 2-3 (c).

(iv) **Helicopter flight with payload:** While carrying a payload, the helicopter needs greater amounts of thrust force. After the payload drop, the amount of thrust greatly exceeds the weight of the helicopter and thus the helicopter keeps flying up. The thrust of the helicopter needs to be decreased to keep the helicopter stable. Hence, a controller is needed to reduce the collective input of the helicopter after the drop of payload, which will reduce the thrust force.
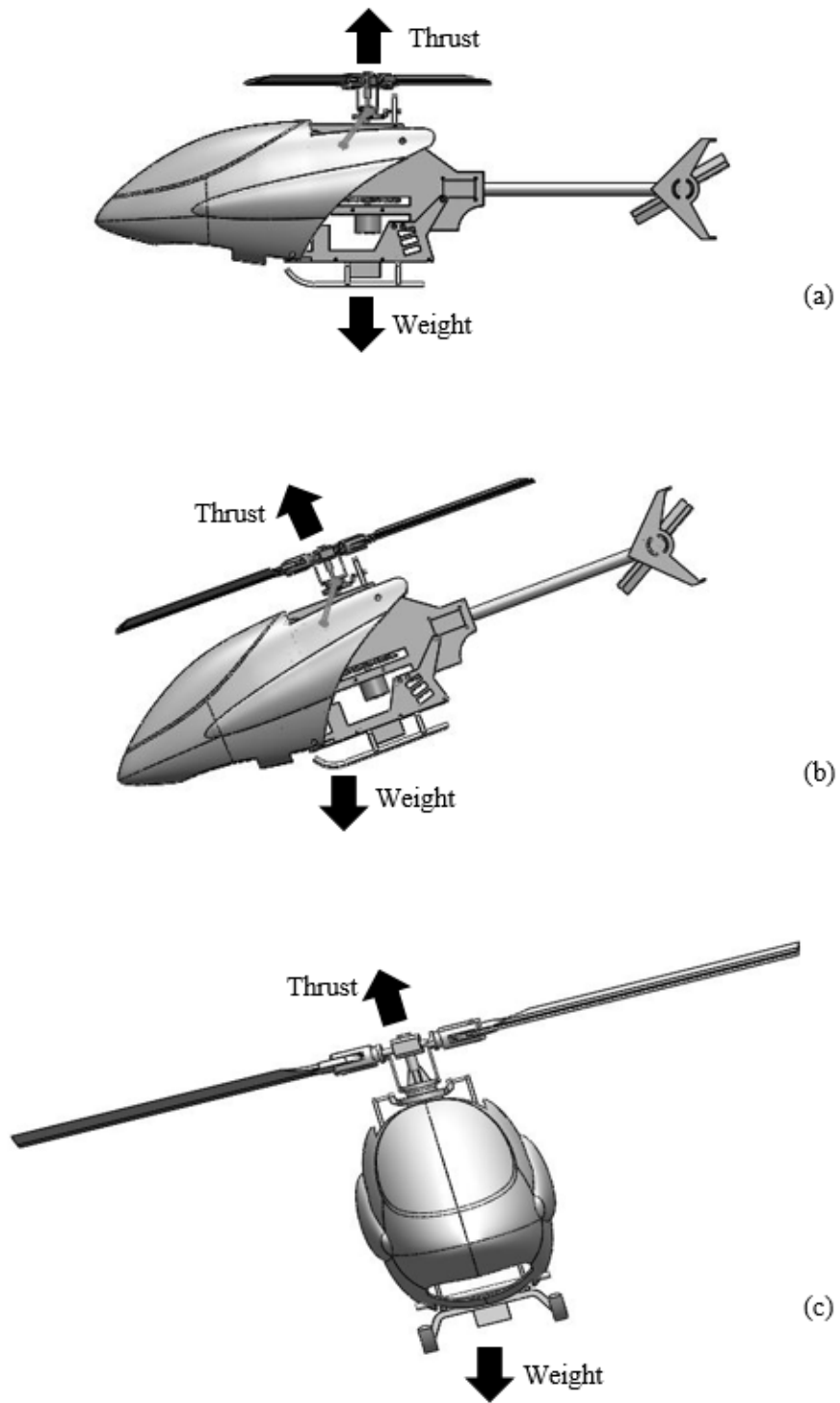
Figure 2-3: Helicopter weight-thrust balance and orientation; (a) hover mode (stationary); (b) longitudinal mode (forward motion); (c) lateral mode (sideways motion)

2.2 Literature Review

Research for unmanned helicopter dates back to 1990 and started with a small-scale helicopter attached to a test fixture. The advantage of using a test rig is that it keeps the helicopter safe and simplifies the dynamics. For example, Weilmenmann and Geering [1] used a rigged helicopter attached to a delta robot structure and designed a control for a six degree of freedom model. However, the hover performance was restricted due to the added motion of delta robot structure. Hence, the true control performance of the helicopter could not be evaluated.

Within the unmanned autonomous helicopter research literature, several models have been developed depending on application. A common approach is to apply laws of motion and principles such as Momentum Theory and Blade Element Theory [2], [3]. Some researchers implemented an advanced model that incorporates detailed modeling of the rotor, blade and nonlinear aerodynamic airflow effects with the rigid body equations of motion [4]. Typically, a 12th order model [5] is used in which the rigid body is modeled with position, orientation, linear and angular velocities considered as states. Higher order models are also used such as a sixteen states model used by Koo *et al.* [6] to account for rotor dynamics. For control system design, a lower degree of freedom model is used to reduce the computational load.

Most researchers currently focus on developing mathematical simulation models to help them design different UAVs and designing controllers to either assist the pilots while flying or make UAVs completely automated like research done by Y. Tang and Y. Li [7]. Secondly, some researchers also focus on system identification techniques to identify different parameters to improve the performance of the UAV like Z. Bai *et al.* [8]. This is the first step and most important part of all the techniques as creating an accurate mathematical model will help in creating a simulation model that closely represents the actual helicopter motion.

MATLAB, Simulink and C/C++ are the most commonly used software packages to model the complex nonlinear multi-input-multi-output unmanned helicopter system. The

advantage of using Simulink is that it allows us to integrate virtual visualizing techniques to help us visualize the real flight performance of the helicopter.

Simulation is a very important and useful technique that helps us while developing controllers by allowing us to visualize the performance of the helicopter in different flight conditions without damaging the actual helicopter. Since buying different UAVs to test is extremely costly, a computer simulation provides a very easy and effective way of testing many designs in the same simulation by merely changing some parameters in the mathematical model.

Some researchers have also used Hardware in Loop (HIL) simulation technique, which provides a physical platform to observe and implement a test algorithm on a physical plant system. The HIL system needs a simulation computer that has full mathematical model, a flight control computer that acts as a link between hardware and simulation, and real hardware to extract data from the actuators and sensors in order to help identify the real performance of the system. C. Yoo *et al.* [9] used a fixed hardware configuration where the UAV model is connected to a test bed, which is fixed to the ground. This provides simulation structure that could be placed indoors. However, this is an expensive method and adds to the complexity to an already complex system by adding the dynamics of the test bed. As the objective for this research is to develop different control algorithms, a mathematical simulation will be used.

Over the years, several controllers have been proposed in literature for autonomous helicopters. They can be categorized into three types: navigational, position and attitude controllers. Navigational controller's primary task includes path and trajectory planning with collision avoidance. Similar to navigation control, position control also emphasizes on path or trajectory planning but primary focus is on tracking instead of path generation. However, Attitude control is the most extensively researched controller in which the primary focus is on orientation of the helicopter. Proportional-Integral-Derivative (PID) controller is the most commonly used controller for position and attitude control [10].

Koo and Sastry [6] show that approximate linearization has an advantage over exact linearization for tracking control, as exact linearization would result in undesirable internal dynamics. Typically, the helicopter body is slower to respond than the rotor

blades. Hence, they developed a hybrid controller that consists of fast and slow components. This allowed them to link the discrete helicopter operations to be linked to the underlying continuous dynamics of the helicopter. However, they neglect the coupling between the rolling moments and lateral accelerations and focus on stabilizing the internal dynamics.

The primary focus for most control research has been on the hover flight. Sanders *et al.* [11] designed an inner-loop hover control system with a navigation filter and a waypoint guidance system. Simple PID controllers were used for each inner loop. Similarly, Lai *et al.* [12] designed a navigation controller in combination with a flight path controller and height-stabilizing controller. They designed a time varying control scheme on the nonlinear model to achieve attitude stabilizing with the PI controller as the outer loop to control the altitude. Mahony *et al.* [13] used the Lyapunov based controller for hover control using the back stepping technique. This puts heavy load on the computer, as it is an iterative process where a feedback input is generated at each step. It is dependent on finding a Lyapunov function, which would result in stable flight.

Robust control design is a relatively new field in unmanned helicopter research. Shim *et al.* [14] made an early attempt to compare three different control strategies: linear robust multivariable control, fuzzy logic control and nonlinear tracking control, these techniques were only tested in simulation and have not yet been implemented. There is also a growing need of designing a robust controller that has full control on all three channels of the helicopter (vertical, longitudinal and lateral). Quantitative Feedback Theory (QFT) is one such method that is a promising technique for the design of a controller that will satisfy both frequency domain and time domain performance criteria when specified uncertainty exist in the dynamics of the system.

Hess *et al.* [15] used QFT techniques applied to the longitudinal flight control system for an AH-64 Rotorcraft. The uncertainty in this approach is assigned to the actual uncertainty in the dynamic and aerodynamic characteristics of the vehicle. As this was the first attempt to apply such a complicated control system, a simplified longitudinal model was used. It was noted that if a full model were to be used, sixteen QFT designs would have to be performed instead of four making it rather complex.

Payload drop is an important application for an unmanned helicopter. Both civil and military operations need the helicopter to move loads to locations that are inaccessible by land and are difficult for crew operated flights. This requires the helicopter to remain stable and balanced. Pounds *et al.* [16] explored the effect of load disturbances introduced by adding and dropping of payload using PID controller while in hover. The dynamic response of the helicopter changed with added payload. However, the PID controllers have been proven effective in keeping the helicopter stable throughout the flight plan. The stability of the helicopter is studied using the Routh-Hurwitz criterion. So-Ryeok *et al.* [17] studied the dynamics of helicopter carrying a payload using a cable-suspended robot. However, the aerodynamic effects of both helicopter and the robot are ignored and the controller was designed for the robot instead of the helicopter

.

3. Helicopter Dynamics

Helicopter dynamics are complex and developing a model that accurately mimics the real helicopter flight for control design is challenging. The helicopter model is developed by deriving the equations of motion needed for the simulation studies where the total forces and torques generated by the blades are calculated using blade element theory. These equations were derived from the book written by Raymond Prouty [2].

3.1 Derivation of Dynamic Equations

The equations of motion needed to simulate the helicopter are derived by assuming it as a rigid body with six degrees of freedom and applying the Newton's second law. Several assumptions are needed to help formulate the equations for the helicopter:

1. Helicopter body is considered as a rigid body. Flex effects of the helicopter body are ignored.
2. Gravity is constant. Thus, the changes in acceleration at different altitudes are ignored.
3. Air is considered static and density is constant. Thus, any changes caused due to wind gusts on the helicopter is ignored.
4. Earth is fixed and flat hence, ignoring effects of the curvature of the earth for the altitude calculations
5. Mass of the helicopter is constant.

3.1.1 Reference Frame

North-East-Down reference system, $F_I = \{O_I, \vec{\imath_I}, \vec{\jmath_I}, \vec{k_I}\}$ is used as inertial frame for the helicopter where the vector $\vec{\imath_I}$ points North, $\vec{\jmath_I}$ points East, $\vec{k_I}$ points at the center of the Earth and origin (O_I) is located at the center of gravity (CG) of the helicopter as shown in Figure 3-1.
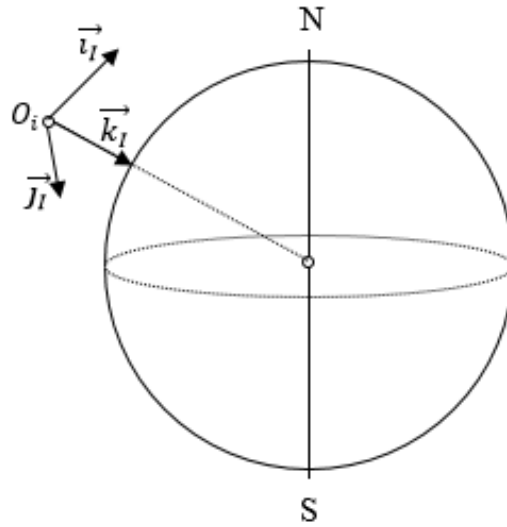
Figure 3-1: North-East-Down reference system; vector $\vec{\imath_I}$ points North, $\vec{\jmath_I}$ points East, $\vec{k_I}$ points at the center of the Earth and origin (O_I) is located at the center of gravity (CG) of the helicopter

Since the inertial frame changes over time, it makes it difficult to calculate the moments and products of inertia [18]. Hence, a second frame is used to derive the equations of motion. Body-fixed reference frame defined as $F_B = \{O_B, \vec{\imath_B}, \vec{\jmath_B}, \vec{k_B}\}$ were the vector $\vec{\imath_B}$ points away from the nose, $\vec{\jmath_B}$ points to the right of the fuselage, $\vec{k_B}$ points downwards and origin (O_B) is located at the CG of the helicopter as shown in Figure 3-2.

The linear velocity vector of the helicopter in body-fixed frame is denoted by $V_B = [u, v, w]^T$. Similarly, the angular velocity vector is denoted by $\omega_B = [p, q, r]^T$, the Euler angle orientation vector is denoted by $\Theta = [\Phi, \Theta, \Psi]^T$, force vector is denoted by $F_B = [F_x, F_y, F_z]^T$ and the moment is denoted by $T_B = [L, M, N]^T$. The Euler angles are defined with a specific sequence of rotations about the vehicle body axis. Where yaw (Ψ) is the angle about the z-axis, pitch (Θ) is the angle about the y-axis and roll (Φ) is angle about the x-axis.
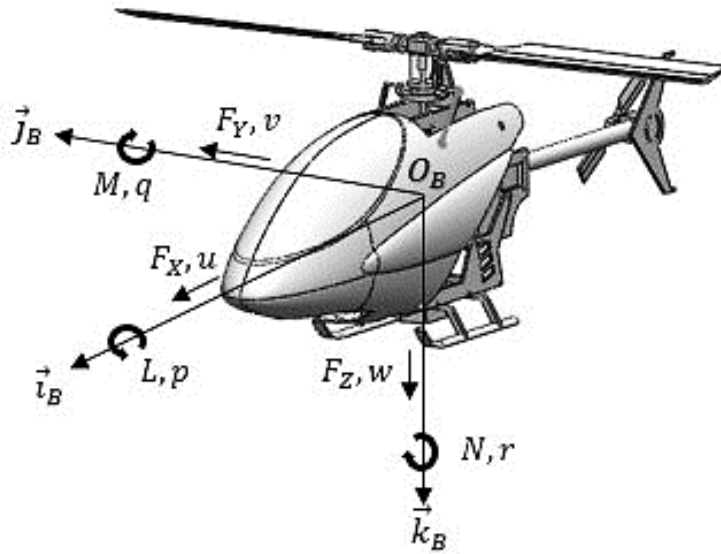
Figure 3-2: Body fixed frame; Forces and moments acting on the body are denoted by $F_B = [F_x, F_y, F_z]$ and $T_B = [L, M, N]$; Linear and angular velocity components are denoted by $V_B = [u, v, w]$ and $\omega_B = [p, q, r]$

Positive direction for rotation is assigned by the right hand thumb rule where the thumb points in the positive axis direction. The rotation matrix is used to transform from body-fixed frame to inertial frame of the helicopter and is shown in Equation (3-1).

$$R(\Theta) = \begin{bmatrix} \cos\theta\cos\Psi & \sin\Phi\sin\theta\cos\Psi - \cos\Phi\sin\Psi & \cos\Phi\sin\theta\cos\Psi + \sin\Phi\sin\Psi \\ \cos\theta\sin\Psi & \sin\Phi\sin\theta\sin\Psi + \cos\Phi\cos\Psi & \cos\Phi\sin\theta\sin\Psi - \sin\Phi\cos\Psi \\ -\sin\theta & \sin\Phi\cos\theta & \cos\Phi\cos\theta \end{bmatrix} \quad (3\text{-}1)$$

3.1.2 Equations of Motion

Newton-Euler equations of motion are used to describe the translational and rotational dynamics of the helicopter. A relation between velocities, forces and torques are derived with respect to the CG of the helicopter in inertial frame using body-fixed frame variables. The main rotor and tail rotor, and gravitational forces produce the external forces and moments. Using the kinematic principles, the equations of motion with respect to body-fixed frame are given by:

$$\vec{F} = m\frac{d\,\vec{v_I}}{dt} = m\left(\frac{d\,\vec{v_B}}{dt} + \vec{\omega}\times\vec{v_B}\right) \tag{3-2}$$

$$\vec{T} = \frac{d\,(I.\vec{\omega_I})}{dt} = \frac{d\,(I.\vec{\omega_B})}{dt} + \vec{\omega_B}\times(I.\vec{\omega_B}) \tag{3-3}$$

where I is the moment of inertia matrix of the helicopter.

$$I = \begin{bmatrix} I_{xx} & -I_{xy} & -I_{xz} \\ -I_{yx} & I_{yy} & -I_{yz} \\ -I_{zx} & -I_{zy} & I_{zz} \end{bmatrix} \tag{3-4}$$

The principle axis of the helicopter is assumed to coincide with the body-fixed frame. Hence,

$$I_{xy} = I_{yx} = I_{zy} = I_{yz} = I_{xz} = I_{zx} = 0 \tag{3-5}$$

Three equations for the translational motion are derived as a function of translational velocities (u, v, w) and forces (F_x, F_y, F_z) acting on the body CG where G.M is the total mass of the helicopter. Equation (3-6) displays three differential equations that describe helicopter translation motion in body fixed frame:

$$\dot{u} = \frac{F_x}{M_H} + vr - wq$$

$$\dot{v} = \frac{F_y}{M_H} + wp - ur \tag{3-6}$$

$$\dot{w} = \frac{F_z}{M_H} + uq - vp$$

Similarly, Equation (3-7) gives us the three equations for the rotational motion derived as a function of rotational velocities (p, q, r) and moments (L, M, N) acting about the CG.

$$\dot{p} = \frac{(I_{yy} - I_{zz}).q.r + L}{I_{xx}}$$

$$\dot{q} = \frac{(I_{zz} - I_{xx}).p.r - M}{I_{yy}} \tag{3-7}$$

$$\dot{r} = \frac{(I_{xx} - I_{yy}).p.q + N}{I_{zz}}$$

3.1.3 Rotor Dynamics

One of the most complex component of the helicopter is the rotor system, which provides lifting force as well as control forces and torques. The helicopter is piloted using four command inputs; main rotor collective pitch, U_{col}, longitudinal cyclic pitch, U_{lon}, lateral cyclic pitch, U_{lat}, and pedal or tail rotor collective pitch, U_{ped}. The collective pitch command controls the main rotor by changing the pitch of the rotor blades. Similarly, the change in pedal collective pitch increases or decreases the tail rotor thrust. Cyclic commands change the inclination of Tip-Path-Plane (TPP) that results in longitudinal and lateral motions of the helicopter.

To understand the rotor dynamics, the blade motion needs to be understood. Rotor blades are attached to the shaft via the rotor head, which spins at speed Ω. The blade can also rotate about three DOF as shown in Figure 3-3:

- Feathering is the motion of blade about its length or span and is denoted by blade pitch angle, θ.
- Flapping is the motion of blade in the direction normal to the rotor disc described by flapping angle, β.
- Lead lagging is the motion of the blade in the rotor disc plane and is denoted by angle, ξ.
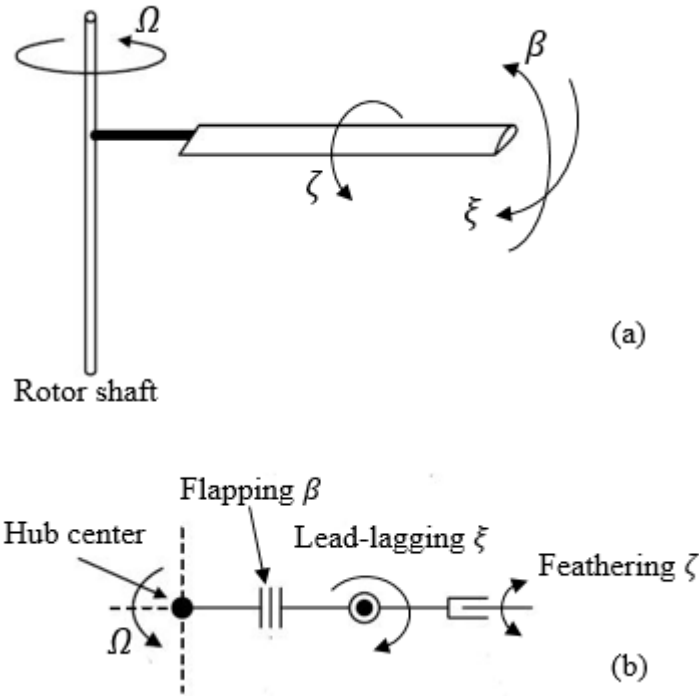
Figure 3-3: Rotor degrees of freedom adapted from [18]; (a) rotor blade motion; (b) top view of the rotor hub

The rotor speed in a helicopter is kept constant whereas the thrust and rotor moments are produced because of changing blade pitch using a swash plate mechanism. The blade pitch is defined as function of the blade position, ψ_b around the hub where the zero position is assigned when the blade is above the tail.

$$\theta = \theta_o - A_1 \cos \psi_b - B_1 \sin \psi_b \tag{3-8}$$

where θ_o is the average pitch angle of the blade and is assigned by the collective pitch input, U_{col}. A_1 is the coefficient that converts the lateral cyclic pitch inputs into angular pitch and B_1 is the coefficient that converts the longitudinal cyclic pitch input as shown in Equation (3-9).

$$A_1 = B_{lat} U_{lat}$$
$$B_1 = A_{lon} U_{lon} \tag{3-9}$$
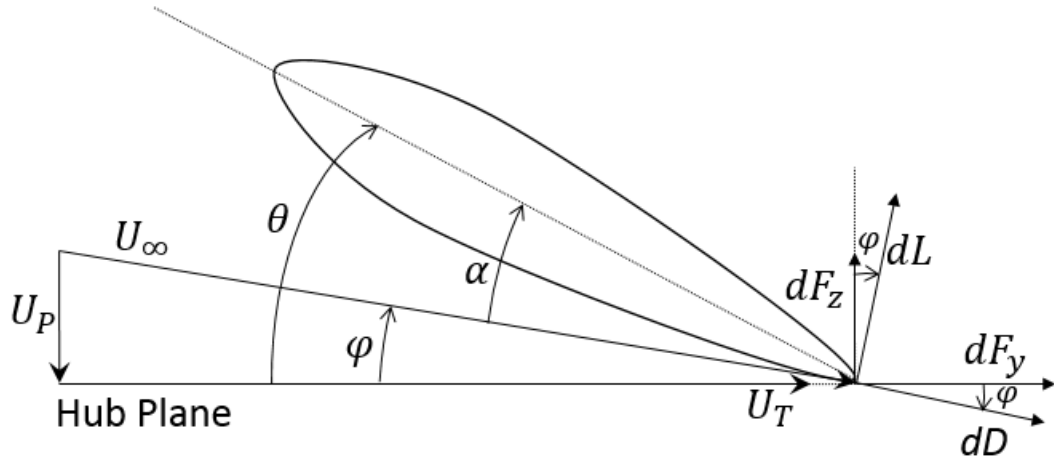
Figure 3-4: Typical blade element adapted from [3]; This illustrates the velocities seen by the blade element and forces generated relative to the hub plane

The local angle of attack, α, is determined by the geometric pitch of the blade, θ, and the local inflow angle, φ. The inflow angle is calculated using the induced velocity, v_i, which is the velocity induced at the wake of the rotor due to generation of lift.

$$\alpha = \theta - \varphi = \theta - \tan^{-1}\left(\frac{v_i}{\Omega r_b}\right) \tag{3-10}$$

In hovering flight, the thrust equals the weight of the helicopter, W_H and the induced velocity, v_{hover} is given as follows.

$$v_{hover} = \sqrt{\frac{W_H}{2\rho\pi r_b^2}} \tag{3-11}$$

In vertical climb, the combined momentum and blade element method can be modified to include the effects of climb velocity, V_c as shown in Equation (3-12) .

$$v_c = \frac{-\left(\left(\frac{\Omega}{2} a\, c\, b\right) + (4\,\pi\, V_c)\right) + \sqrt{\left(\left(\frac{\Omega}{2} a\, c\, b\right) + (4\,\pi\, V_c)\right)^2 + \left(8\,\pi\, b\, \Omega^2\, a\, c\, r_b \left(\theta - \frac{V_c}{\Omega\, r_b}\right)\right)}}{8\,\pi} \tag{3-12}$$

In forward flight, the induced velocity depends on the blade position, ψ_b, and the forward velocity of the helicopter, V_f, and is given by:

$$v_f = \left(\sqrt{-\frac{V_f^2}{2} + \sqrt{\left(\frac{V_f^2}{2}\right)^2 + (v_{hover})^4}} \right) \left(1 + \left(\frac{r_{be}}{r_b}\right) \cos(\psi_b) \right) \qquad (3\text{-}13)$$

However, a simplified model of the induced velocity for the forward flight as shown in Equation (3-14) was implemented instead of Equation (3-13).

$$v_f = \left(\sqrt{-\frac{V_f^2}{2} + \sqrt{\left(\frac{V_f^2}{2}\right)^2 + (v_{hover})^4}} \right) \qquad (3\text{-}14)$$

The velocity tangential to the hub plane, U_T, is dependent on the forward velocity of the helicopter and the velocity due to the rotation, Ωr_b. While in hover, it is only dependent on the rotational component of the velocity. Thus, the tangential velocity is calculated with respect to azimuthal angle, ψ_b, and the radial distance, r_b, of the blade and is given by:

$$U_T = \Omega r_b + V_f \sin(\psi_b) \qquad (3\text{-}15)$$

The perpendicular velocity in vertical flight is calculated as the sum of the climbing velocity (V_c) and the induced velocity (v_c) at the blade and is given as:

$$U_P = V_c + v_c \qquad (3\text{-}16)$$

In forward flight, the perpendicular velocity is dependent on the four components: forward velocity in the radial direction, induced velocity at the blade, and flapping characteristics of the blade.

The flapping motion of the blade is a 2π periodic function and is given by the Fourier series:

$$\beta(\psi_b) = \beta_0 - \beta_{1c} \cos(\psi_b) - \beta_{1s} \sin(\psi_b) - \beta_{2c} \cos(2\psi_b)$$
$$- \beta_{2s} \sin(2\psi_b) - \cdots .. \qquad (3\text{-}17)$$

However, small-unmanned helicopters, the flapping angle is only dependent on the lower harmonic components of the equation. Hence, the flapping angle is reduced to Equation (3-18).

$$\beta(\psi_b) = \beta_0 - \beta_{1c}\cos(\psi_b) - \beta_{1s}\sin(\psi_b) \qquad (3\text{-}18)$$

where term, β_0, describes the coning angle and coefficients, β_{1c} and β_{1s} describe the tilting of the rotor tip path plane in the longitudinal and lateral direction, respectively.

The tip path plane (TPP) rotor dynamics have three oscillatory motions, the coning, the advancing blade and retreating blade. To simplify the TPP model several assumptions are made:

1. The blade is considered rigid. Hence, no bending and torsion occur and the blade twist is linear and the flapping angles are considered small.
2. The aerodynamic factors are simplified by ignoring the inflow ratio, blade stall, and losses due to blade tip or root cutout.
3. The lead-lag motion due to the Coriolis forces induced by flapping motion is ignored.
4. The effects of the hinge offset are disregarded.
5. The blade-element drag coefficient is considered constant.

The equations used to describe the TPP motion are given as follows:

$$\dot{\beta}_{1c} = \frac{-\beta_{1c} - (\tau_f q) + A_b \beta_{1s} + A_{lon} U_{lon}}{\tau_f}$$

$$\dot{\beta}_{1s} = \frac{-\beta_{1s} - (\tau_f p) + B_a \beta_{1c} + B_{lat} U_{lat}}{\tau_f} \qquad (3\text{-}19)$$

where τ_f, denotes the main rotor time constant, which depends on the angular velocity, Ω, of the main rotor and the lock number, γ, which is the measure of balance between the aerodynamic forces and inertial forces on the rotor.

$$\tau_f = \frac{16}{\Omega\gamma} \qquad (3\text{-}20)$$

$$\gamma = \frac{\rho\, a\, c\, r_b{}^4}{I_b} \qquad (3\text{-}21)$$

where ρ is density of air, a is slope of lift curve, c is chord of blade, r_b is the radius of blade and I_b is moment of inertia of blade. The main rotor cross coupling terms A_b and B_a

are dependent on the natural frequency ratio, λ_β, of the flapping response and are given by:

$$A_b = -B_a = \frac{8\left(\lambda_\beta^2 - 1\right)}{\gamma} \tag{3-22}$$

$$\lambda_\beta^2 = \frac{K_\beta}{\Omega^2 I_b} + 1 \tag{3-23}$$

Equation (3-23) is used to model the flapping where K_β is the stiffness of the torsional spring added at the hinge [10]. Hence, using Equations (3-18) to (3-23) the perpendicular velocity for the forward flight can be calculated and is given by:

$$U_P = V_f \sin(\alpha_{hb}) - v_f - r\dot{\beta} - V_f\beta\cos(\psi_b) \tag{3-24}$$

The total velocity generated by the blade is calculated as the resultant of the tangential and perpendicular velocity and is given by resultant velocity (U) shown in Equation (3-25).

$$U = \sqrt{U_T^2 + U_P^2} \tag{3-25}$$

The incremental lift produced at the blade is perpendicular to the resultant velocity and is given by:

$$dL = \frac{1}{2}\rho U^2 c\, a\, \alpha\, dr \tag{3-26}$$

where a is slope of lift curve, c is chord of the blade and ρ is air density. Similarly, the drag component at the blade acts in line with the resultant velocity and is given by:

$$dD = \frac{1}{2}\rho U^2 c\, c_d\, dr \tag{3-27}$$

The components of the forces acting parallel (dF_x) and perpendicular (dF_z) to the rotor plane can be calculated and are given by:

$$dF_x = dL \sin(\varphi) + dD \cos(\varphi)$$
$$dF_z = dL \cos(\varphi) - dD \sin(\varphi) \tag{3-28}$$

The thrust of the main rotor can be calculated by integrating the perpendicular force for the entire blade element along the blade's length and for number blades, b:

$$T_{MR} = b \int_0^{r_b} dF_z \, dr \tag{3-29}$$

Torque introduced on the helicopter body due to the rotation of blades can be calculated by using Equation (3-30).

$$Q_{MR} = b \int_0^{r_b} dF_x \, r_{be} \, dr \tag{3-30}$$

The tail rotor provides the moment to negate the moment produced by the main rotor. The tail rotor thrust, T_{TR}, required to balance main rotor torque is given by:

$$T_{TR} = \left(\frac{F_{y,MR} x_{MR} + F_{x,MR} y_{MR} + Q_{MR} \cos(\beta_{1s}) \cos(\beta_{1c})}{x_{TR}} \right) + T_{TC} \tag{3-31}$$

The tail rotor thrust, T_{TC} is calculated similar to the thrust calculations of the main rotor in vertical flight using the Blade Element Theory.

3.1.4 Force and Torque Calculations

Forces (X, Y, Z) acting on the helicopter are calculated by relating the total thrust generated by the main rotor, tail rotor and the weight of the helicopter and is given by:

$$F = \begin{bmatrix} F_x \\ F_y \\ F_z \end{bmatrix} = F_{MR} + F_{TR} + F_W \tag{3-32}$$

The forces generated by the main rotor can be calculated using the main rotor thrust translated to the body fixed frame using β_{1c} and β_{1s}, the flapping angles of the blade, and is given by:

$$F_{MR} = \begin{bmatrix} F_{x,MR} \\ F_{y,MR} \\ F_{z,MR} \end{bmatrix} = \begin{bmatrix} -T_{MR} \sin(\beta_{1c}) \\ T_{MR} \sin(\beta_{1s}) \\ -T_{MR} \cos(\beta_{1s}) \cos(\beta_{1c}) \end{bmatrix} \tag{3-33}$$

The forces generated by the tail rotor only applies a force in y direction and is given by:

$$F_{TR} = \begin{bmatrix} F_{x,TR} \\ F_{y,TR} \\ F_{z,TR} \end{bmatrix} = \begin{bmatrix} 0 \\ T_{TR} \\ 0 \end{bmatrix} \tag{3-34}$$

The force generated by weight of the helicopter with the payload is calculated by deriving the components in the body fixed frame using the Euler angles θ and ϕ.

$$F_W = \begin{bmatrix} -(M_H)g\,\sin(\theta) \\ (M_H)g\,\sin(\Phi)\cos(\theta) \\ (M_H)g\,\cos(\Phi)\cos(\theta) \end{bmatrix} \tag{3-35}$$

Torque (L, M, N) acting on the helicopter in the body fixed frame is calculated using the main rotor force and main rotors torque which (x_{MR}, y_{MR}, z_{MR}) away from the CG and are calculated by:

$$T = \begin{bmatrix} L \\ M \\ N \end{bmatrix} = \begin{bmatrix} F_{y,MR}z_{MR} - F_{z,MR}y_{MR} + F_{y,TR}z_{TR} + Q_{MR}\sin(\beta_{1c}) \\ -F_{x,MR}z_{MR} - F_{z,MR}x_{MR} - Q_{MR}\sin(\beta_{1s}) \\ F_{x,MR}y_{MR} + F_{y,MR}x_{MR} - F_{y,TR}x_{TR} + Q_{MR}\cos(\beta_{1c})\cos(\beta_{1s}) \end{bmatrix} \tag{3-36}$$

3.1.5 Summary

Equations of motion of a helicopter can be summarized as shown in Equation (3-37).

$$\begin{bmatrix} \dot{\vec{v_B}} \\ \dot{\vec{\theta}} \\ \dot{\vec{\omega}} \end{bmatrix} = \begin{bmatrix} \dfrac{1}{m}\vec{F} - \vec{\omega} \times \vec{v_B} \\ R(\theta).\vec{\omega} \\ I^{-1}\left(\vec{T} - \vec{\omega} \times (I.\vec{\omega})\right) \end{bmatrix} \tag{3-37}$$

where $\dot{\vec{v_B}}$, $\dot{\vec{\theta}}$, and $\dot{\vec{\omega}}$ are the states of the helicopter. The velocity vector can be expanded as shown in Equation (3-38).

$$\dot{v}_B = \begin{bmatrix} \dot{u} \\ \dot{v} \\ \dot{w} \end{bmatrix} = \begin{bmatrix} \dfrac{F_x}{M_H} + vr - wq \\ \dfrac{F_y}{M_H} + wp - ur \\ \dfrac{F_z}{M_H} + uq - vp \end{bmatrix} \tag{3-38}$$

where (F_x, F_y, F_z) are forces acting on helicopter body, (u, v, w) are translation velocities and (p, q, r) are rotational velocities of the helicopter and M_H is the mass of the helicopter. The Euler angle vector, Θ, can be expanded as shown in Equation (3-39).

$$\dot{\Theta} = \begin{bmatrix} \dot{\Phi} \\ \dot{\Theta} \\ \dot{\psi} \end{bmatrix} = \begin{bmatrix} p + (\sin(\Phi)\tan(\Theta)\,q) + (\cos(\Phi)\tan(\Theta)\,r) \\ \cos(\Phi)\,q - \sin(\Phi)\,r \\ \dfrac{\sin(\Phi)}{\cos(\Theta)}q + \dfrac{\cos(\Phi)}{\cos(\Theta)}r \end{bmatrix} \tag{3-39}$$

The rotational velocity vector, ω, can be expanded as shown in Equation (3-40).

$$\dot{\omega} = \begin{bmatrix} \dot{p} \\ \dot{q} \\ \dot{r} \end{bmatrix} = \begin{bmatrix} \dfrac{(I_{yy} - I_{zz}).q.r + L}{I_{xx}} \\ \dfrac{(I_{zz} - I_{xx}).p.r - M}{I_{yy}} \\ \dfrac{(I_{xx} - I_{yy}).p.q + N}{I_{zz}} \end{bmatrix} \tag{3-40}$$

where (L, M, N) are the moments acting about the center of gravity of helicopter and (I_{xx}, I_{yy}, I_{zz}) are moment of inertia of helicopter.

3.2 Simulation Studies

Using the mathematical equations in the previous section, a simulation program for helicopter was developed to test different control algorithm.

3.2.1 Simulation Platform

The simulation was developed in Simulink environment of MATLAB software. The helicopter that was simulated in the simulation was the X-Cell 60 and the parameters for the model were taken from MicroPilot Horizon simulation model. Fourth-order Runga-Kutta method was used in the simulation with integration time of 0.001 s. The controllers that will be designed later will be inserted in the simulation and will run at the same speed as the simulation. All units are in imperial system and the parameters of the helicopter are shown in Table 3-1.

Table 3-1: Parameters of the X-Cell 60 helicopter

Parameter	Values
Rotor Speed, Ω	1500 rpm
Main rotor radius, r_b	2.25 ft
Helicopter weight, W_H	19.5 lb
Payload weight, W_P	10 lb
Number of blades, b	2
Chord of main blade, c	0.1979 ft
Main rotor blade twist, θ_T	0 rad
Main blade lift slope, a	$6.0 \ rad^{-1}$
Drag coefficient, c_d	0.01
Natural flapping frequency, λ_β	1.00
Main rotor blade moment of inertia, I_b	$0.0847 \ slug.ft^2$
Longitudinal coefficient, A_{long}	0.53
Lateral coefficient, B_{lat}	0.42
Distance of the main rotor from center of gravity of helicopter in z direction, z_{main}	0.9 ft
Helicopter moment of inertia, (I_{xx}, I_{yy}, I_{zz})	$(0.2184 , 0.3214, 0.4608) \ slug.ft^2$

3.2.2 Results

After developing the simulation, it is important to verify that the simulation runs accurately for different flight plans. The simulations are conducted using the open loop system, i.e. no controllers are implemented and the variations in the variables are qualitatively verified. To see if the simulation is generating accurate parameters, the collective pitch is changed for the vertical flight while the longitudinal and lateral cyclic pitch are changed for the longitudinal and lateral flight respectively.

3.2.2.1 Vertical Flight

The vertical channel of the helicopter simulation is verified by adding a positive pulse input followed by a negative pulse input to the trim collective pitch as shown in Figure 3-5 (a). Because of the positive input change to the collective pitch, the vertical velocity becomes positive while the negative input creates a negative vertical velocity as shown in Figure 3-5 (b).
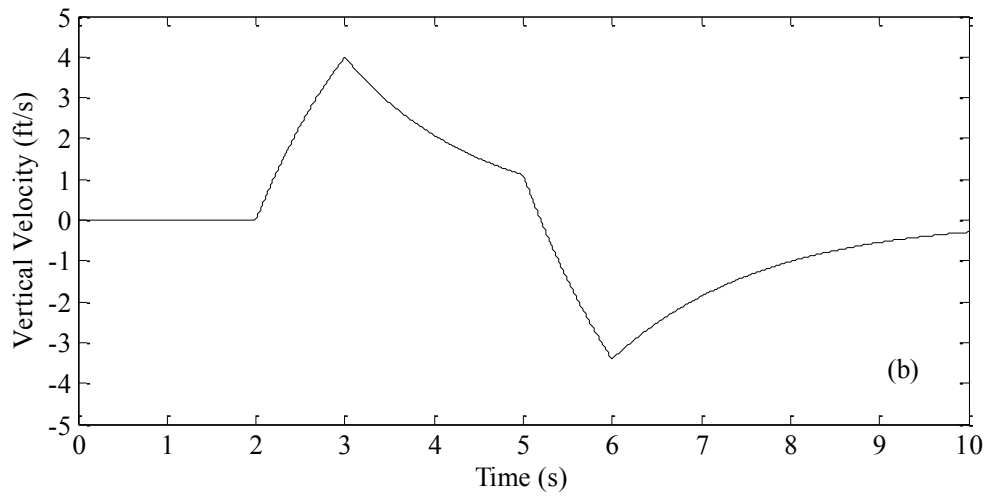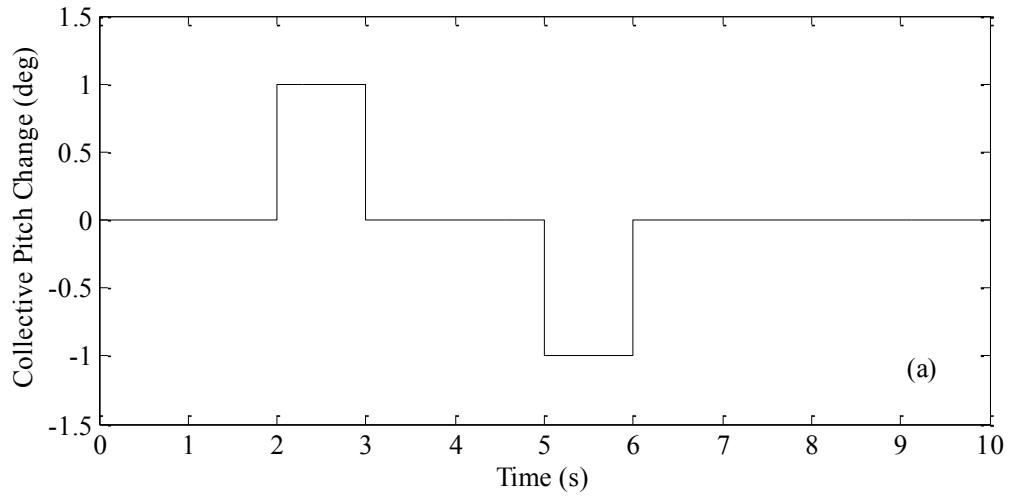
Figure 3-5: Response to collective pitch input; (a) collective pitch; (b) vertical velocity

The positive input at 2.0 s increases the altitude in flight while the negative input at 5.0 s decreases the altitude as shown in Figure 3-6. While the translation velocities ('u' and 'v') and the rotational velocities (p and q) stay zero.
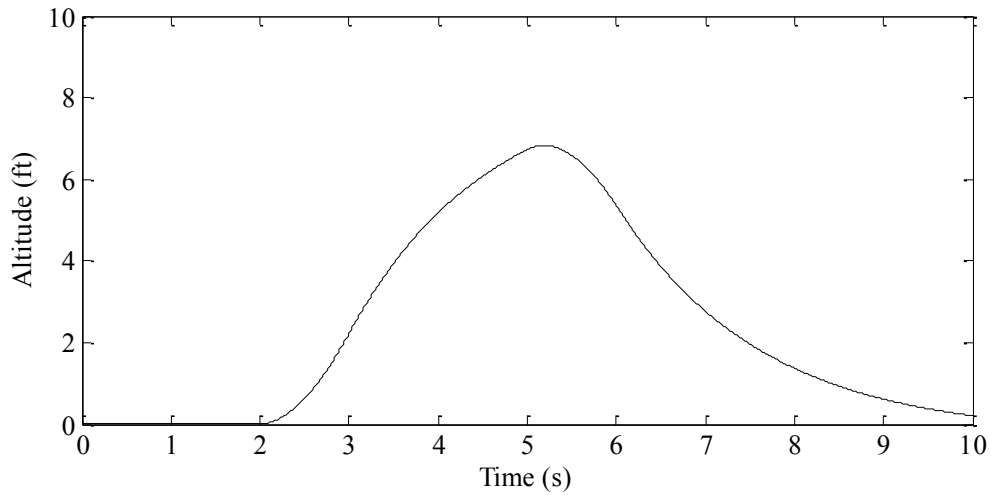
Figure 3-6: Altitude response to collective pitch input

With increase in collective pitch, the main rotor thrust increases while decrease in the collective pitch causes the thrust to decrease as well, as shown in Figure 3-7.
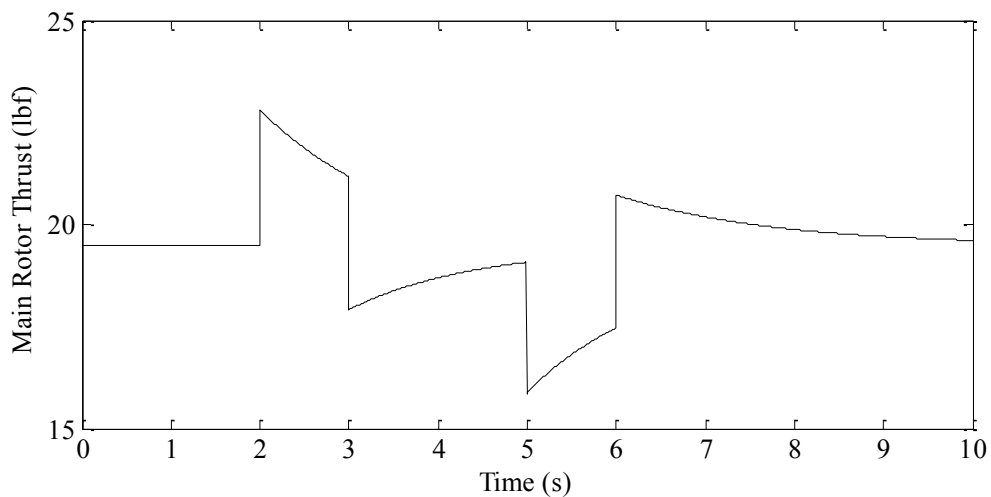
Figure 3-7: Thrust generated by main rotor

The positive collective pitch results in increase in main rotor moment generated on the helicopter body while the negative input results in opposite change as shown in Figure 3-8.
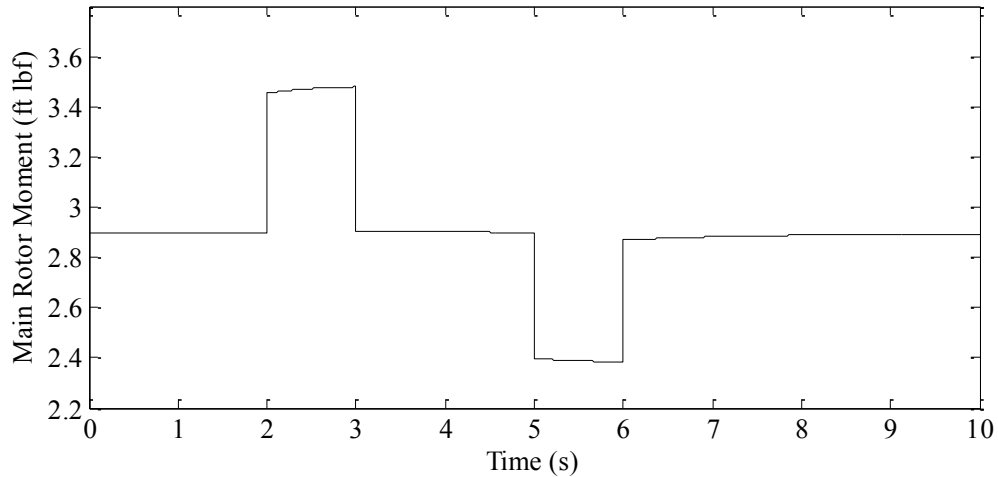
Figure 3-8: Moment generated due to main rotor rotation

To counter the moment, the tail rotor thrust needs to increase and decrease accordingly as seen in Figure 3-9.
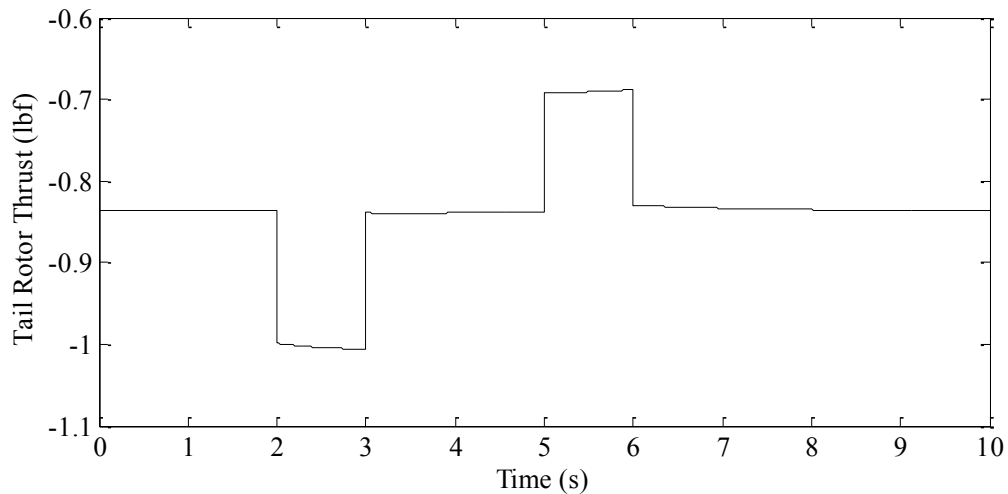
Figure 3-9: Tail rotor thrust

As a result, it can be inferred that the simulation is working as expected and hence, it can be used to evaluate the different controllers that will be designed for the helicopter. The simulation will be further verified through the outputs resulted due to the controllers that will provide us with further information if the variables are generated as intended.

3.2.2.2 Forward Flight: Longitudinal Motion

Forward flight is difficult to verify in open loop. Without controllers for the other channels, the change in one channel will appear in all channels. To see if the longitudinal channel is working properly, the effects of positive step input at 1.0 s to the longitudinal cyclic pitch shown in Figure 3-10 are observed. As a result the input at 1.0 s the pitch rate, q, increases as shown in Figure 3-11.
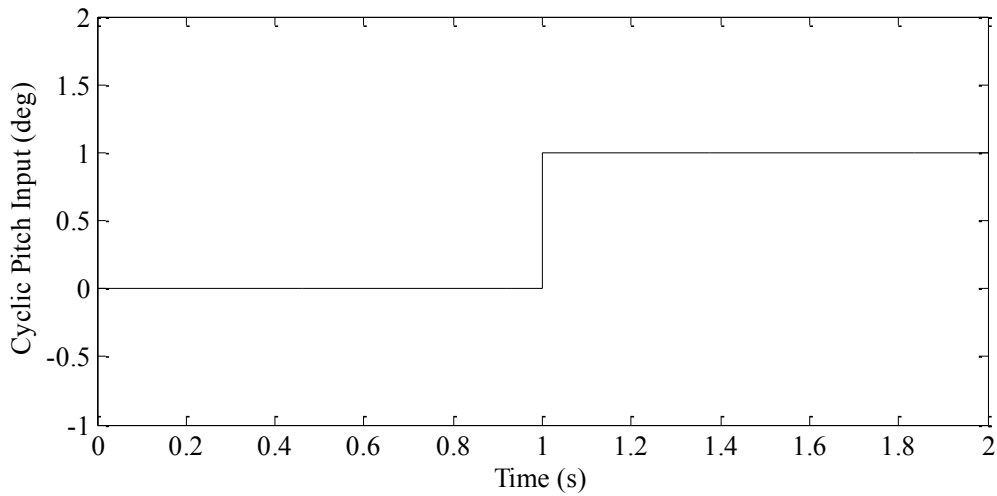
Figure 3-10: Longitudinal cyclic pitch input
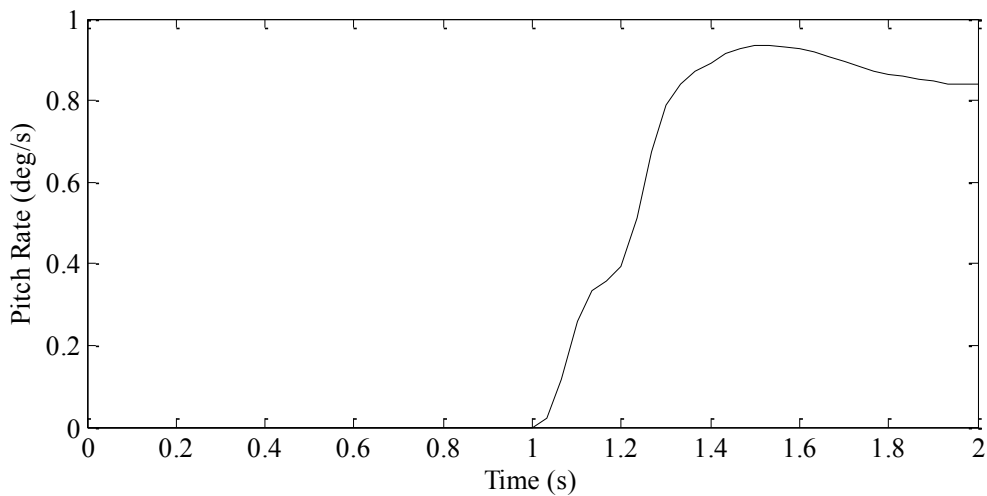
Figure 3-11: Pitch rate longitudinal mode

The positive longitudinal cyclic pitch command also increase the forward velocity, u as shown in Figure 3-12 (a) and moves the helicopter in the forward direction as shown in Figure 3-12 (b).

(a)

(b)
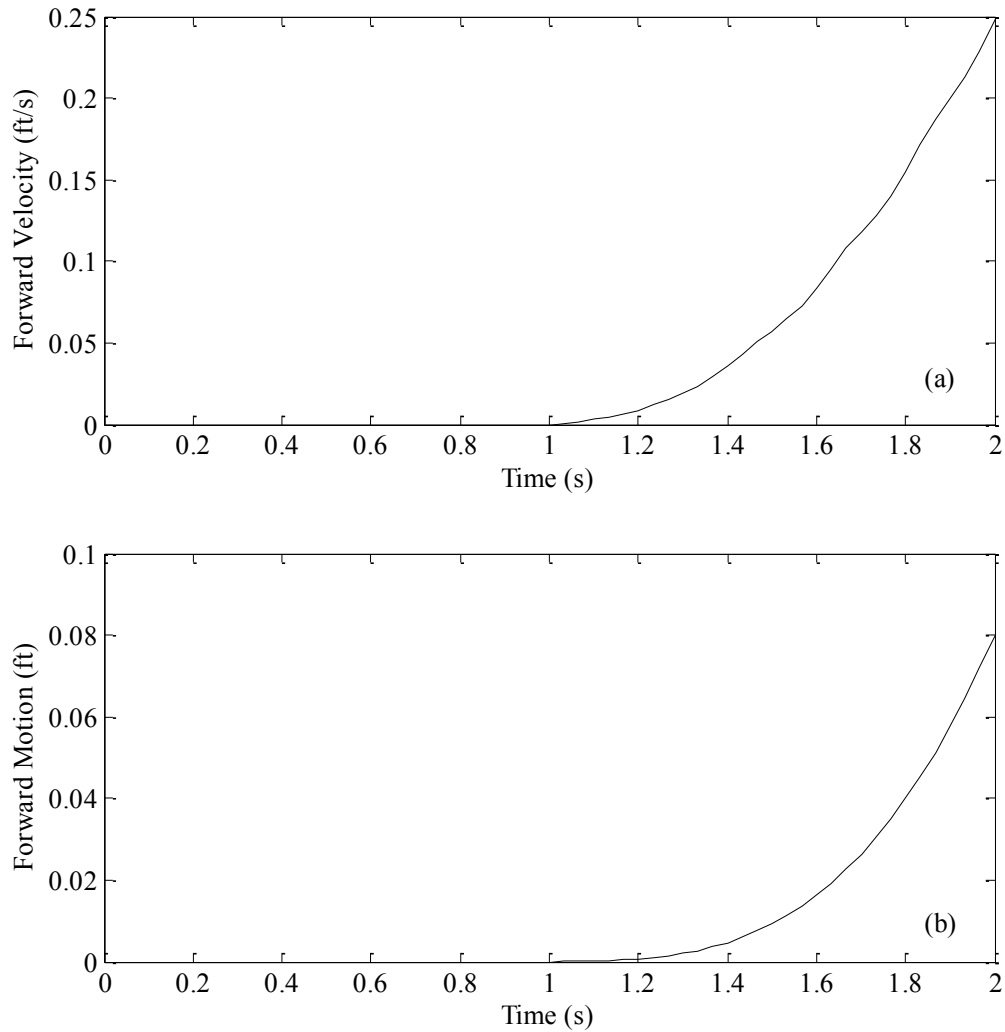
Figure 3-12: Longitudinal mode; (a) velocity; (b) forward motion

As no controller was implemented in the vertical channel, the velocity in the vertical direction becomes negative as shown in Figure 3-13 causing the helicopter to fly down as shown in Figure 3-14.
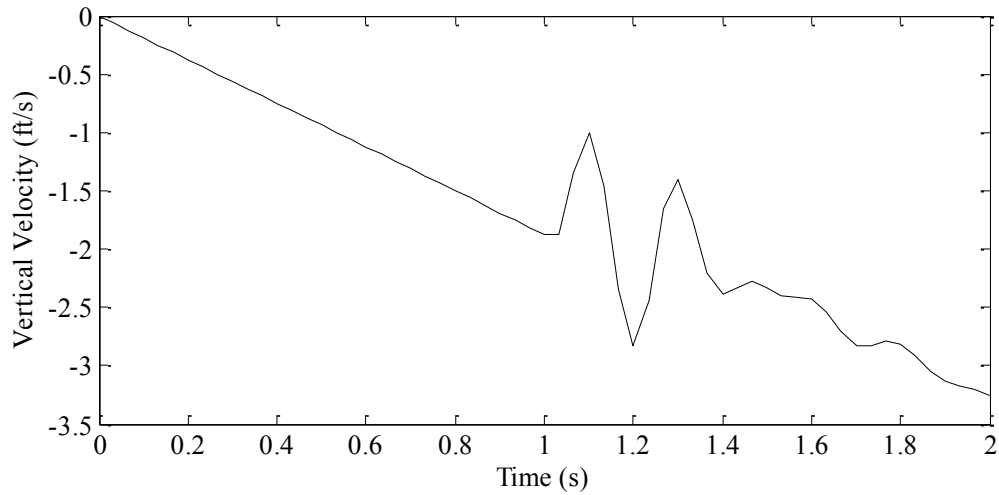
Figure 3-13: Vertical velocity
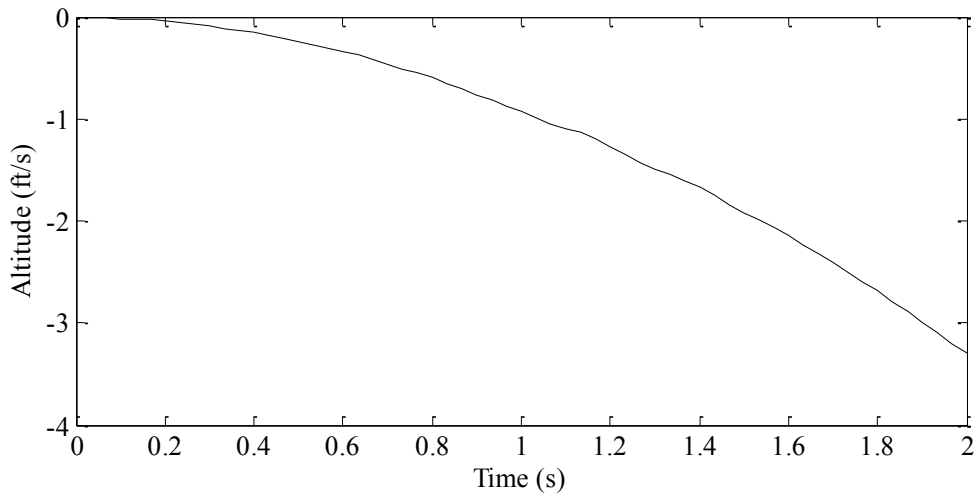
Figure 3-14: Altitude response

The translational and the rotational velocities (v and p) in the lateral direction remain unchanged as expected. Hence, the simulation is running properly in the longitudinal channel.

3.2.2.3 Forward Flight: Lateral Motion

To see if the lateral channel works properly the lateral cyclic pitch command was replaced with a step input at 1.0 s as shown in Figure 3-15 and the effects on the variables are observed.
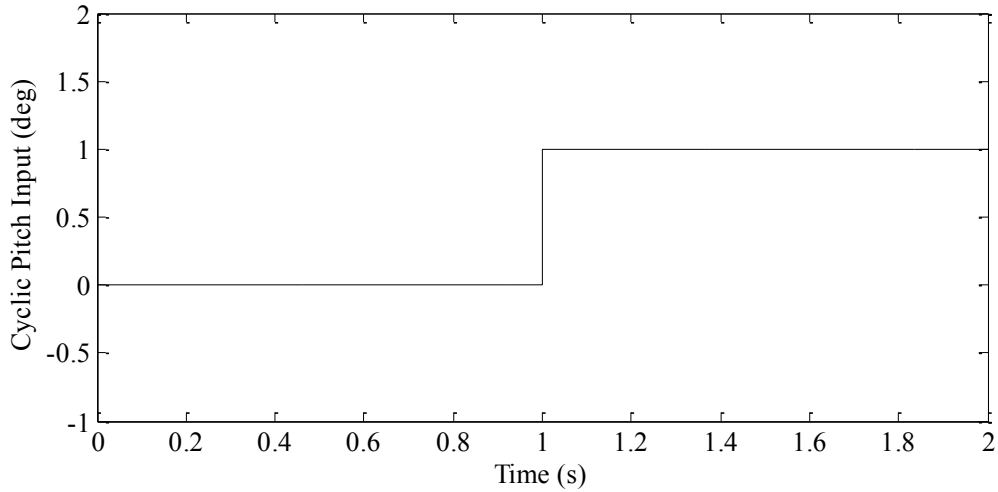
Figure 3-15: Lateral cyclic pitch input

As shown in Figure 3-16, an increase in the lateral cyclic pitch causes an increase in the roll rate, p.
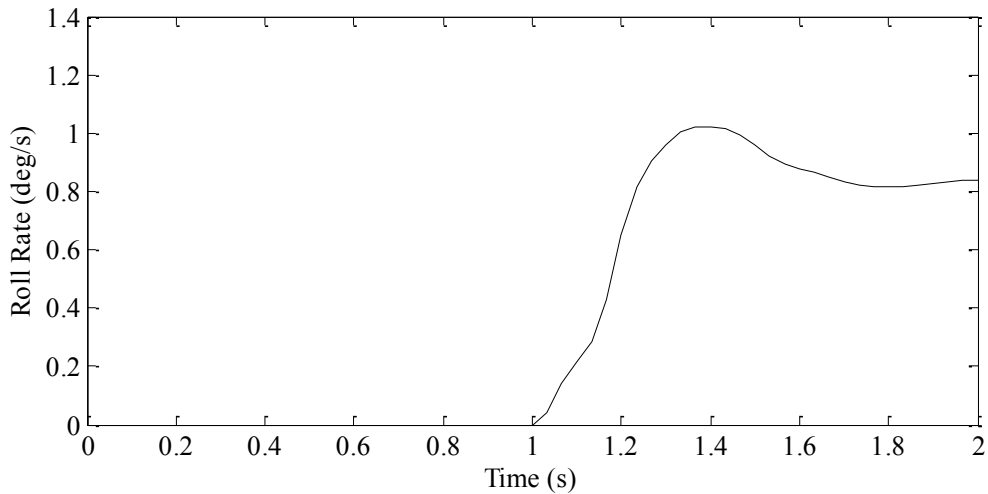
Figure 3-16: Roll rate lateral mode

The positive lateral cyclic pitch command also increases the velocity in the lateral direction, v, as shown in Figure 3-17 and causes the helicopter to move in lateral direction as shown in Figure 3-18.
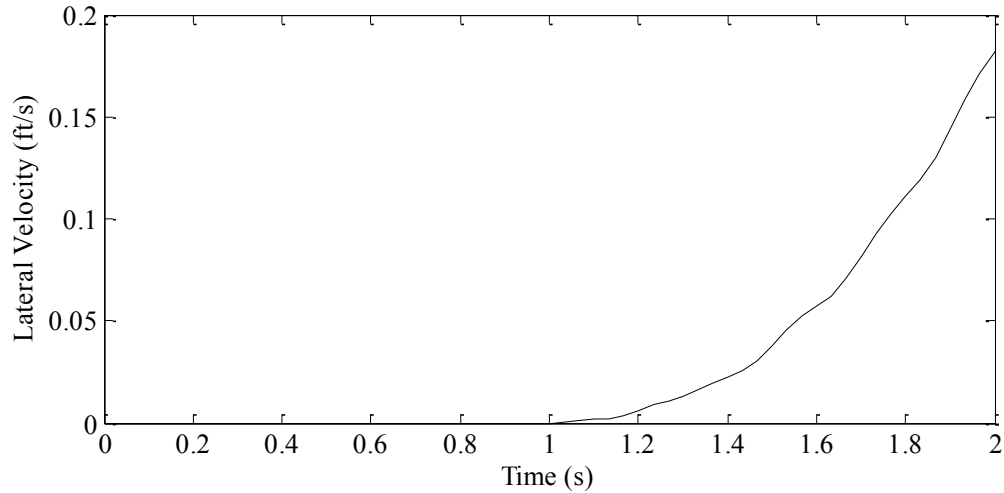
Figure 3-17: Lateral velocity
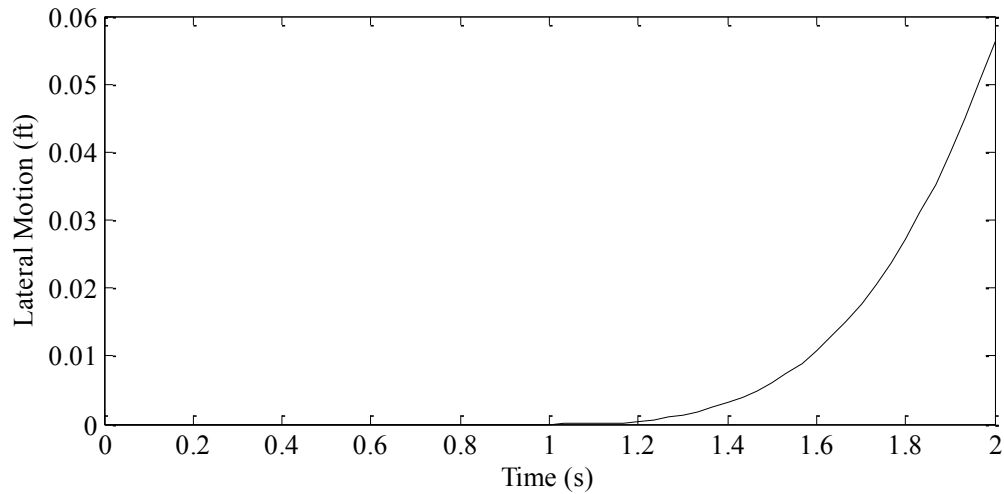
Figure 3-18: Lateral motion

Similar to the longitudinal motion, the helicopter altitude also decreases as seen in Figure 3-14, as no controller was implemented. Hence, we can infer that the simulation is generating the expected changes caused by the inputs in all three channels. However, to verify if the variables are generating accurate values, controllers need to be implemented for all the channels.

4. Controller Design of Vertical Channel

Design of various controllers for the vertical channel of the helicopter while carrying and dropping the payload. The vertical control loop as shown in Figure 4-1 is a two-loop process, where the outer loop is calculated using altitude and the inner loop a vertical velocity. The reference signal for the inner loop is desired vertical velocity, which is the output of the outer loop. A simple proportional controller is used for the outer altitude control. The gain for the altitude controller was set to 0.25 ft/s/ft is a good estimate for a small-scale helicopter. The primary objective is to design a controller for the inner loop that calculates the control signal collective pitch command needed to fly the helicopter in the vertical direction.
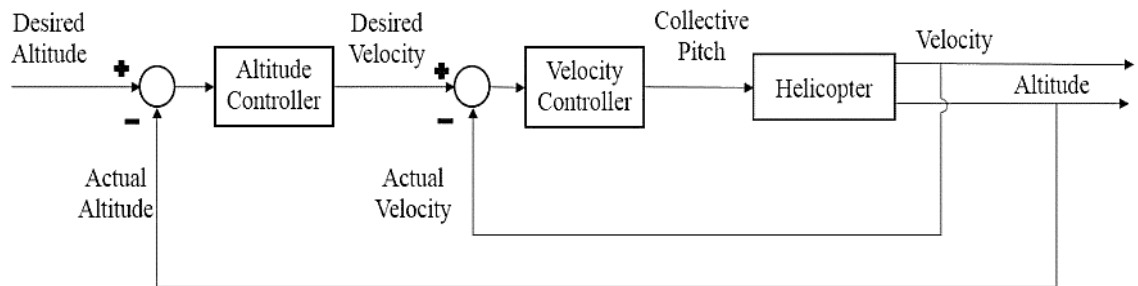
Figure 4-1: Vertical channel control loop

There are several control design techniques used for automatic control in the industry. The key for most designs is ease of implementation. Linear controllers such as PID controllers therefore have an advantage as long as the performance is acceptable. However, PID controllers are either tuned experimentally or designed for specific operating point. The performance may deteriorate or the system may become unstable if the operating point is too far from the design point due to the nonlinearities in the system. Hence, the idea is to design a controller that is robust in the sense that it has acceptable performance for a large rang of operating conditions. One such technique is Quantitative Feedback Theory (QFT) developed by Isaac Horowitz [19].

4.1 Quantitative Feedback Theory Controller Design

Quantitative Feedback Theory (QFT) is a frequency domain method for control system design to design a fixed gain controller given robust performance specification. The advantageous of the QFT design technique may be summarized [20] as follows:

1. It results in a robust design that is insensitive to structured plant parameter variation.
2. There can be one robust design for the full, operating envelope.
3. Design limitations and achievable performance specifications can be determined in the early stages of design process.
4. If necessary, one can redesign for changes in the specifications quickly with the aid of the QFT CAD package.
5. Reduces the cost of feedback by designing a low bandwidth controller that allows avoiding the problems associated with high loop gains such as sensor noise amplification, saturation and high frequency uncertainties.

As shown in Figure 4-2, the QFT control loop consists of the plant , $P(\alpha, s)$, controller to be designed, $G(s)$, reference signal, $R(s)$, pre-filter to be designed, $F(s)$, error signal generated, $E(s)$, disturbance to the plant output, $D(s)$ and the output signal, $Y(s)$.
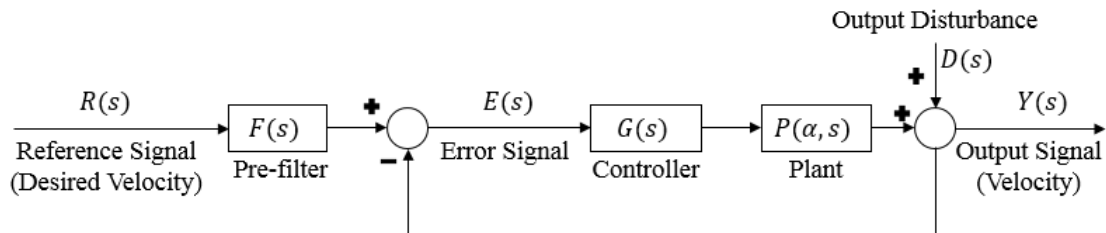
Figure 4-2: QFT control loop

QFT design procedure involves four steps [20], [21]:

1. **Generating plant templates**: The first step in the QFT design process is generating the plant templates. The plant templates capture the uncertainties in the plant transfer function, $P(\alpha, s)$ and are plotted as boundaries of magnitude and phase variations on the Nichols chart at specific design frequencies. These templates are then used to create bounds on the Nichols chart.

2. **Generating performance bounds**: Given the templates, QFT converts the closed loop magnitude specifications into magnitude and phase constraint on the open loop transfer function for the nominal plant $\left(L_o = G(s)P_o(s)\right)$. Usually system performance is described as robust stability, rejection to input disturbance and reference tracking.

   a. **Reference Tracking**: To meet the tracking performance the controller should meet the following:

$$|T_l| \leq \left|F\frac{PG}{1 + PG}\right| \leq |T_u| \qquad (4\text{-}1)$$

   where the upper, T_u and lower, T_l bounds are defined using time domain figures of merit such as peak overshoot and settling time.

   b. **Robust Stability**: Robust stability in QFT amounts to checking stability using nominal plant $\left(L_o(s) = G(s)P_o(s)\right)$ and then demonstrating stability of the whole set plants by assigning a sensitivity rating, W_{s1} given by:

$$\left|\frac{PG}{1 + PG}\right| \leq W_{s1} \qquad (4\text{-}2)$$

Oded Yaniv [21] in his book translated these to desired phase margin (PM) shown in Equation (4-3) and gain margin (GM) shown in Equations (4-4).

$$PM = 2\sin^{-1}\frac{1}{2(W_{s1})} \ deg \qquad (4\text{-}3)$$

$$GM = 20\log\left(\frac{W_{s1} + 1}{W_{s1}}\right) dB \qquad (4\text{-}4)$$

   c. **Disturbance rejection at plant output**: An upper limit is set to the sensitivity function to limit the peak value of disturbance amplification to the plant output as shown:

$$\left|\frac{1}{1 + PG}\right| \leq W_{dr} \qquad (4\text{-}5)$$

These bounds are then used for loop shaping to design a controller.

3. **Controller Design**: The controller is designed by adding poles and zeroes to the nominal transfer function by satisfying all bounds at each frequency. During this stage, the designer considers a trade-off between the specification, controller complexity and the cost of feedback in the bandwidth.

4. **Pre-filter Design**: A pre-filter is needed to bring the response within the reference tracking tolerances, T_l and T_u and is done by adding poles and zeroes.

4.2 QFT Controller for Vertical Channel (Controller I)

4.2.1 Transfer Function Estimation

The first step to design a controller is to estimate a transfer function for the vertical flight (Heave) dynamics. This is done by analyzing the response between the vertical velocity, w and the collective pitch input, δ_{col}. Bernard Mettler *et al.* [22] have estimated the transfer for the heave dynamics using the frequency domain techniques to be a first-order:

$$\frac{w}{\delta_{col}} = \frac{k_h}{\tau_h s + 1} \tag{4-6}$$

This was confirmed by applying a 1-degree step input to the collective pitch in open loop and analyzing the vertical velocity response. k_h is the max output at which the vertical velocity settles and τ_h is the time taken for the vertical velocity after the step input reaches 63% of the max vertical velocity. Values of k_h and τ_h for the transfer function when carrying a 10 lb load or no load were estimated from the simulation output as shown in Figure 4-3.
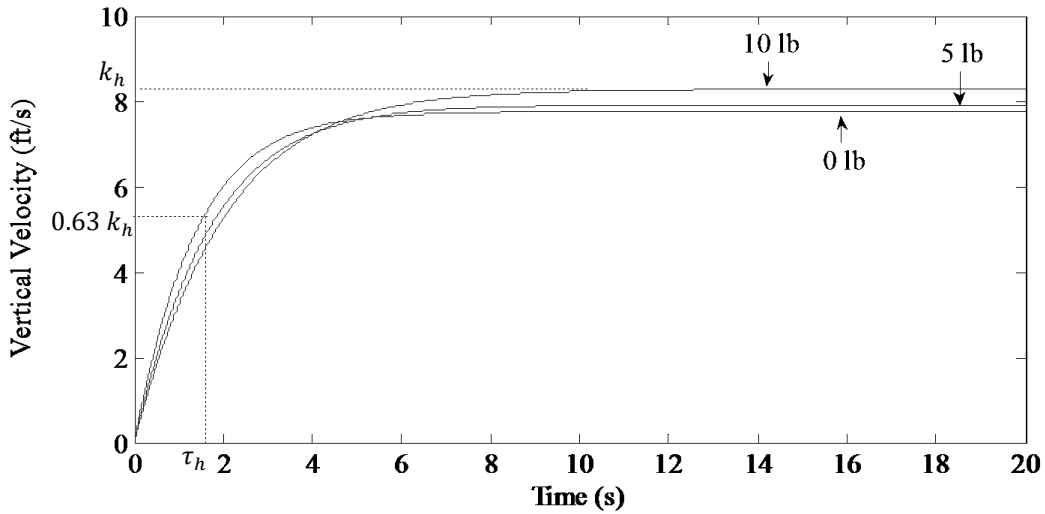
Figure 4-3: Heave response to step input

It is seen that as the payload increases both k_h and τ_h increases, which confirms that payload does affect the dynamics of the helicopter. The range for the transfer function variables are summarized in the Equation (4-7).

$$7.75 \le k_h \le 8.28 \quad \left(\frac{\frac{ft}{s}}{deg} \right)$$

$$1.35 \le \tau_h \le 1.97 \ (s)$$

(4-7)

To validate the estimation further, the input and output data from the simulation were used in CIFER software package [23], which uses frequency domain system identification techniques to estimate the transfer function. Figure 4-4 shows the output of the CIFER software without carrying a payload and Equation (4-8) displays the estimated transfer function.
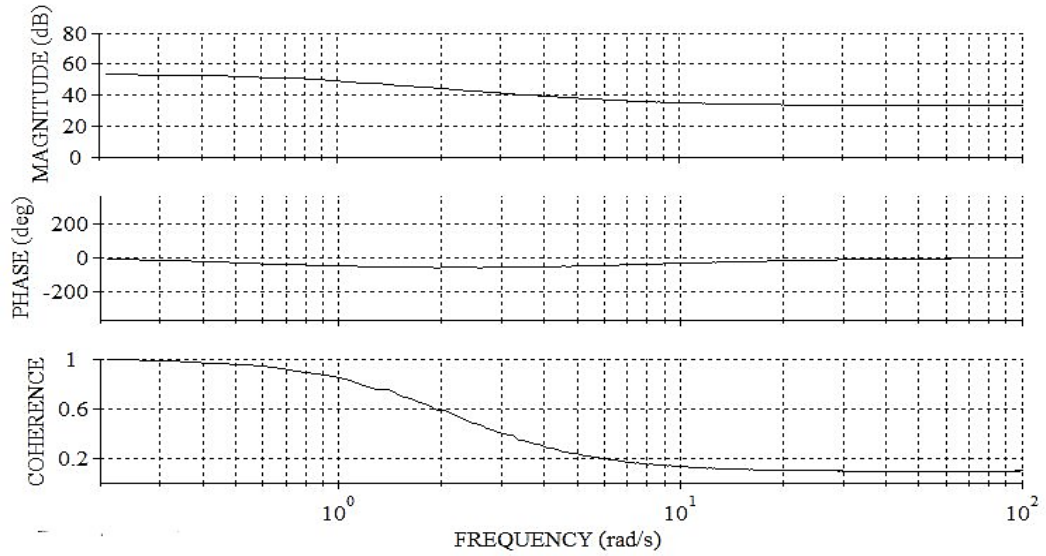
Figure 4-4: No payload CIFER output

$$\frac{314.765 \, e^{0.0458}}{s + 0.71762} \frac{\frac{ft}{s}}{rad} = \frac{8.01}{1.39s + 1} \frac{\frac{ft}{s}}{deg} \qquad (4\text{-}8)$$

Similarly, the input and output of the simulation while carrying a 10 lb payload was inputted into CIFER and the output of CIFER is shown in Figure 4-5 while the estimated transfer function is displayed as Equation (4-9).
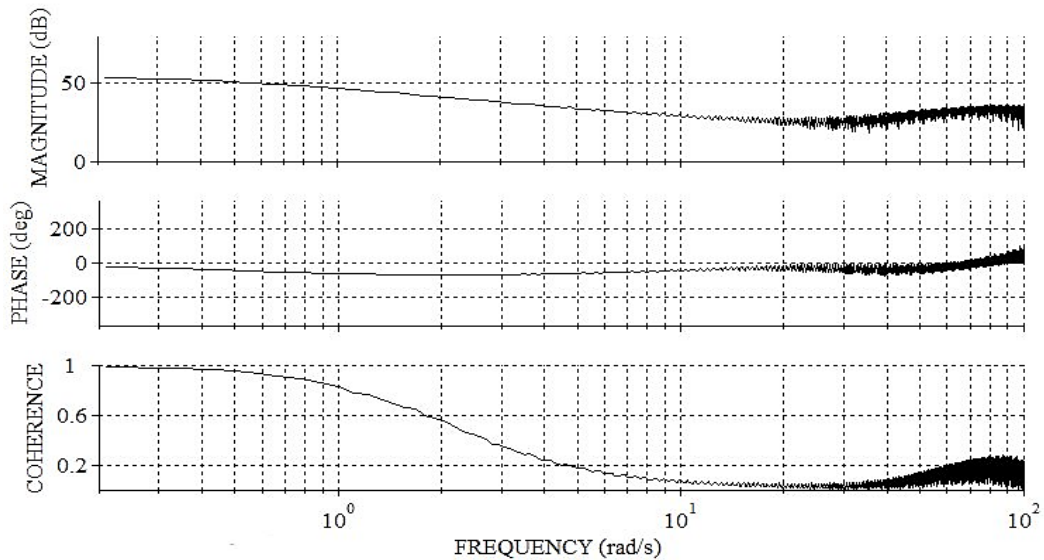
Figure 4-5: 10 lb payload CIFER output

$$\frac{230.88 \, e^{0.077}}{s + 0.48766} \frac{\frac{ft}{s}}{rad} = \frac{8.92}{2.05s + 1} \frac{\frac{ft}{s}}{deg} \qquad (4\text{-}9)$$

The ranges for uncertainties in the transfer function variables estimated from CIFER are summarized in Equation (4-10).

$$8.01 \leq k_h \leq 8.92 \quad \left(\frac{\frac{ft}{s}}{deg} \right)$$

$$1.39 \leq \tau_h \leq 2.05 \ (s)$$

(4-10)

Comparing equation (4-7) and (4-10), it is seen that the value of k_h and τ_h estimated using the first-order estimation technique in simulation and CIFER are different. This is because the results from CIFER have low coherence meaning lower accuracy [22]. Nevertheless, for the design process a closed estimate of the values is good enough. Hence, for the QFT design the following plant uncertainties that cover both the estimation results will be used:

$$7.5 \leq k_h \leq 9.5 \quad \left(\frac{\frac{ft}{s}}{deg} \right)$$

$$1.3 \leq \tau_h \leq 2.3 \ (s)$$

(4-11)

4.2.2 Controller Design

The frequency range from 0.01 to 100 rad/s was selected for the QFT controller design. This covers the full range of frequencies for a typical unmanned helicopter. The first step of the QFT design is to generate the plant templates, which characterize the uncertainties in the plant as shown in Equation *(4-11)* at given frequencies. These plant templates were generated using the Matlab QFT toolbox and are shown in Figure 4-6.
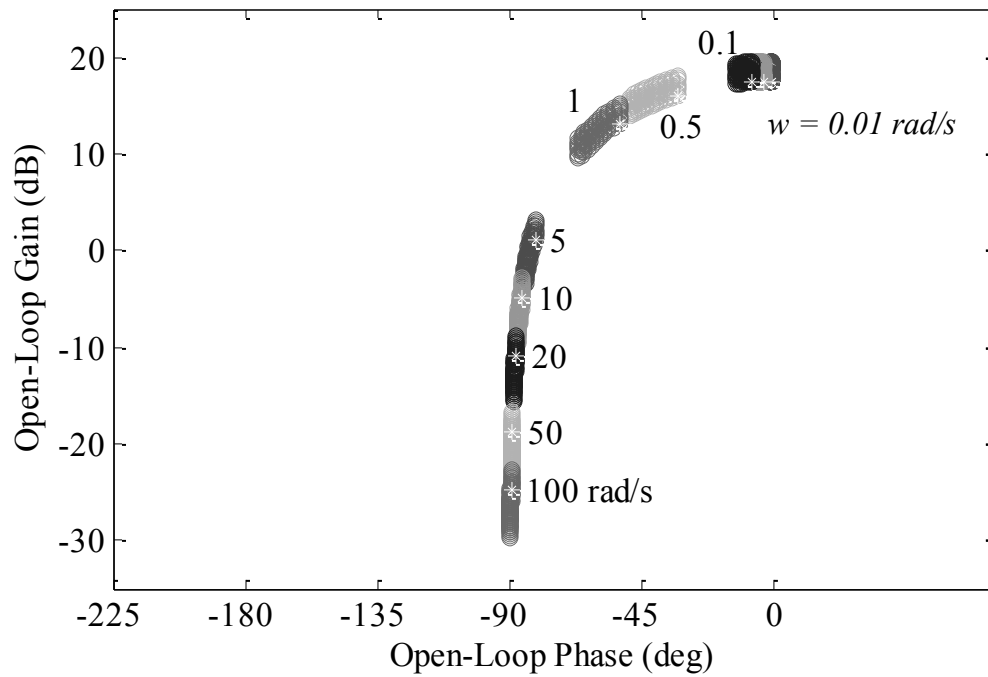
Figure 4-6: Plant templates

Criterions needed for the designing of the controller are:

Tracking Criterion: The upper bound for the tracking criterion was generated by considering 1% overshoot and settling time of 0.3 s. The transfer function used for the upper bound is:

$$T_u = \frac{(15)^2}{s^2 + 21s + (15)^2} \qquad (4\text{-}12)$$

Similarly, the lower bound was generated by considering no overshoot and settling time of 1.0 s. The transfer function used for the lower bound is:

$$T_l = \frac{35}{s^2 + 12s + 35} \qquad (4\text{-}13)$$

These bounds in time domain and frequency domain are shown in Figure 4-7.
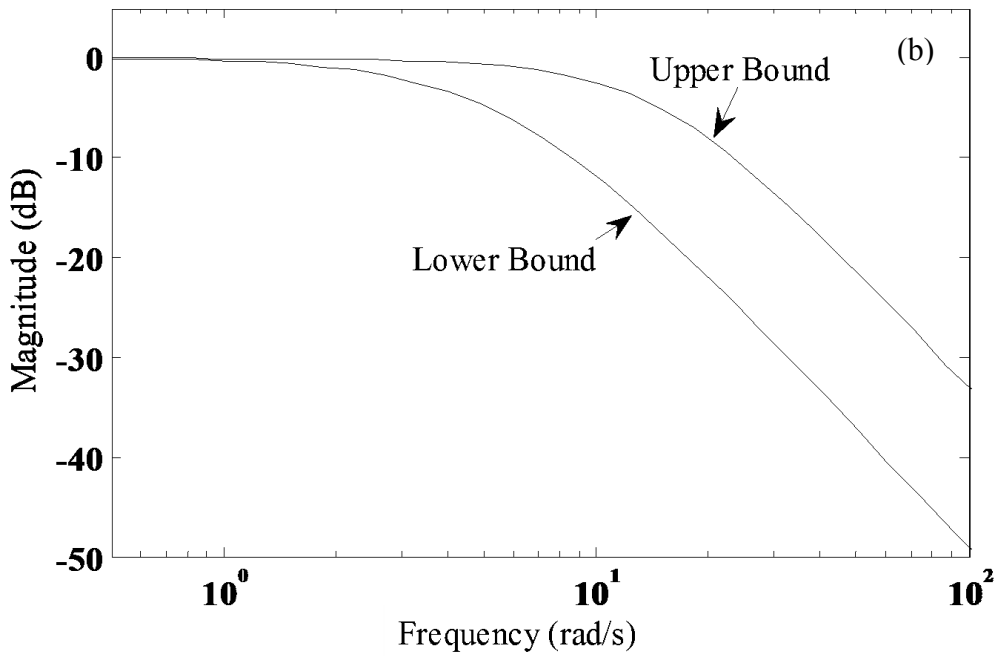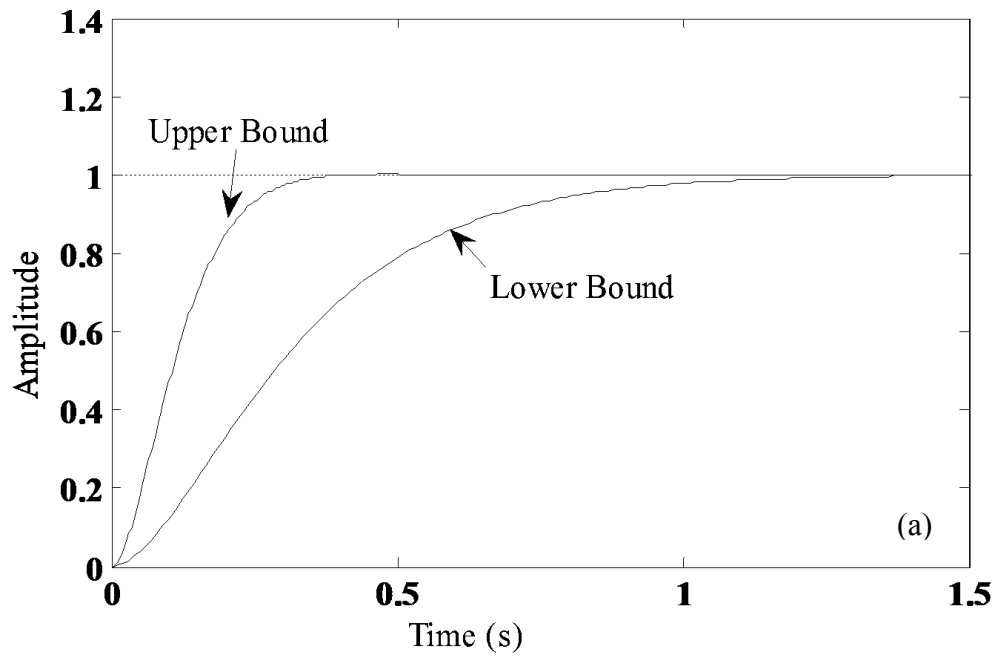
Figure 4-7: Tracking bounds; (a) time domain; (b) frequency domain

The tracking bounds are shown in the Nyquist plot in Figure 4-8.
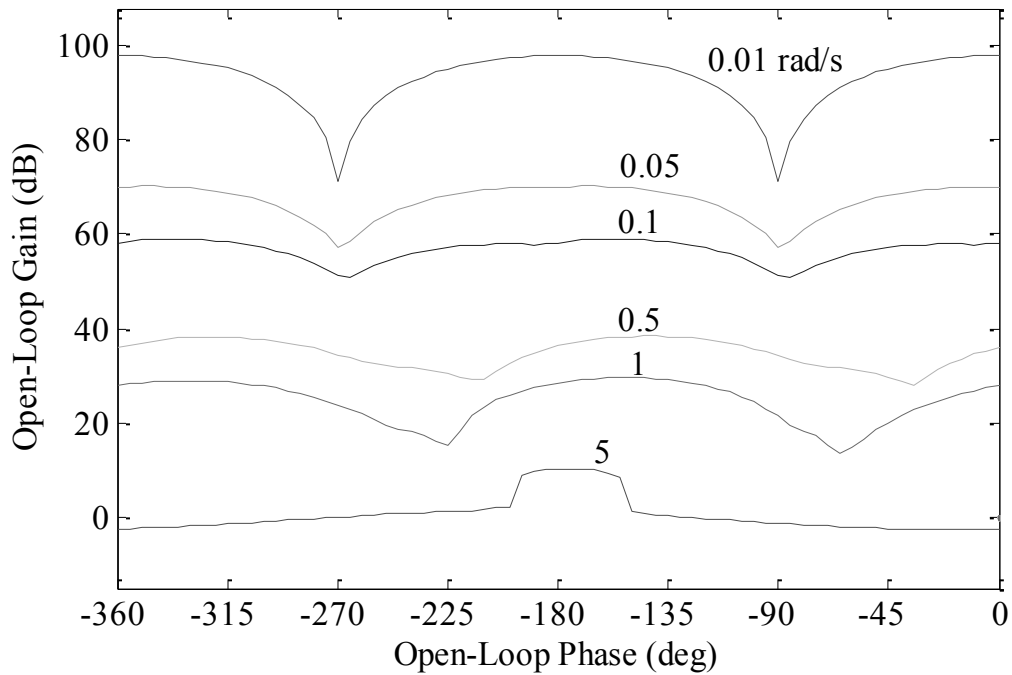
Figure 4-8: Tracking bounds

Stability criterion: The sensitivity value, W_s, for the stability criterion is set to 1.3 which translates to an allowable phase margin of 45.2 deg and a gain margin of 4.95 dB using Equations (4-3) and (4-4). The stability bounds are generated on a Nyquist plot and are shown in Figure 4-9.
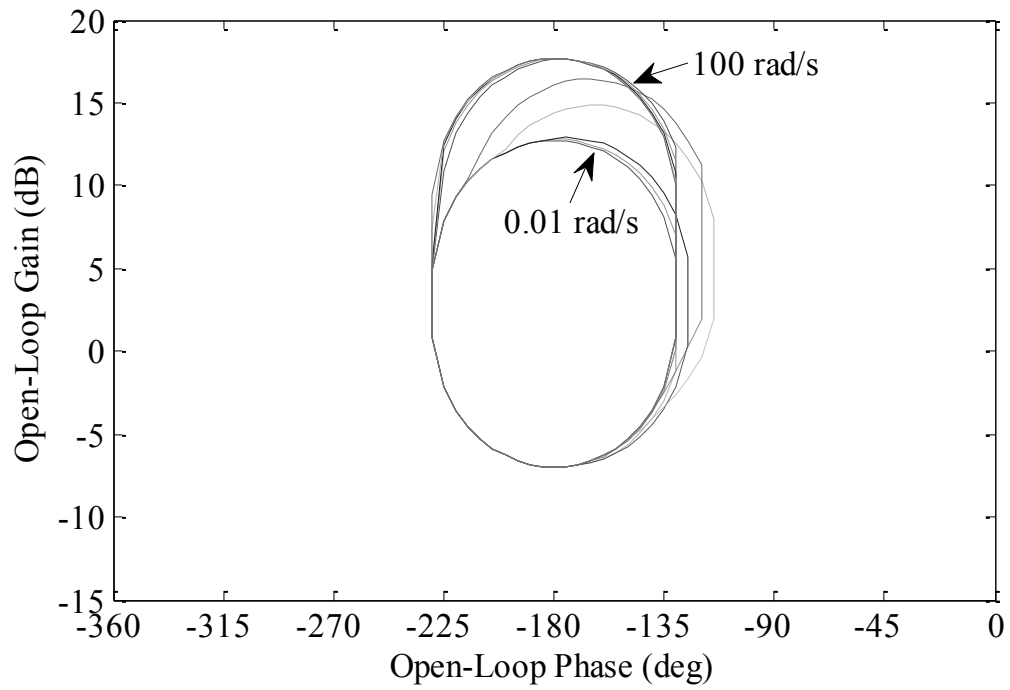
Figure 4-9: Stability bounds

Disturbance rejection in the plant output: A performance criteria was set to reject disturbance in the output signal by setting the sensitivity value (W_{dr}) to 1.1. The resulting bounds are displayed in Figure 4-10.
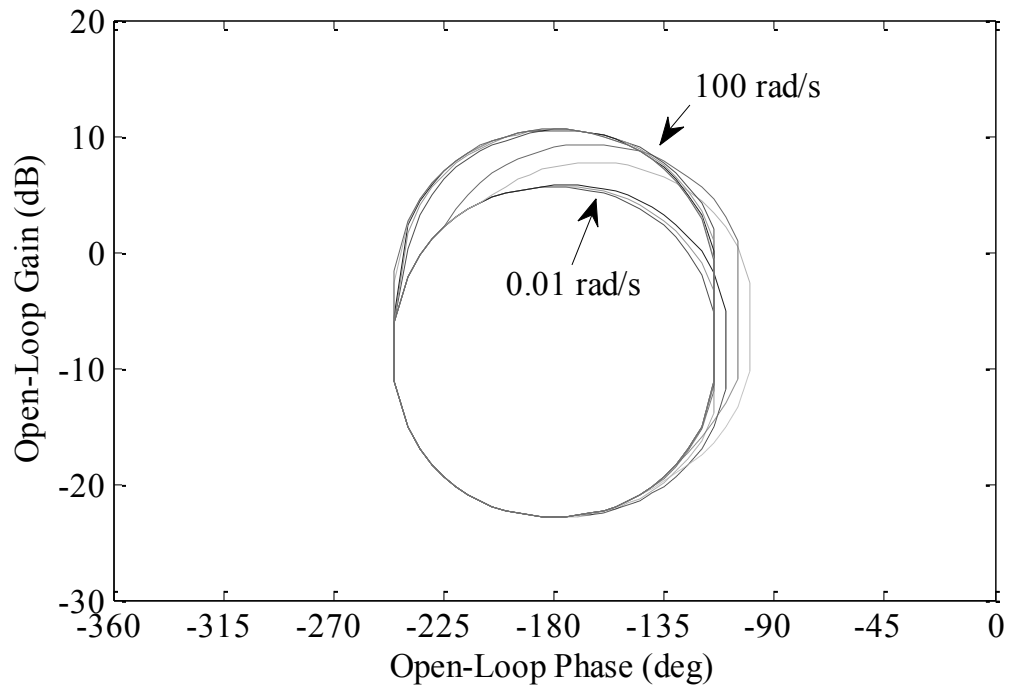
Figure 4-10: Disturbance rejection bounds

The stability bounds, tracking bounds and the disturbance bounds are combined into one Nyquist plot. At each frequency the bound that has the highest gain are kept while the bounds with lower gains are rejected. These bounds as shown in Figure 4-11 and will be used to design the controller. The intersection bounds with nominal loop function without the controller are shown in Figure 4-12.
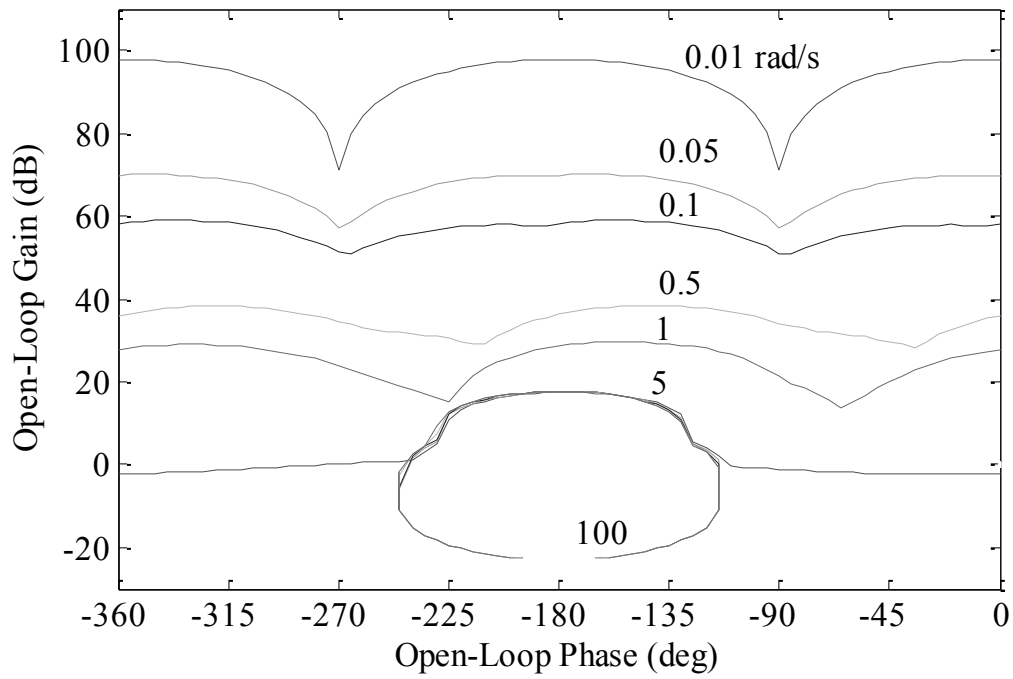
Figure 4-11: Intersection bounds
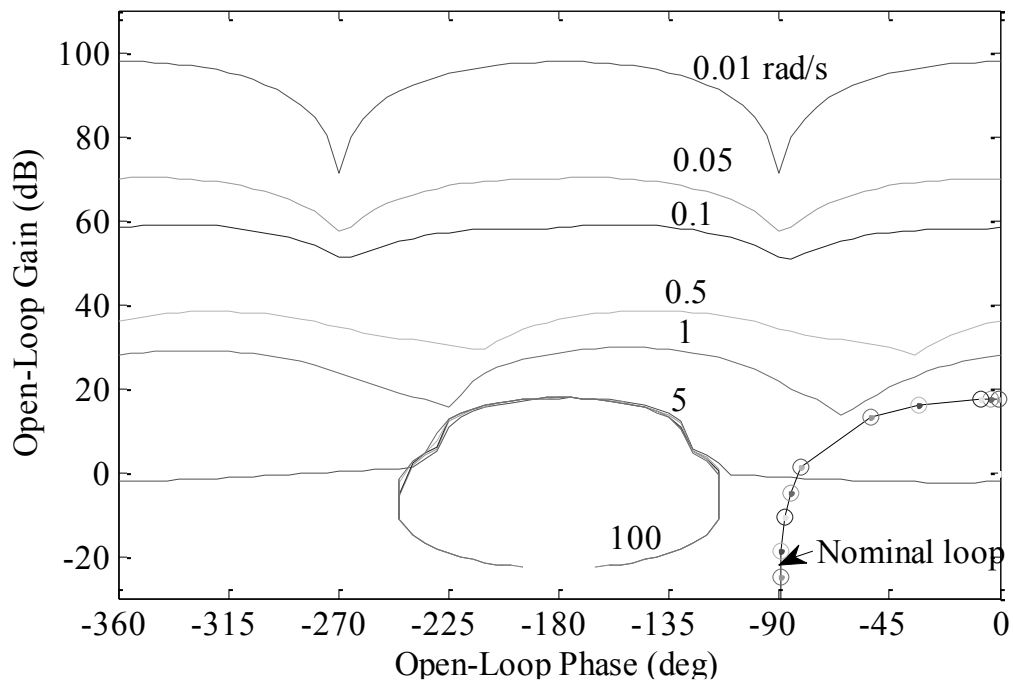
Figure 4-12: Nominal plant without controller

The nominal loop function shown in Figure 4-12 is the product of the nominal plant and the controller (to be designed) [24]. As seen the points at each frequencies represented by the circles on the nominal loop are below the allowable gain and does not meet the specifications. The shape of the nominal loop function is changed by changing the gain of the controller and placing poles and zeros so that it meets the lowest possible gain required at each frequencies. Placing a real pole pushes the loop function to the left whereas adding a real zero pushes the loop function to the right. Increasing the gain of the controller increases the gain of the loop function thereby moving the loop up on the Nyquist plot. The controller designed to satisfy the performance criterion is shown in Equation (4-14) and the tuned loop function is Figure 4-13.

$$G(s) = \frac{6.5\left(\frac{s}{4}+1\right)}{s} \tag{4-14}$$
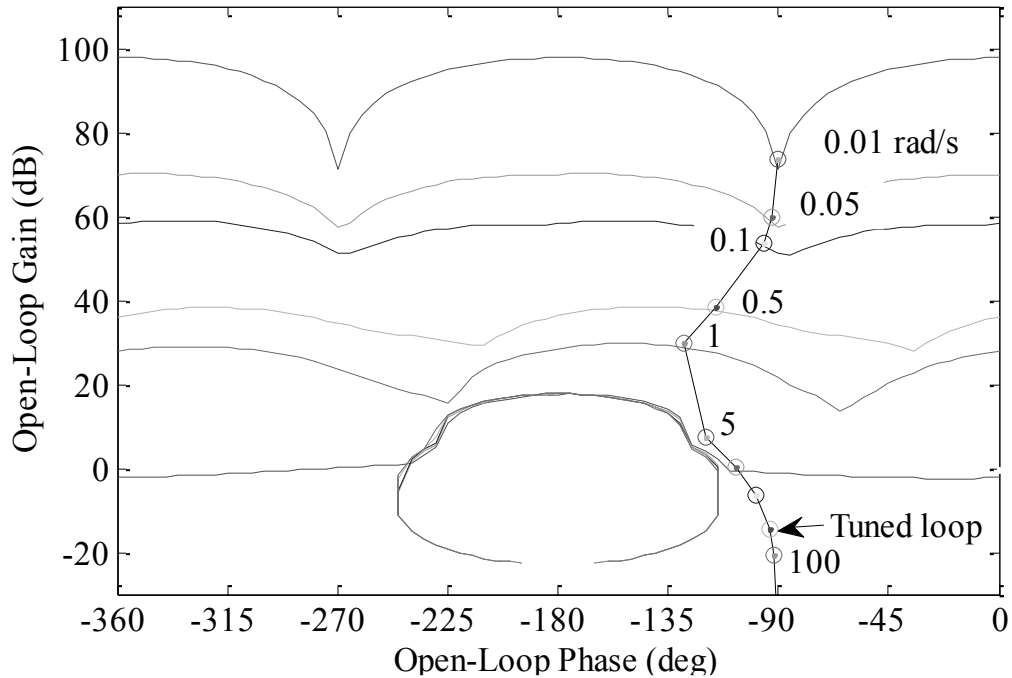
Figure 4-13: Tuned nominal plant (Controller I)

It can be seen that the nominal loop gain at each frequency is above the corresponding bound and is outside the stability bound; hence meeting all performance criteria. However, a prefilter has to be designed to meet the tracking criterion. Similar to the controller design, the prefilter is designed by placing poles and zeros to bring the response within the lower and upper bound of tracking criterion. Figure 4-14 shows the closed loop response of the plant with controller in frequency domain. It can be seen that the frequency response of the plant is above the upper bound limit.
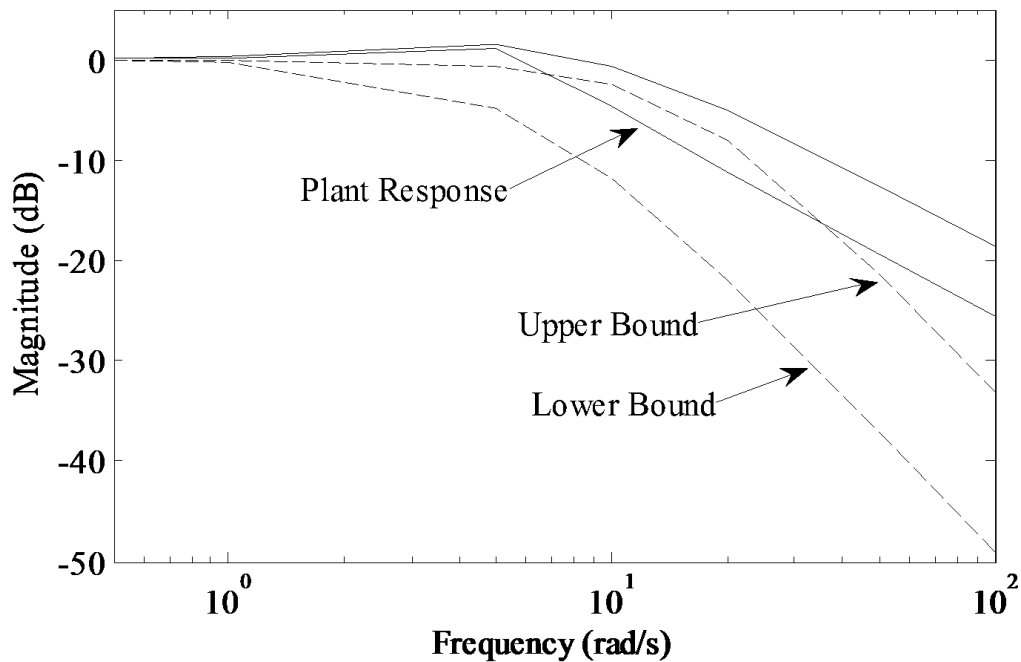
Figure 4-14: Plant response without prefilter

Hence, Prefilter is needed to push the response below the upper bound limits. The prefilter designed to satisfy the tracking criterion is shown below and the plant response with prefilter is shown in Figure 4-15.

$$F(s) = \frac{\left(\frac{s}{22} + 1\right)}{\left(\frac{s}{3.3} + 1\right)} \tag{4-15}$$
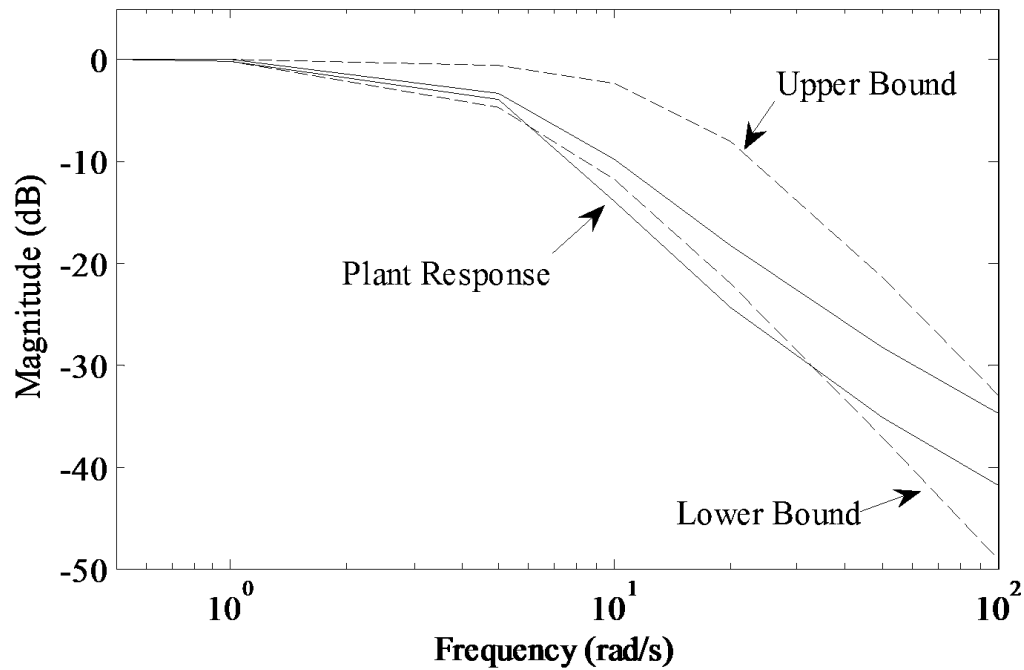
Figure 4-15: Plant response with prefilter

4.2.3 Simulation Results

The controller and prefilter designed were implemented in the helicopter simulation developed in Simulink. The helicopter was given a command to go to an altitude of 100 ft at 10 s with a payload of 10 lb. The payload was then dropped after the simulation reached 50 s. Figure 4-16 shows the altitude response of the helicopter. It is seen that the helicopter starts with a negative altitude and settles back to zero altitude as seen at time eight second. This is due to the fact we start with zero collective pitch as no trim collective pitch was added and hence no thrust. Thus, the collective pitch increases to the point where the thrust generated is enough to balance the weight of the helicopter.
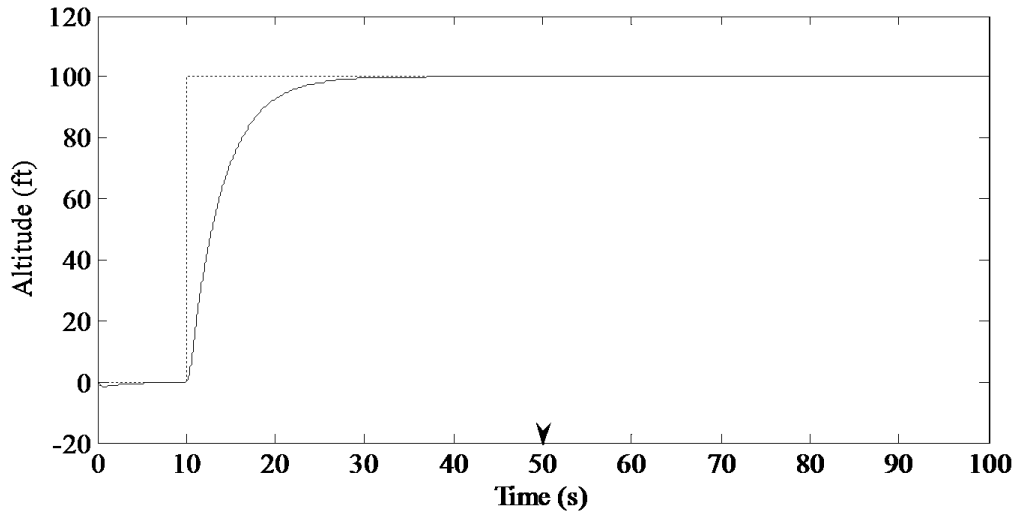
Figure 4-16: Altitude response with 10 lb payload (Controller I); payload dropped at 50 s, dotted line represents desired and solid line represents actual altitude

Figure 4-17 shows the zoom in view of the change in altitude after the payload drop (2 lb, 5 lb and 10 lb). For a 10 lb payload, the altitude changes by 0.43 ft and for 2 lb payload drop, the altitude only changes by 0.09 ft. Hence, the greater the payload attached to the helicopter, greater change is observed in the altitude after the payload drop. The time taken to recover within 2 % of the change in altitude observed after the 10 lb payload drop is 15.20 s.
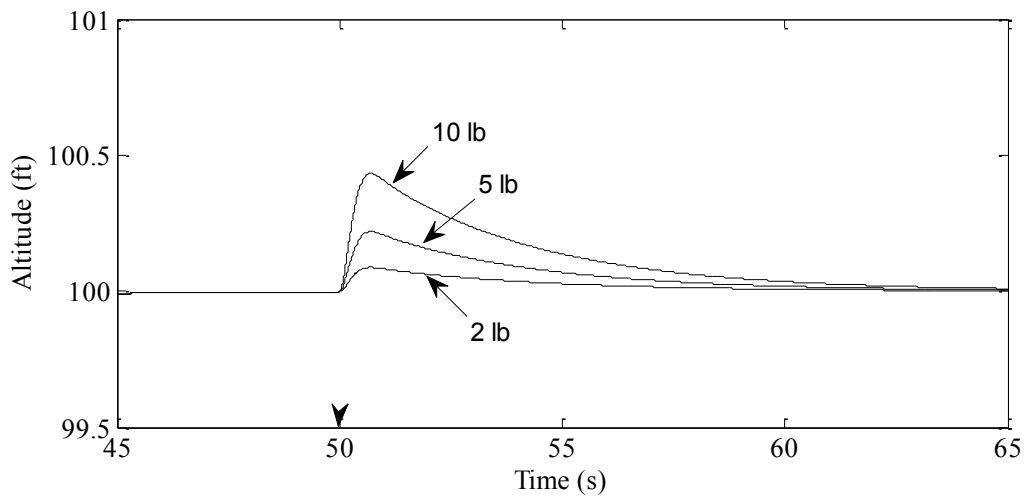
Figure 4-17: Altitude change after payload drop (Controller I); payloads (10 lb, 5 lb, 2 lb)

Figure 4-18 shows the velocity response of the helicopter with 10 lb payload. As the helicopter takes off and flies to 100 ft, the vertical velocity increases and settles back to 0 ft/s as soon as it reaches 100 ft.
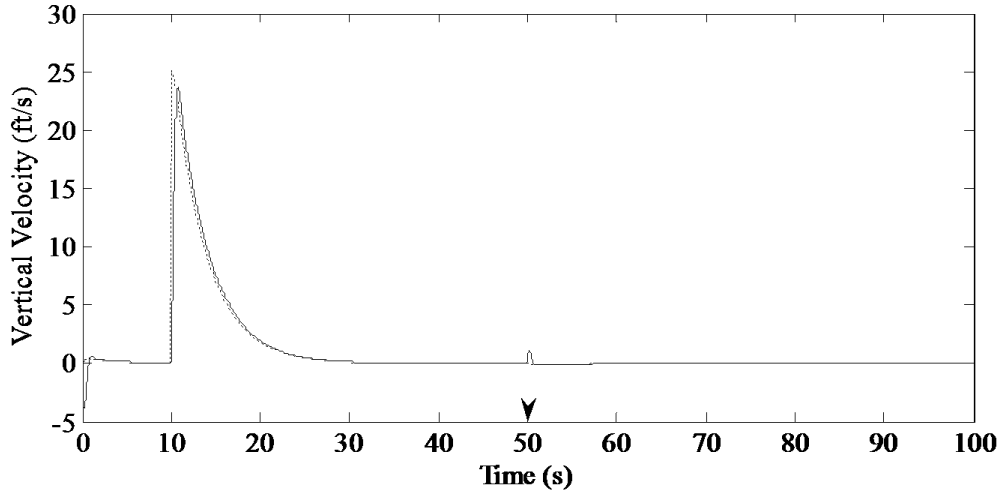
Figure 4-18: Vertical velocity response with 10 lb payload (Controller I); payload dropped at 50 s, dotted line represents desired and solid line represents actual velocity

After dropping the payload, the velocity again increases to push the helicopter back to 100 ft as shown in Figure 4-19. Similar to the change in altitude after dropping the payload, the vertical velocity also changes. For a 10 lb payload, the velocity increased to 1.15 ft/s whereas for a payload of 2 lb payload the velocity only changed to 0.24 ft/s.
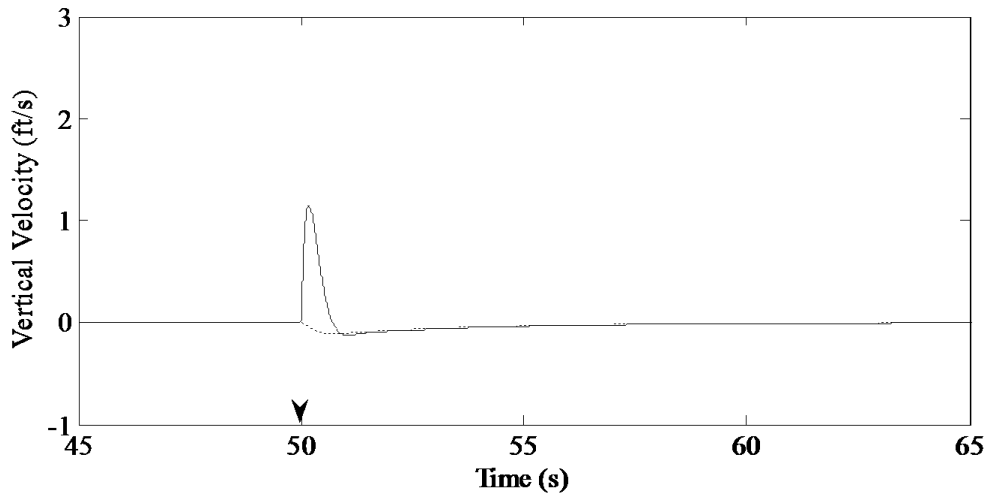
Figure 4-19: Vertical velocity change after 10 lb payload drop (Controller I); change in velocity of - 1.15 ft/s with 10 lb payload dropped at 50 s

Figure 4-20 displays the collective pitch command for a helicopter flying with a payload of 10 lb. To fly the helicopter to 100 ft the collective pitch increases and settles to 12 deg as soon at 100 ft.
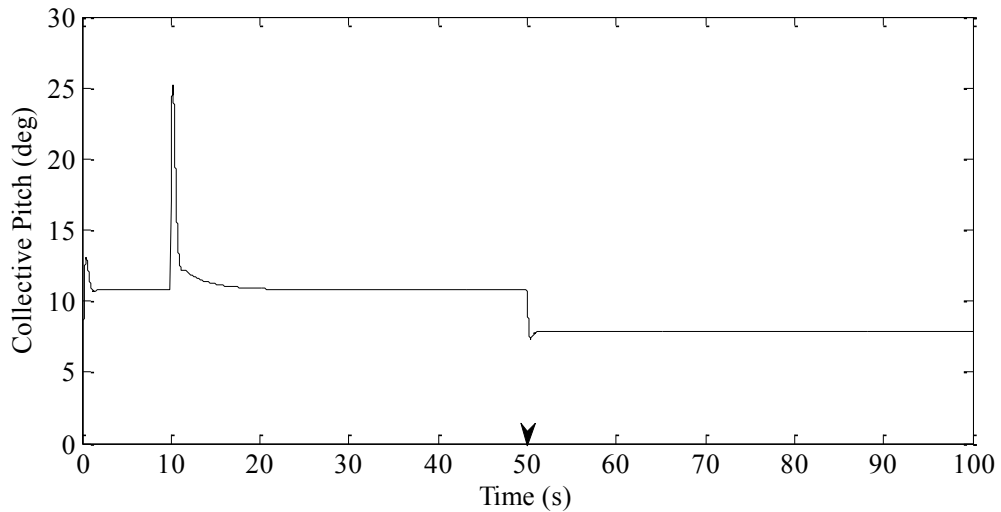
Figure 4-20: Collective pitch with 10 lb payload (Controller I)

After the 10 lb payload is dropped, the collective pitch command reduces to 7.85 deg as shown in Figure 4-21.
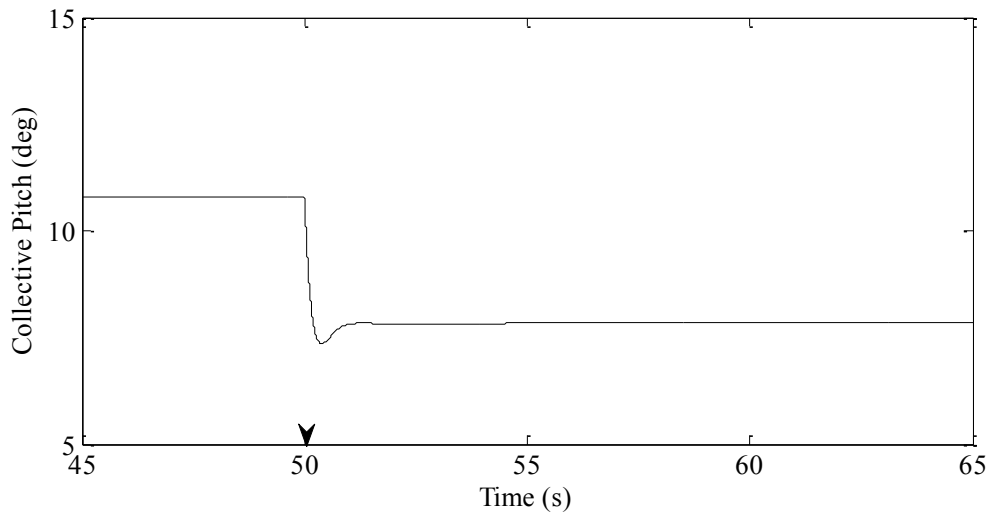
Figure 4-21: Collective pitch change after 10 lb payload drop (Controller I)

The main rotor thrust increases in take-off while decreases after dropping the payload but remains constant in hover mode as shown in Figure 4-22. The amount of thrust generated with a payload of 10 lb and helicopter weight of 19.5 lb is 29.5 lb while hovering at 100 ft. Similarly, after the 10 lb payload drop, the simulation accurately generates the thrust equal to the weight of the helicopter.
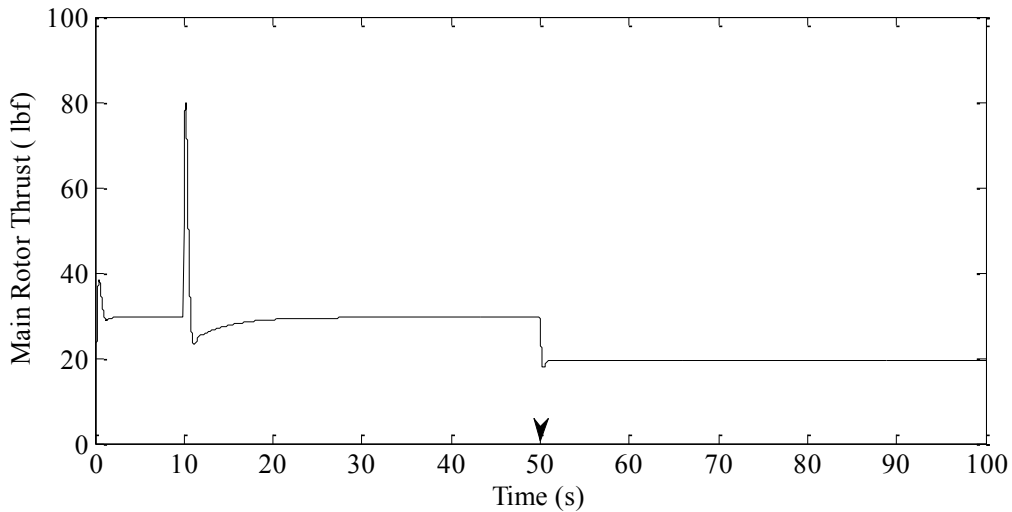
Figure 4-22: Main rotor thrust with 10 lb payload (Controller I)

The rotation of the helicopter rotors creates a moment as shown in Figure 4-23. As seen the moment increases as the helicopter flies to 100 ft and reduces while hovering.
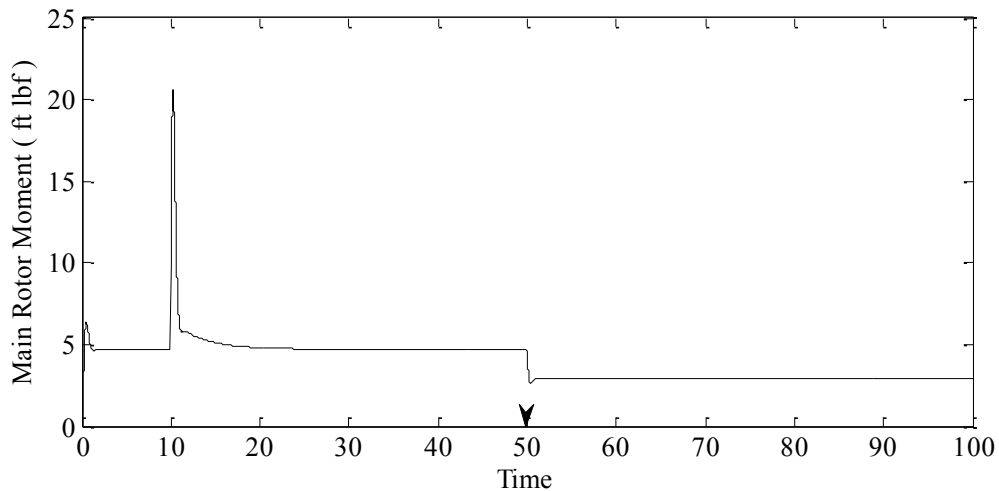
Figure 4-23: Main rotor moment with 10 lb payload (Controller I)

To counter this moment, the tail rotor thrust has to be adjusted as seen in Figure 4-24.
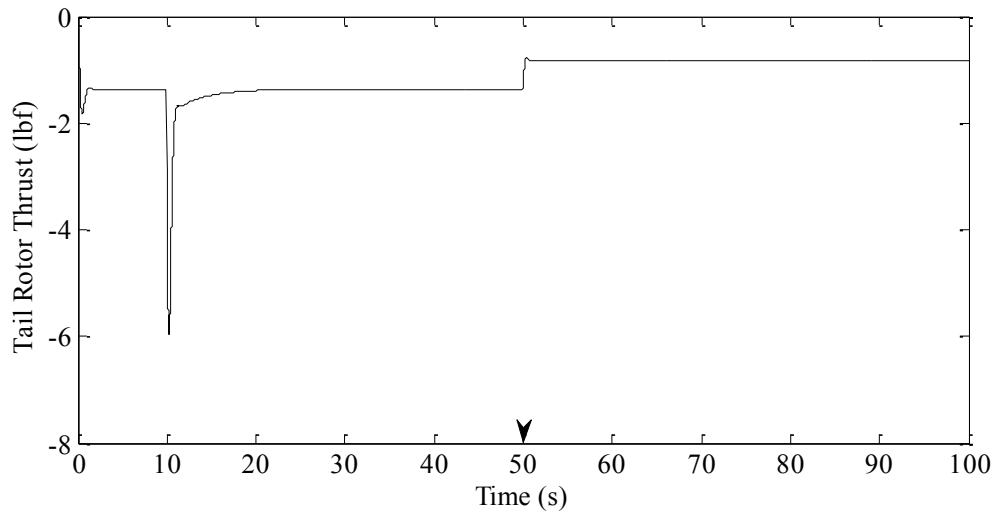
Figure 4-24: Tail rotor thrust with 10 lb payload (Controller I)

The Xcell 60 helicopter has a hardware limitation that limits the maximum collective pitch attainable to 20 deg. Blade stall may also occur before the hardware limit is achieved but this can be updated by testing it on the real helicopter and lowering it in the simulation. As the collective pitch command does not reach 20 degree at the payload drop, the results should not be affected. From Figure 4-20, it is seen that the helicopter while flying to 100 ft reaches a collective pitch of 25 deg that exceeds the limit. Hence, the saturation limit was added to the collective pitch command by adding a maximum limit of 20 deg to simulate the helicopter model similar to the real system as shown in Figure 4-25.
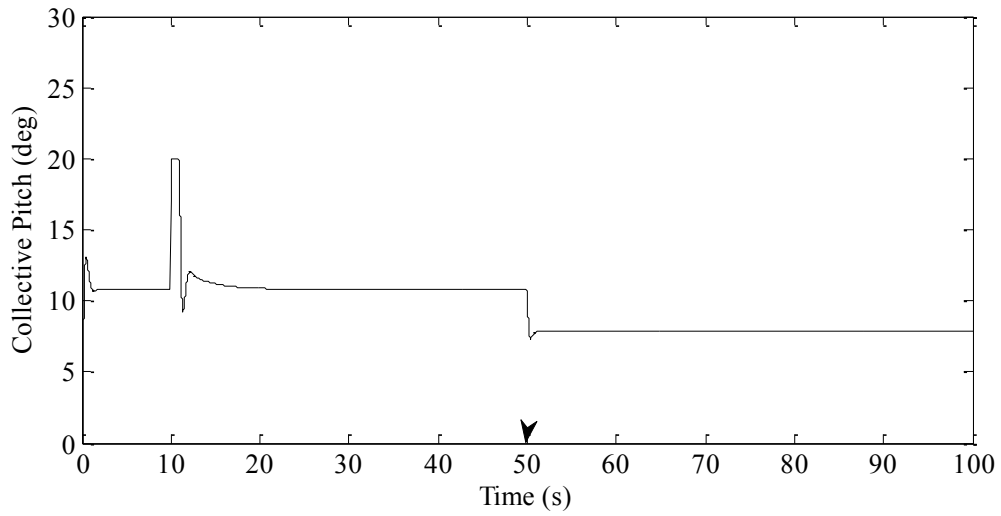
Figure 4-25: Collective pitch with saturation limit and 10 lb payload (Controller I)

After the 10 lb payload is dropped the collective pitch command changes to 7.85 deg as seen in Figure 4-26 same as that observed without the saturation limit seen in Figure 4-21.
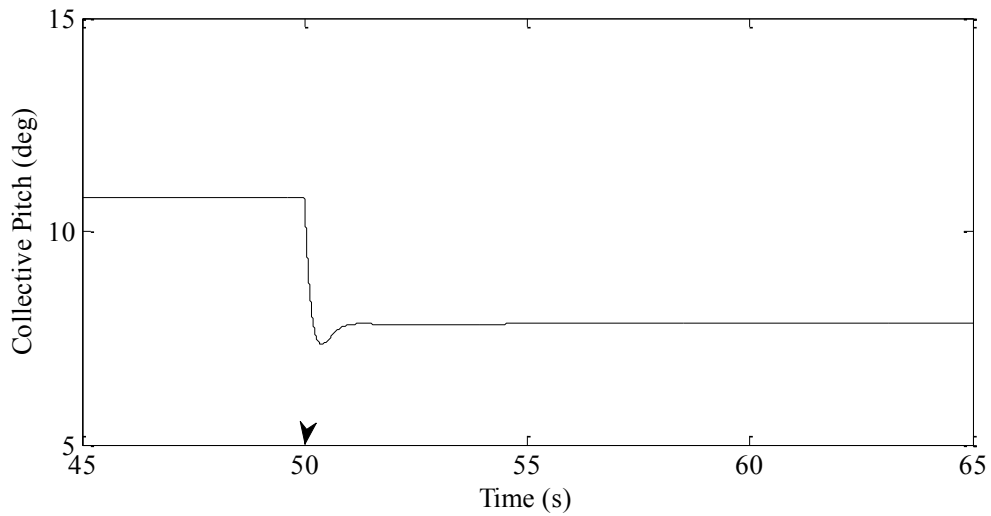
Figure 4-26: Collective pitch change after 10 lb payload drop with saturation limit (Controller I)

The altitude response did not change much due to the addition of the saturation limit as seen in Figure 4-27.
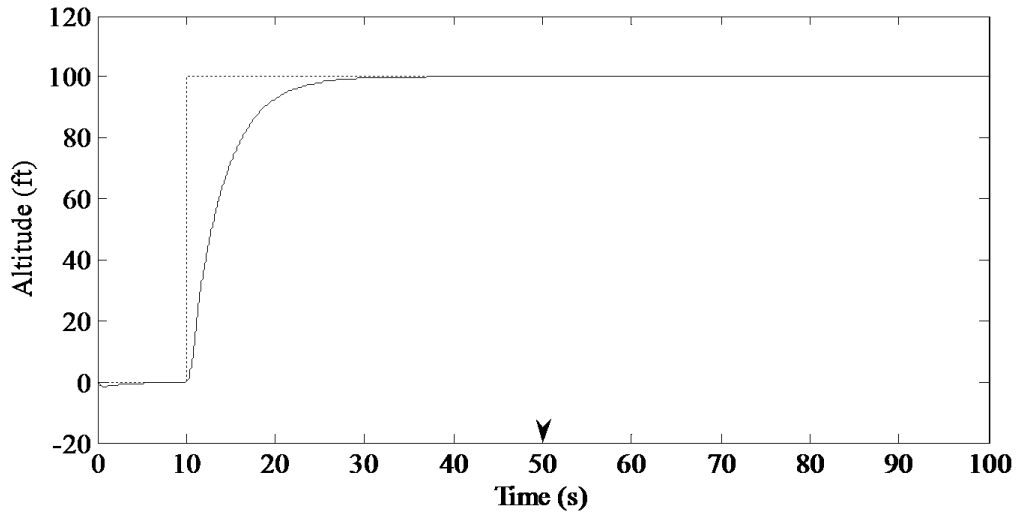
Figure 4-27: Altitude response with saturation limit and 10 lb payload (Controller I)

The velocity response after the 10 lb payload drop changes as seen in Figure 4-28. The velocity achieved at takeoff increases from 24 ft/s seen in Figure 4-18 to 28 ft/s.
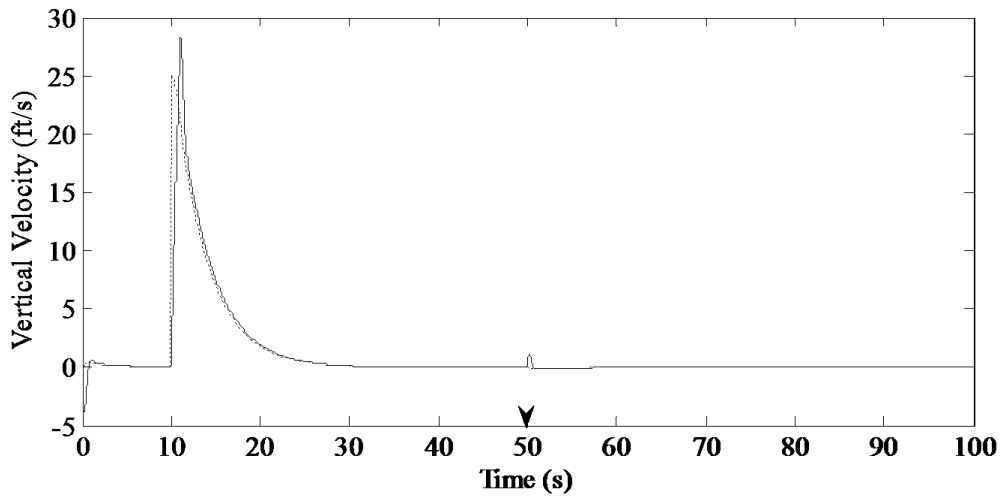
Figure 4-28: Vertical velocity response with saturation limit and 10 lb payload (Controller I)

The change in vertical velocity after the payload drop is seen in Figure 4-29. It is seen that the change in velocity after the payload drop is same as that observed without saturation limit seen in Figure 4-19 since the collective pitch does not reach the saturation limit.
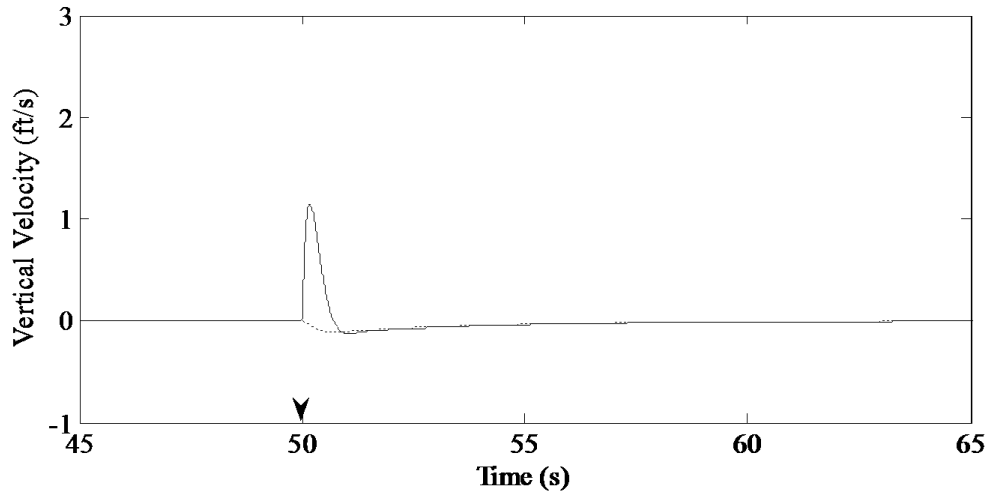
Figure 4-29: Vertical velocity change after 10 lb payload drop with saturation limit (Controller I)

The results of the Controller I with saturation limit and 10 lb payload are summarized in Table 4-1.

Table 4-1: Controller I results with saturation limit (10 lb payload)

Performance index	Value
Time taken after takeoff to reach 100 ft	34.44 s
Maximum change in altitude after payload drop	0.43 ft
Maximum change in velocity after payload drop	1.15 ft/s
Time to recover within 2% of change in altitude after payload drop	15.20 s

4.2.4 Comparison with PID Controller

The Proportional-Integral-Derivative controller (PID) is the most common type of controller currently used in the industry. It is therefore, important to compare the results of the QFT controller with the PID controller. The structure of the controller is shown below where the gains of the controller (K_P, K_I, K_D) are tuned until the desired performance is obtained.

$$G(s) = K_P e(t) + K_I \int e(t)dt + K_D \frac{d}{dt} e(t) \qquad (4\text{-}16)$$

Similar to the QFT controller, the PID controller was implemented in the simulation with the same flight plan, first flying to 100 ft and then dropping a payload at 50 s. The gains for the PID controller were determined using Ziegler Nichols Method are shown in Equation (4-17).

$$K_P = 0.035 \left(\frac{rad}{\frac{ft}{s}}\right)$$

$$K_I = 0.0087 \left(\frac{rad}{ft}\right) \qquad (4\text{-}17)$$
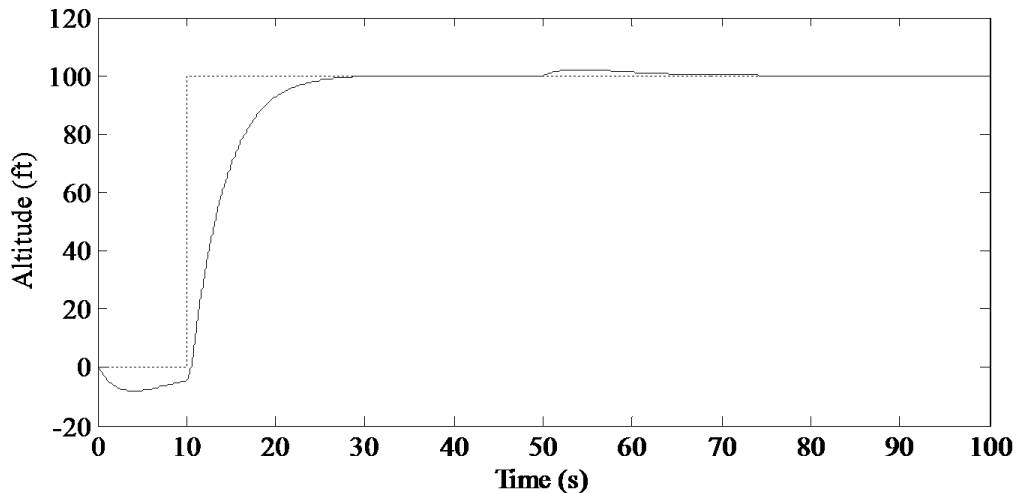
Figure 4-30: Altitude response with 10 lb payload (PID Controller I)

As seen that the controller performance is poor, actual altitude is not able to follow the desire altitude accurately. The change in altitude after the payload drop is clearly visible. The altitude changed by 2.19 ft after the 10 lb payload drop. The changes in altitude for payloads, 2 lb, 5 lb and 10 lb are shown in Figure 4-31. As the payload increased the change in altitude also increased. While the time taken to recover within 2 % change in altitude after the drop also increased significantly.
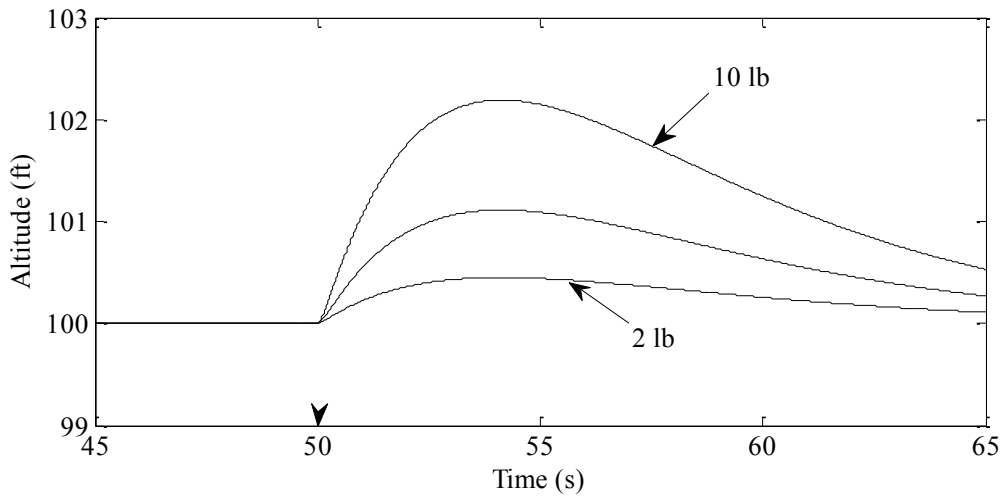
Figure 4-31: Altitude change after payload drop (PID Controller I); payloads (10 lb, 5 lb, 2 lb)

The results for the PID controller tuned with Ziegler Nichols (PID Controller I) and 10 lb payload are summarized in Table 4-2.

Table 4-2: PID Controller I results with 10 lb payload

Performance index	Value
Time taken after takeoff to reach 100 ft	26.25 s
Maximum change in altitude after payload drop	2.19 ft
Maximum change in velocity after payload drop	1.26 ft/s
Time to recover within 2% of change in altitude after payload drop	26.90 s

The controller obtained from the Ziegler Nichols method has often proven to be ineffective such as in our case where the performance is poor. However, the gains obtained from the method act as the starting point for tuning a controller to obtain the

desired performance. New gains for the PID controller were obtained by tuning the controller to match the performance obtained from the QFT controller with 2 lb payload. The gains obtained are shown in Equation (4-18).

$$K_P = 0.028 \left(\frac{rad}{\frac{ft}{s}} \right)$$

$$K_I = 0.098 \left(\frac{rad}{ft} \right)$$

(4-18)

The altitude response with the new gains and with 10 lb payload is shown in Figure 4-32.
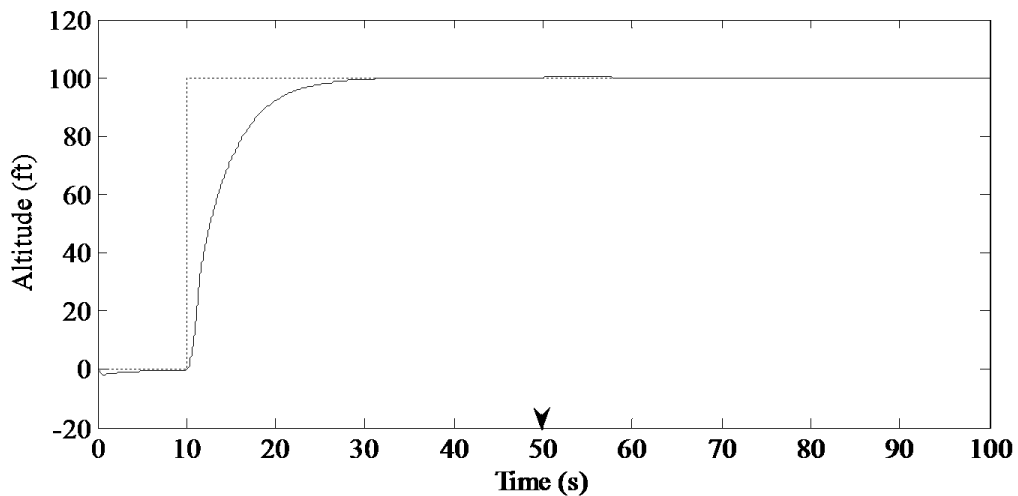
Figure 4-32: Altitude response with 10 lb payload (PID Controller II)

As seen the controller performance improved significantly. The altitude change observed for 2 lb payload drop was 0.09 ft similar to that of the QFT controller. While the change observed for 10 lb payload drop was 0.46 ft as compared to 0.43 ft observed with the QFT controller. The changes in altitude for payloads, 2 lb, 5 lb and 10 lb are shown in Figure 4-33. The time taken to recover within 2 % change in altitude after 10 lb payload drop with the new PID controller was 16.43 s much more than that observed with QFT controller.
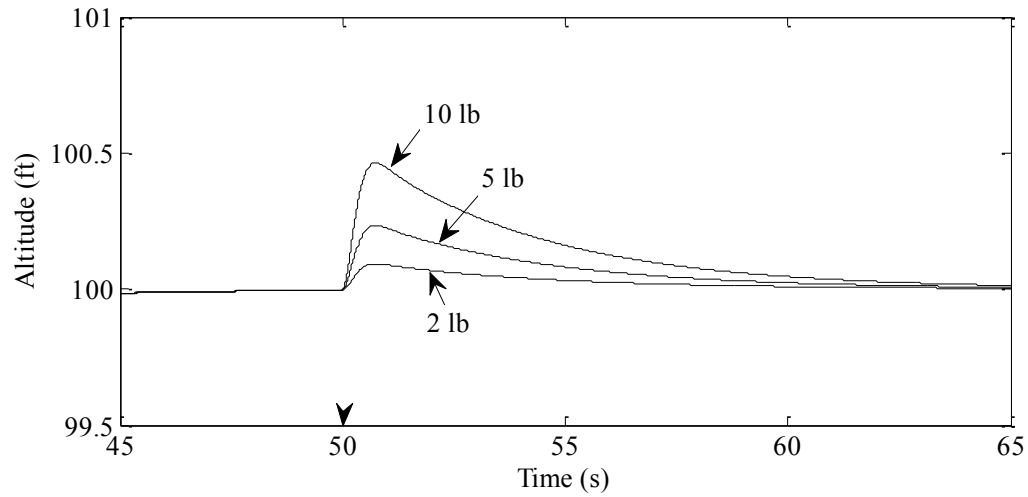
Figure 4-33: Altitude change after payload drop (PID Controller II); payloads (10 lb, 5 lb, 2 lb)

The results for the PID controller II with 10 lb payload are summarized in Table 4-3.

Table 4-3: PID Controller II results with 10 lb payload

Performance index	Value
Time taken after takeoff to reach 100 ft	36.43 s
Maximum change in altitude after payload drop	0.46 ft
Maximum change in velocity after payload drop	1.18 ft/s
Time to recover within 2% of change in altitude after payload drop	16.43 s

Alternately, the gains for the PID controller can also be obtained by matching the performance of that observed with the 10 lb payload with QFT controller.

The gains obtained are shown in Equation (4-19).

$$K_P = 0.035 \left(\frac{rad}{\frac{ft}{s}} \right)$$

$$K_I = 0.098 \left(\frac{rad}{ft} \right)$$

(4-19)

The altitude response of the helicopter is shown in Figure 4-34. As seen, the attitude response with the PID controller is similar to that observed with controller I seen in Figure 4-16. However, the time taken to reach 100 ft after take-off increased from 25 s seen with controller I to 35 s
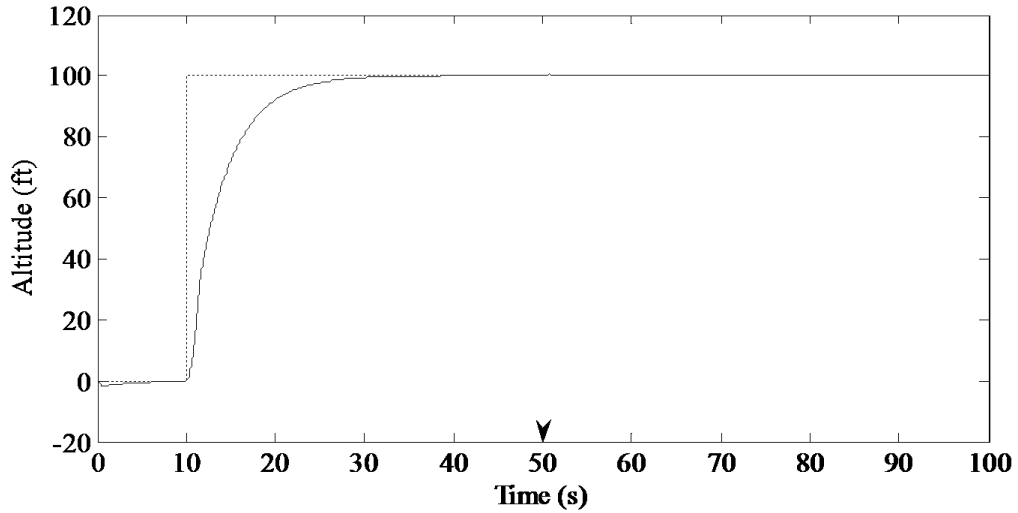
Figure 4-34: Altitude response with 10 lb payload (PID Controller III)

For a payload of 10 lb, the change in altitude observed was same as that observed with controller I as seen in Figure 4-35. However, the time taken to recover within 2 % of the change in altitude observed after 10 lb payload drop was 16.70 s much more than that observed with QFT controller.
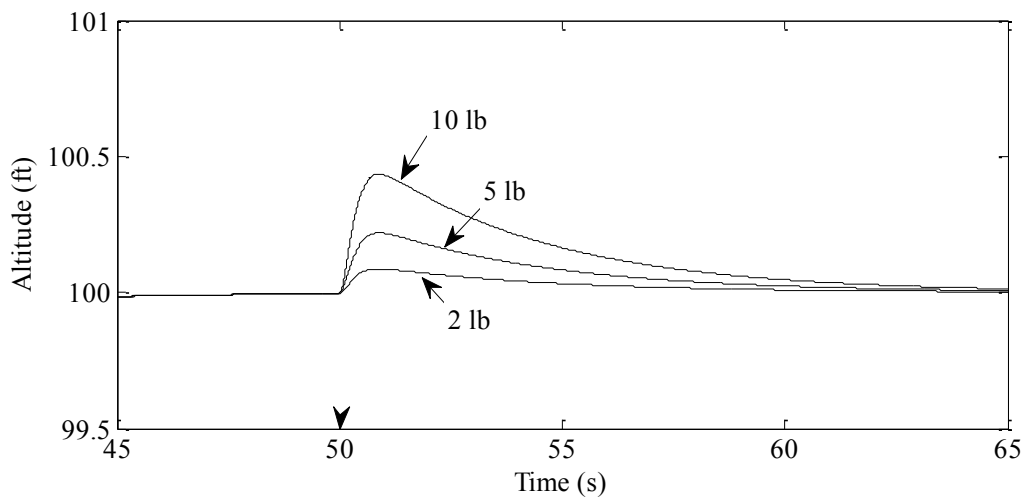
Figure 4-35: Altitude change after payload drop (PID Controller III); payloads (10 lb, 5 lb, 2 lb)

The results of the PID controller with saturation limit and 10 lb payload are summarized in the Table 4-4.

Table 4-4: PID Controller III results with 10 lb payload

Performance index	Value
Time taken after takeoff to reach 100 ft	36.62 s
Maximum change in altitude after payload drop	0.43 ft
Maximum change in velocity after payload drop	1.03 ft/s
Time to recover within 2% of change in altitude after payload drop	16.70 s

4.2.5 Effect of Actuator Dynamics

The collective pitch of the helicopter is changed by the swash plate mechanism. In the helicopter model studied, this mechanism moves up or down by employing motors to create the appropriate collective pitch. Thus, it is important to understand how the performance of the controller is affected by including the actuator dynamics to the simulation. The actuator dynamics is a first-order transfer function as shown in Equation (4-20).

$$\frac{k_m}{\tau_m s + 1} \tag{4-20}$$

The value for k_m is one while the value for τ_m was varied to simulate different motors where lower values would represent a motor with fast response time. Actuator dynamics were then added in the simulation.

The altitude response of the helicopter with τ_m as 0.125 s and saturation limit controller (4-14) and prefilter (4-15) applied as shown in Figure 4-36. The altitude response seems similar to the one without the actuator dynamics.
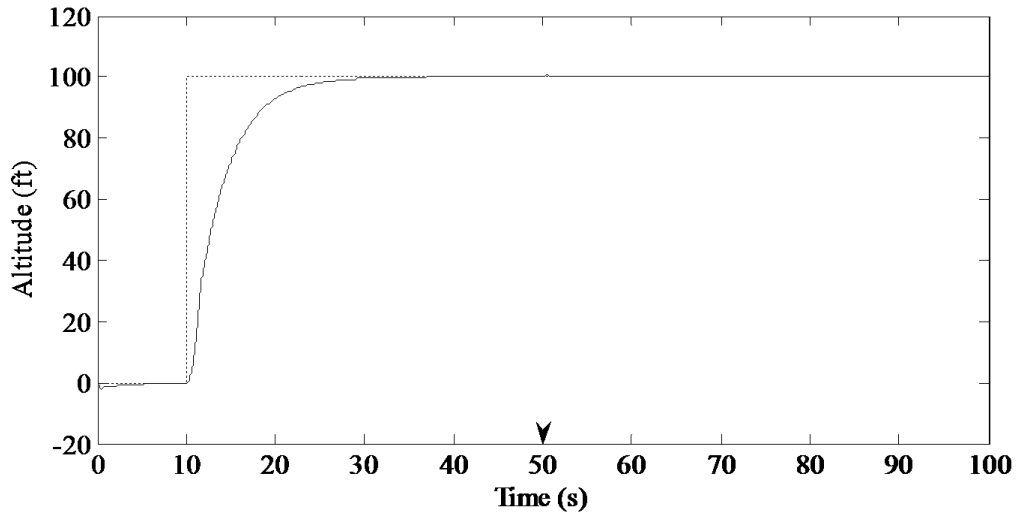
Figure 4-36: Altitude response with actuator dynamics and 10 lb payload (Controller I); motor time constant 0.125 s

The vertical velocity response is shown in Figure 4-37. The velocity achieved after take-off is 32 ft/s compared to 28 ft/s observed with Controller I seen in Figure 4-28.
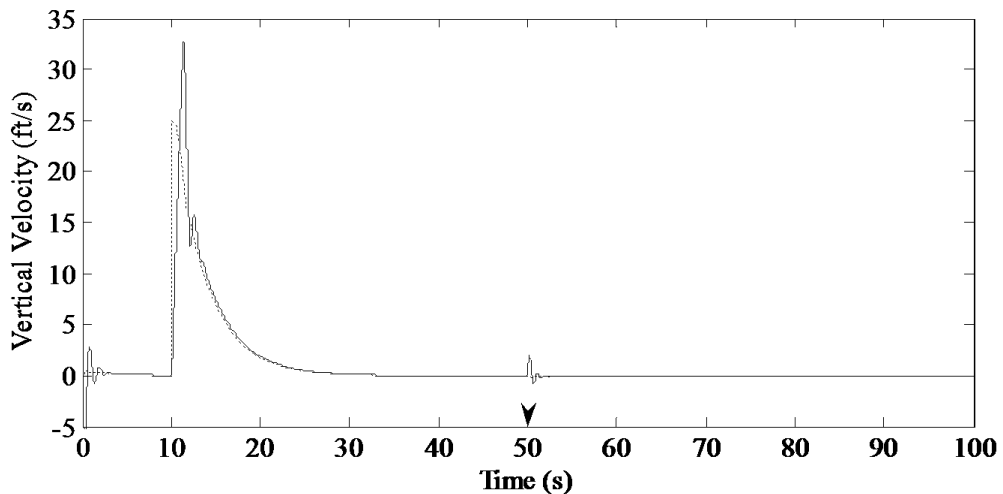
Figure 4-37: Vertical velocity response with actuator dynamics and 10 lb payload (Controller I); motor time constant 0.125 s

After the 10 lb payload drop, the change in velocity increases to 2.00 ft/s with some oscillation as seen in Figure 4-38 compared to 1.15 ft/s seen with Controller I seen in Figure 4-29.
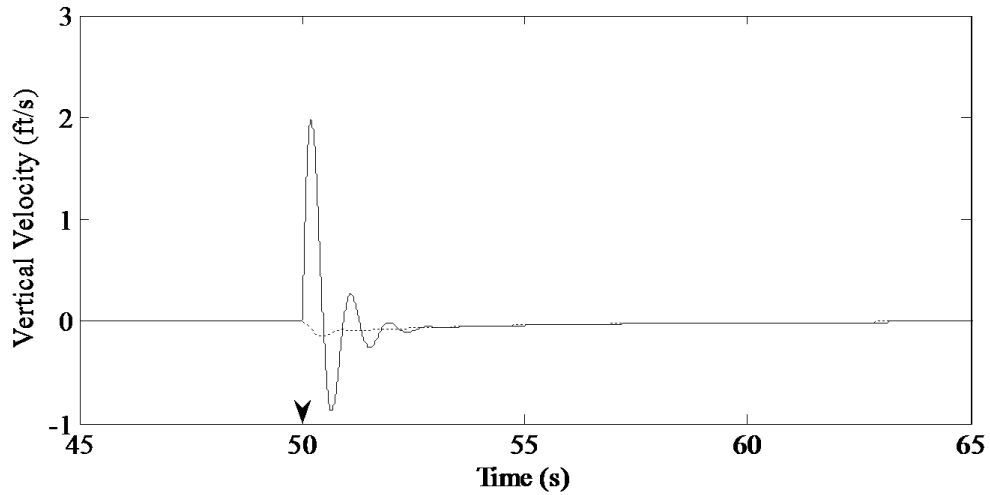
Figure 4-38: Vertical velocity change after 10 lb payload drop with actuator dynamics (Controller I); motor time constant 0.125 s

These oscillations seen the velocity are as result of the controller being very aggressive in changing the collective pitch command as shown in Figure 4-39.
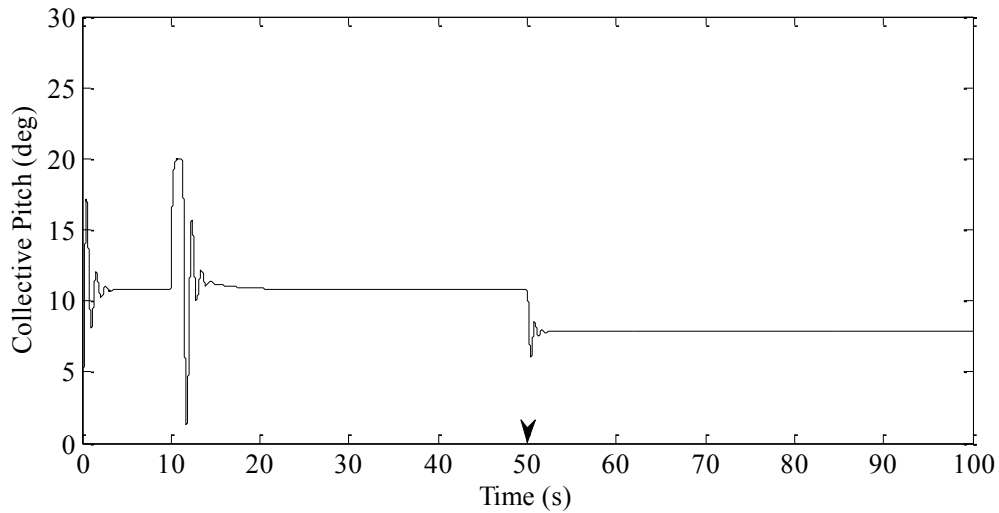
Figure 4-39: Collective pitch with actuator dynamics and 10 lb payload (Controller I); motor time constant 0.125 s

After the 10 lb payload is dropped, the collective pitch commands shows oscillations as seen in Figure 4-40 but settles to 7.8 deg as seen before in Figure 4-26.
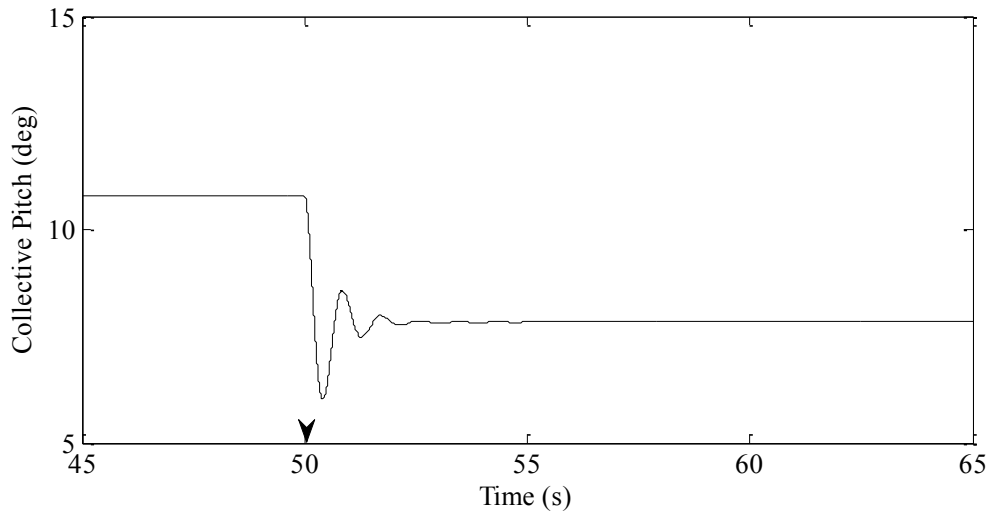
Figure 4-40: Collective pitch change after 10 lb payload drop with actuator dynamics (Controller I); motor time constant 0.125 s

Figure 4-41 shows the effect of payloads (2 lb, 5 lb and 10 lb) with constant motor time constant, τ_m, of 0.125 s. As seen with the increase in payloads, the change in altitude after the payload drop increases with increased oscillations.
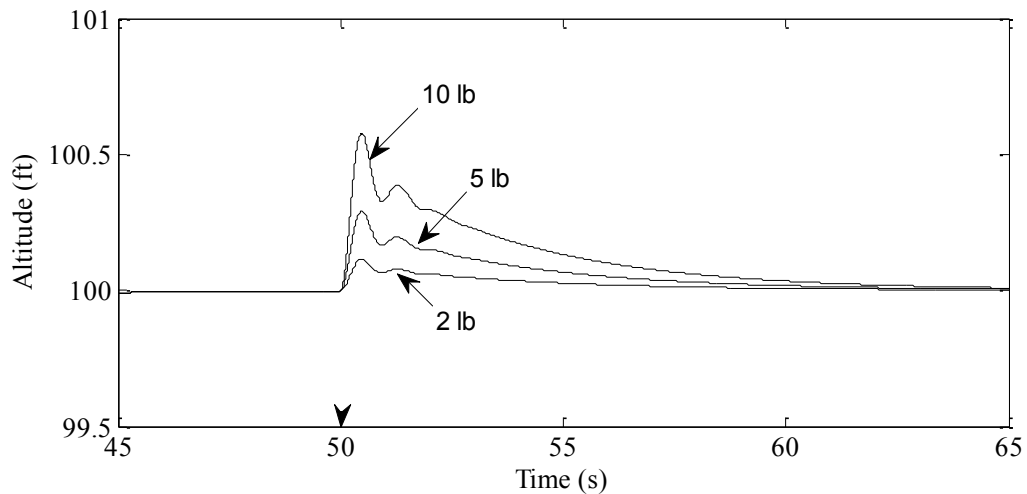
Figure 4-41: Altitude change after payload drop with 0.125 s motor time constant (Controller I); payloads (10 lb, 5 lb, 2 lb)

Some oscillations appear in the altitude while the change in altitude after 10 lb payload drop increases to 0.58 ft as seen in Figure 4-42 as compared to 0.43 ft seen with controller I seen in Figure 4-17. The time to recover within 2% of the change in altitude with 10 lb payload decreases to 14.07 s as shown in Figure 4-42.
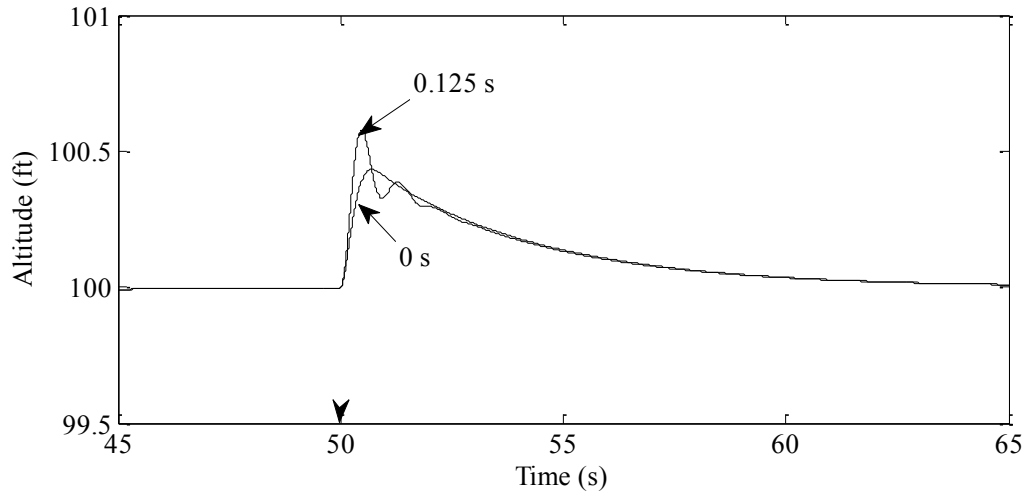
Figure 4-42: Altitude change after 10 lb payload drop (Controller I); motor time constants (0.125 s and 0 s)

The results of the Controller I with motor time constant of 0.125 s and 10 lb payload are summarized in Table 4-5.

Table 4-5: Controller I with 10 lb payload; motor time constant 0.125 s

Performance index	Value
Time taken after takeoff to reach 100 ft	34.44 s
Maximum change in altitude after payload drop	0.58 ft
Maximum change in velocity after payload drop	2.00 ft/s
Time to recover within 2% of change in altitude after payload drop	14.07 s

However, as the value for τ_m is increased further the oscillations increased. The max value for τ_m that can be used in the simulation is 0.145 s.

4.3 Controller Design to cope with Actuator Dynamics (Controller II)

One solution for designing a controller that works with the actuator dynamics without including it in the design process is to modify the tracking criterion of the QFT controller design process. As the controller originally designed was very aggressive, the new tracking criterion have to be relaxed to account for the actuator dynamics. While the bounds for stability and disturbance rejection are kept same as in Figure 4-9 and Figure 4-10. The upper bound for the tracking criterion was generated by using no overshoot and settling time of 2.0 s as the criterion. The transfer function used for the upper bound is:

$$T_u = \frac{(1.3)^2}{(s^2 + 2.6s + (1.3)^2)\left(\frac{s}{10} + 1\right)}$$ (4-21)

The lower bound was generated by settling time criterion of 6.0 s and the transfer function used is:

$$T_l = \frac{1}{(s^2 + 2s + 1)\left(\frac{s}{5} + 1\right)}$$ (4-22)

The tracking bounds in time domain and frequency domain are shown in Figure 4-43.
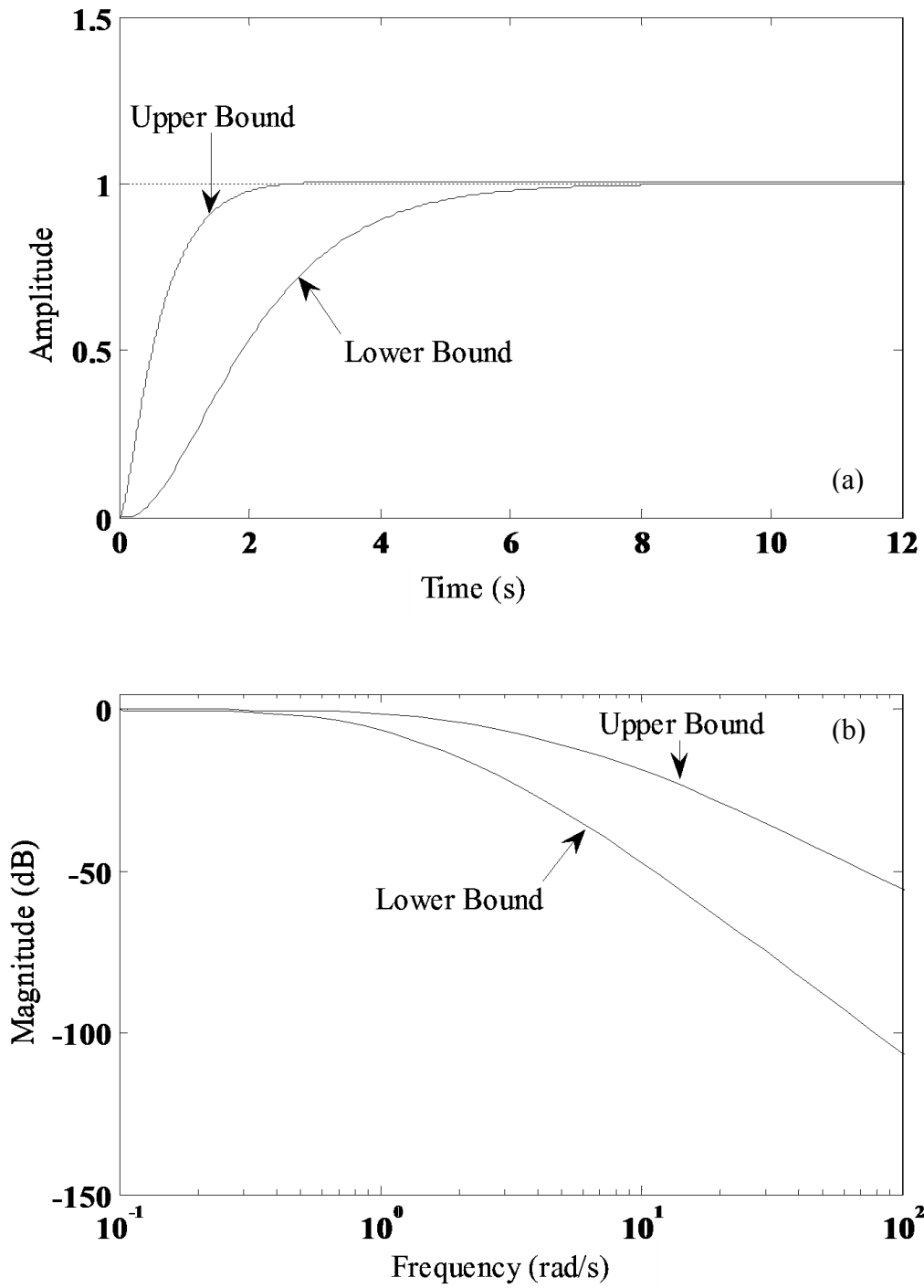
Figure 4-43: Tracking bounds (Controller II) ; (a) time domain; (b) frequency domain

As seen in Figure 4-44 the allowable nominal loop function does not meet the specifications.
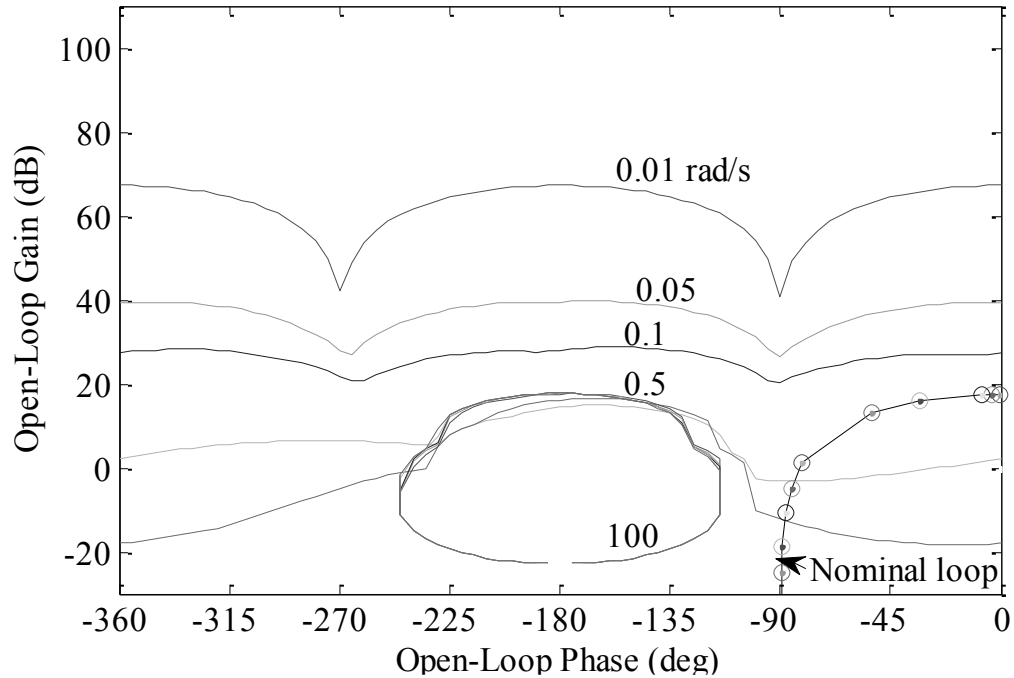
Figure 4-44: Nominal loop gain without controller (Controller II)

A controller is designed to satisfy the performance criterion as shown in Equation (4-23). The results of the nominal loop function with controller are shown in Figure 4-45.

$$G(s) = \frac{\left(\frac{s}{2.5} + 1\right)}{s} \qquad (4\text{-}23)$$
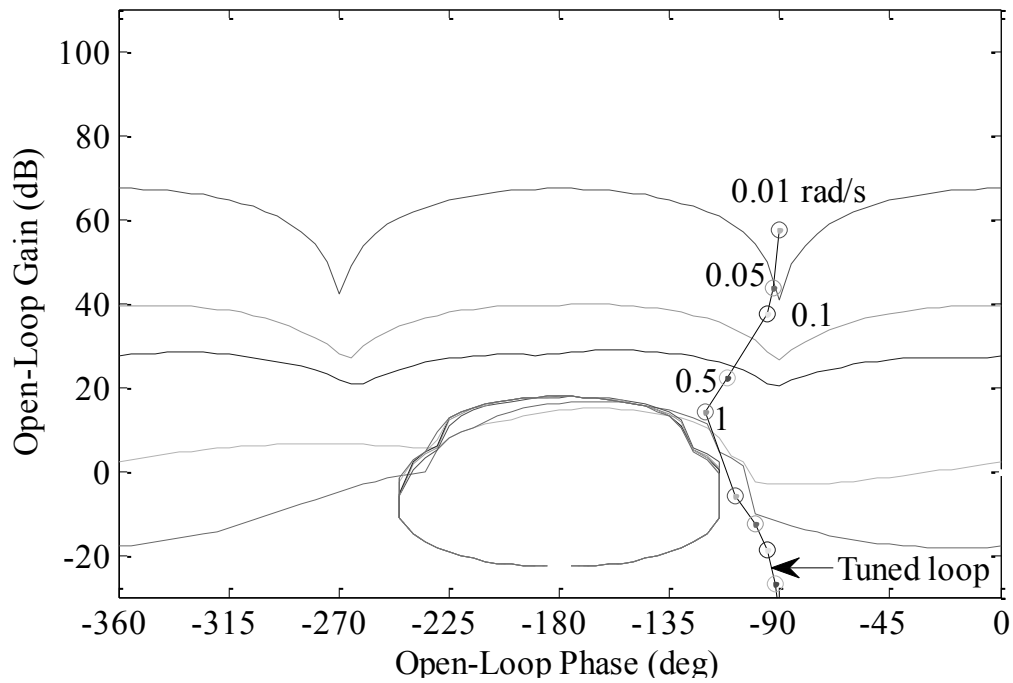
Figure 4-45: Nominal loop gain with controller (Controller II)

The next step of the design is designing a prefilter as shown in Equation (4-24).

$$F(s) = \frac{1}{\left(\frac{s}{0.85} + 1\right)} \tag{4-24}$$

The prefilter pushes the response of the plant with the controller below the upper bound throughout the frequency range as shown in Figure 4-46.
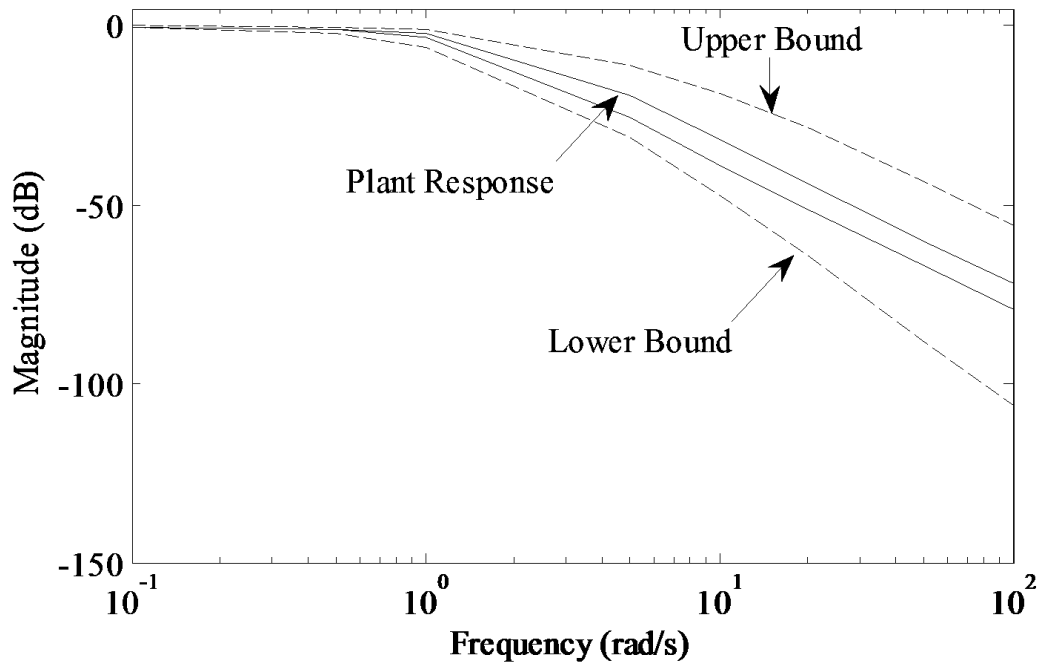
Figure 4-46: Plant response frequency domain with prefilter (Controller II)

The controller and prefilter as designed were than implemented in the simulation with τ_m of 0.25 s for the actuator dynamics and the altitude response as shown in Figure 4-47. It is observed that the time taken to reach 100 ft is reduced to 14.44 s as compared to 34.44 s seen before.
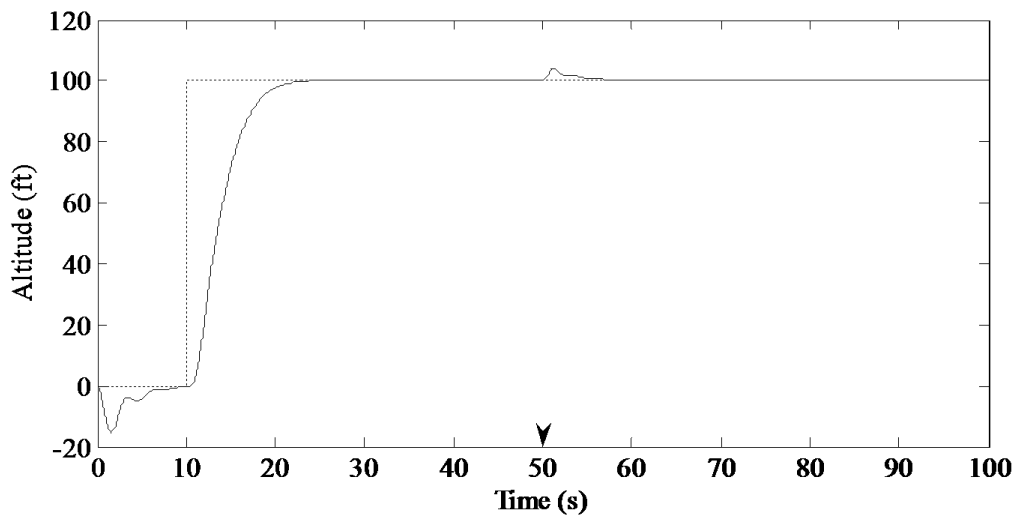
Figure 4-47: Altitude response with 10 lb payload (Controller II); motor time constant 0.25 s

Figure 4-48 displays the vertical velocity response of the helicopter where the maximum velocity attained to reach 100 ft is 23.24 ft/s.
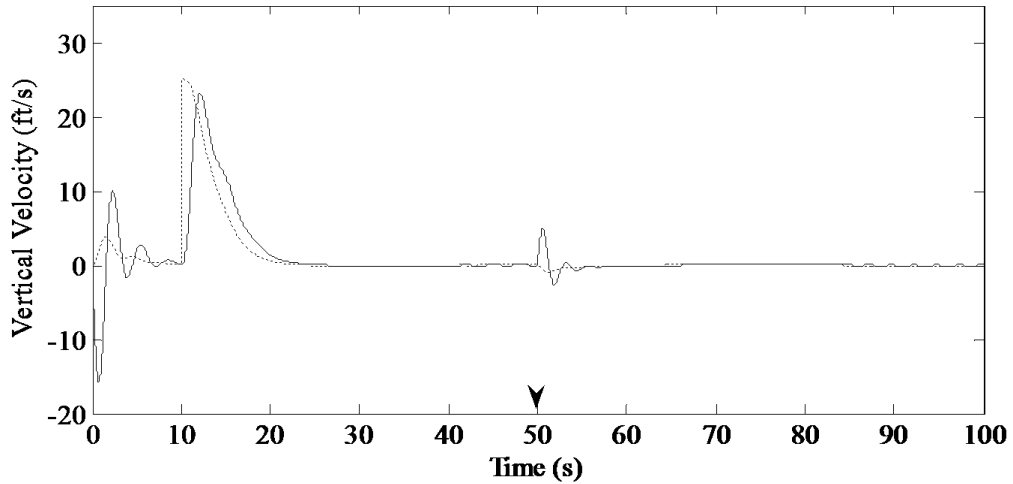
Figure 4-48: Vertical velocity response with 10 lb payload (Controller II); motor time constant 0.25 s

Some oscillations are observed in the vertical velocity while after the 10 lb payload is dropped the change in vertical velocity is 4.97 ft/s as shown in Figure 4-49.
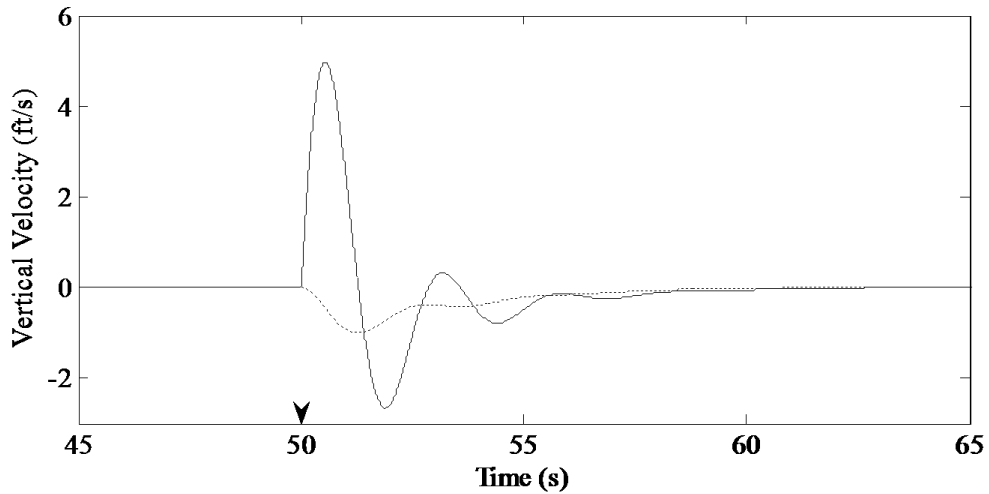
Figure 4-49: Vertical velocity change after 10 lb payload (Controller II); motor time constant 0.25 s

The collective pitch command with 10 lb payload and τ_m of 0.25 s is shown in Figure 4-50. It is observed that the collective pitch command does not saturate and settles to 10.8 deg lower than that observed with 12 deg seen in Figure 4-28.
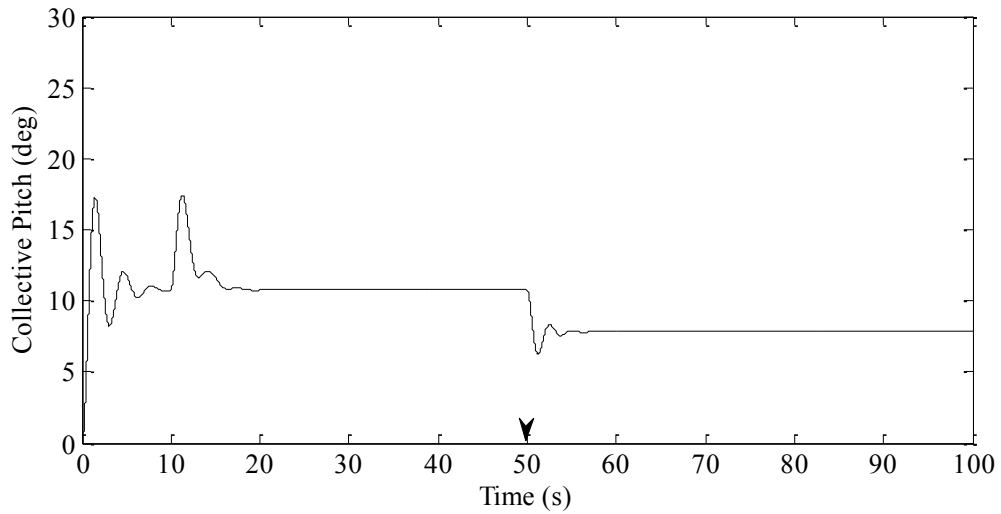
Figure 4-50: Collective pitch with 10 lb payload (Controller II); motor time constant 0.25 s

After the 10 lb payload is dropped, the collective pitch commands shows oscillations as seen in Figure 4-51. The collective pitch command after drop settles to 7.8 deg as seen before in Figure 4-26.
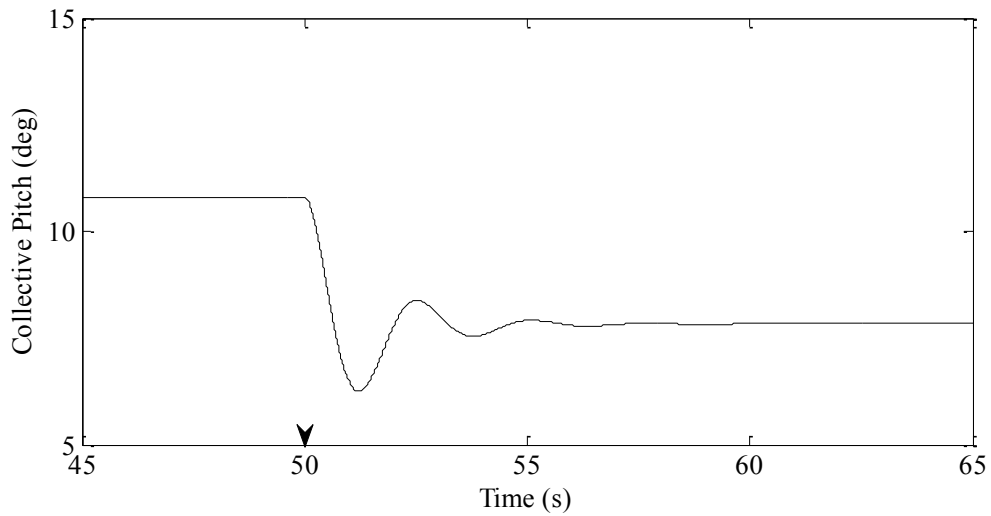
Figure 4-51: Collective pitch change after 10 lb payload drop (Controller II); motor time constant 0.25 s

Figure 4-52 shows the effect of payloads (2 lb, 5 lb and 10 lb) with constant motor time constant, τ_m, of 0.125 s on the change in altitude after the payload drop. As seen with the increase in payloads, the changes in altitude after the payload drop increases.
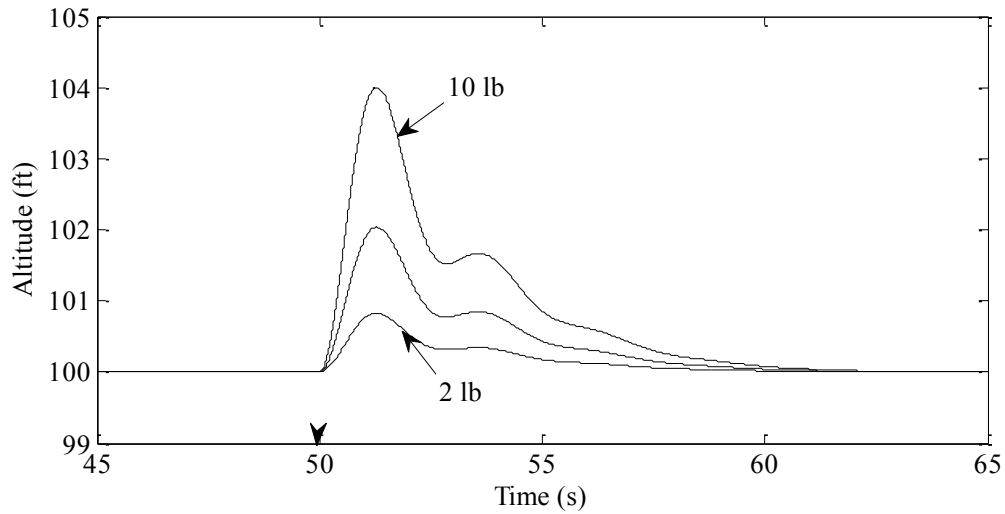
Figure 4-52: Altitude change after payload drop with 0.25 s motor time constant (Controller II); payloads (10 lb, 5 lb, 2 lb)

Figure 4-53 shows the effect of change in τ_m (0.25 s, 0.125 s and 0 s) on the change in altitude after dropping a 10 lb payload. The figure shows that the oscillations are seen for τ_m of 0.25 s. After the 10 lb payload drop with τ_m of 0.25, the change in altitude observed is 4.00 ft.
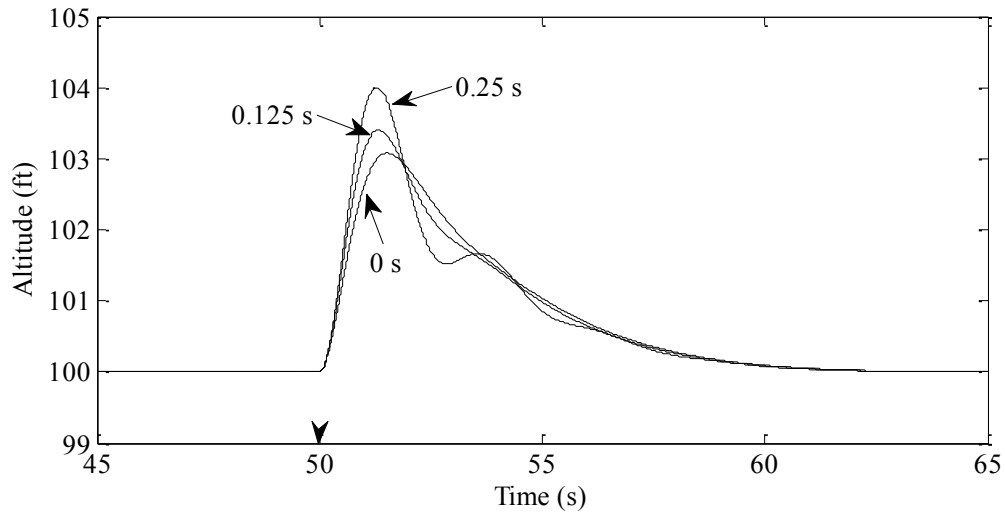
Figure 4-53: Altitude change 10 lb payload with actuator dynamics (Controller II); motor time constant (0.25 s, 0.125 s, 0 s)

The results of the Controller II with motor time constant of 0.25 s and 10 lb payload are summarized in Table 4-6.

Table 4-6: Controller II results with 10 lb payload; motor time constant 0.25 s

Performance index	Value
Time taken after takeoff to reach 100 ft	14.34 s
Maximum change in altitude after payload drop	4.00 ft
Maximum change in velocity after payload drop	4.97 ft/s
Time to recover within 2% of change in altitude after payload drop	10.00 s

While comparing these results to the Controller I, it was observed that by relaxing the tracking requirements for the controller design, the simulation works for a motor with slower time constant but the performance suffers greatly.

4.4 Controller Design Knowing Actuator Dynamics (Controller III)

Another solution for designing a controller relies on the assumption that the actuator dynamics is already known. The actuator dynamics in Equation (4-20) consists of a pole.

By placing a zero at the same location with the Controller I designed in Section 4.2, the effect of the actuator dynamics can be cancelled out [25]. In order to implement the transfer function in Simulink, a far non-dominant pole is also placed with the zero so that the condition to use the block is satisfied i.e., the order of the denominator must be greater than or equal to the order of the numerator [26]. Assuming that the value of τ_m is 0.25 s, the resulting controller transfer function with the prefilter is shown in Equation (4-25).

$$G(s) = \frac{6.5\left(\frac{s}{4}+1\right)(0.25s+1)}{s}$$

$$F(s) = \frac{\left(\frac{s}{22}+1\right)}{\left(\frac{s}{3.3}+1\right)}$$

(4-25)

Figure 4-54 shows the altitude response of the helicopter with 10 lb payload and motor time constant of 0.25 s. It took 34.31 s to reach the altitude of 100 ft compared 34.44 s seen with Controller I in Figure 4-27.
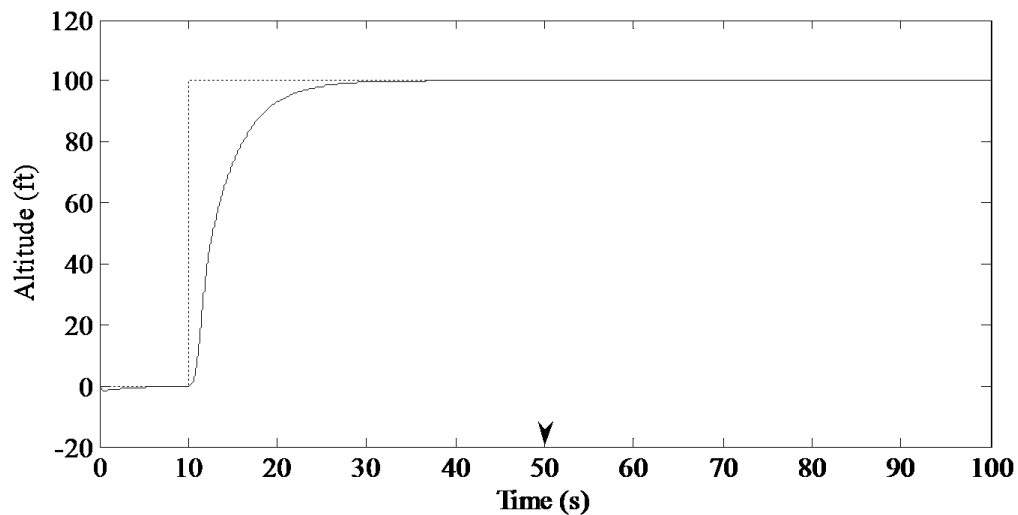
Figure 4-54: Altitude response (Controller III); motor time constant 0.25 s

Figure 4-55 displays the vertical velocity response of the helicopter with 10 lb payload and motor time constant of 0.25 s. The velocity attained to reach 100 ft is 33.32 ft/s while no oscillations are observed.
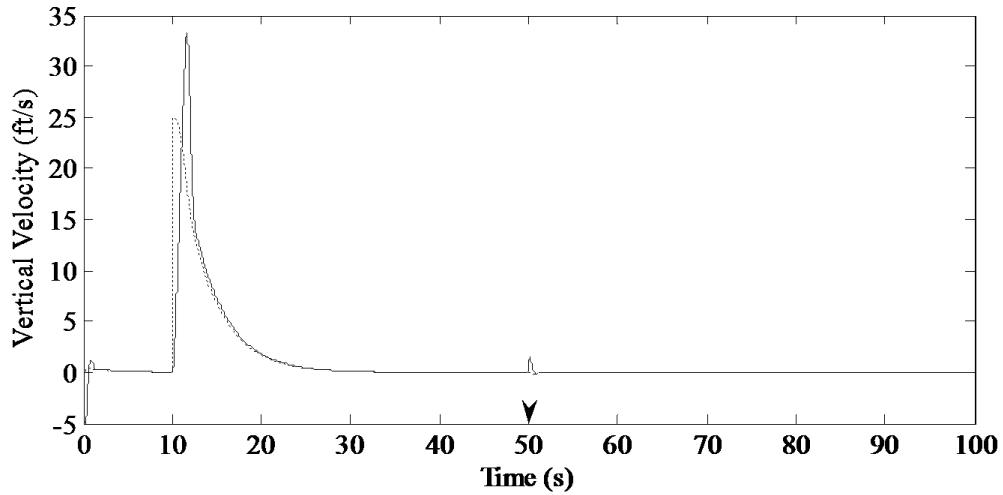
Figure 4-55: Vertical velocity response (Controller III); motor time constant 0.25 s

No oscillations are observed in the vertical velocity after the payload drop as seen in Figure 4-56. The change in vertical velocity after 10 lb payload drop and motor time constant 0.25 s is 1.53 ft/s as compared to 1.15 ft/s for Controller I seen in Figure 4-29.
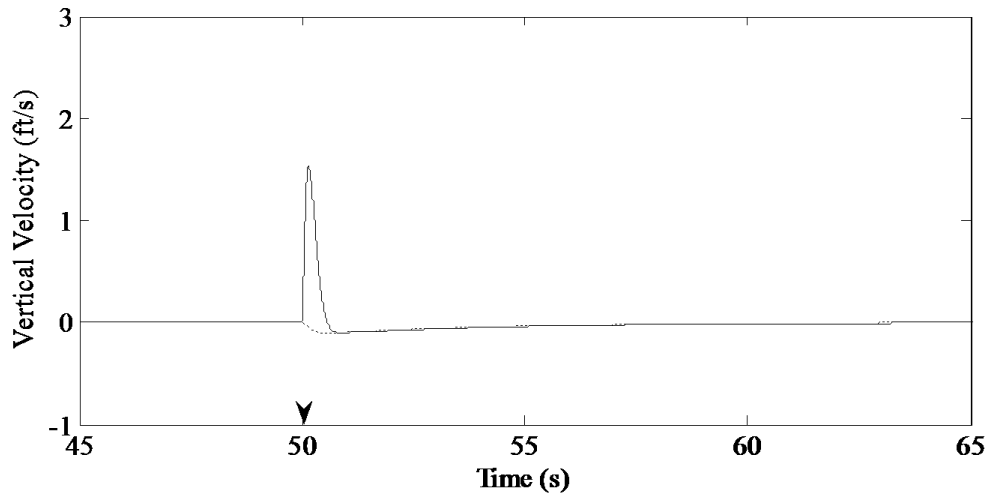
Figure 4-56: Vertical velocity after 10 lb payload drop (Controller III); motor time constant 0.25 s

Figure 4-57 displays the collective pitch command with 10 lb payload and motor time constant of 0.25 s. As before the collective pitch command settles to 12 deg after reaching the altitude of 100 ft.
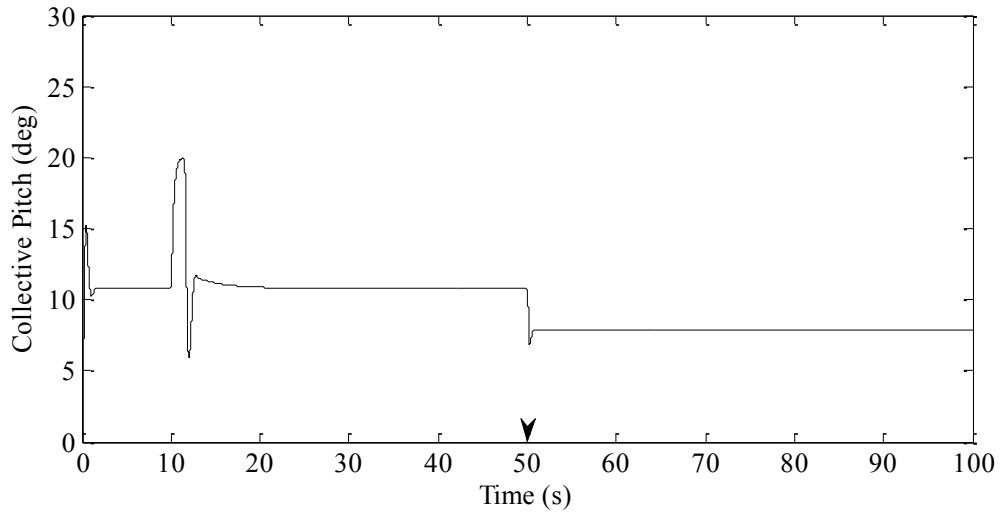
Figure 4-57: Collective pitch with 10 lb payload (Controller III); motor time constant 0.25 s

Figure 4-58 displays the collective pitch command after the 10 lb payload is dropped. As seen with Controller I the collective pitch command settles to 7.8 deg after payload drop.
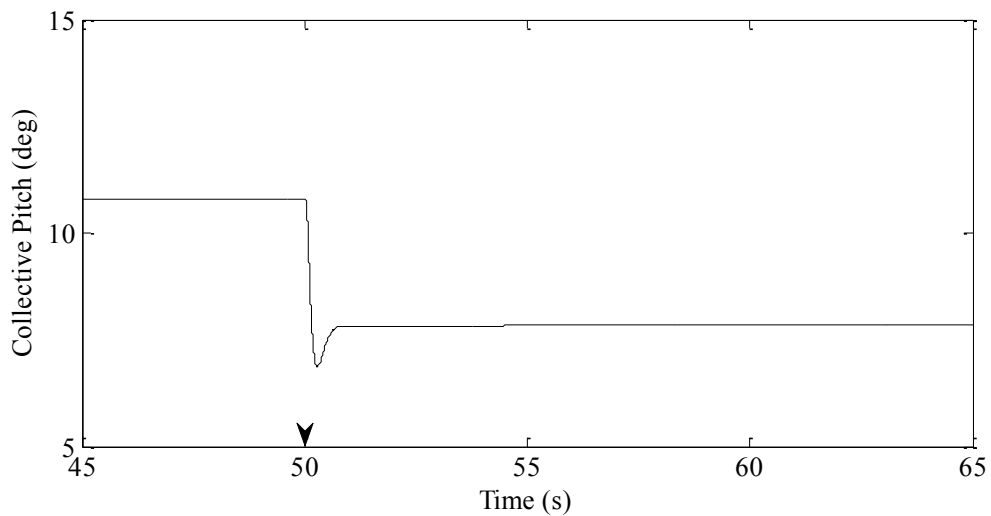
Figure 4-58: Collective pitch after 10 lb payload drop (Controller III); motor time constant 0.25 s

Figure 4-59 shows the change in altitude with a constant τ_m of 0.25 s but with payloads (10 lb, 5 lb and 2 lb). As seen with increasing payloads, the changes in altitude after payload drop increases.
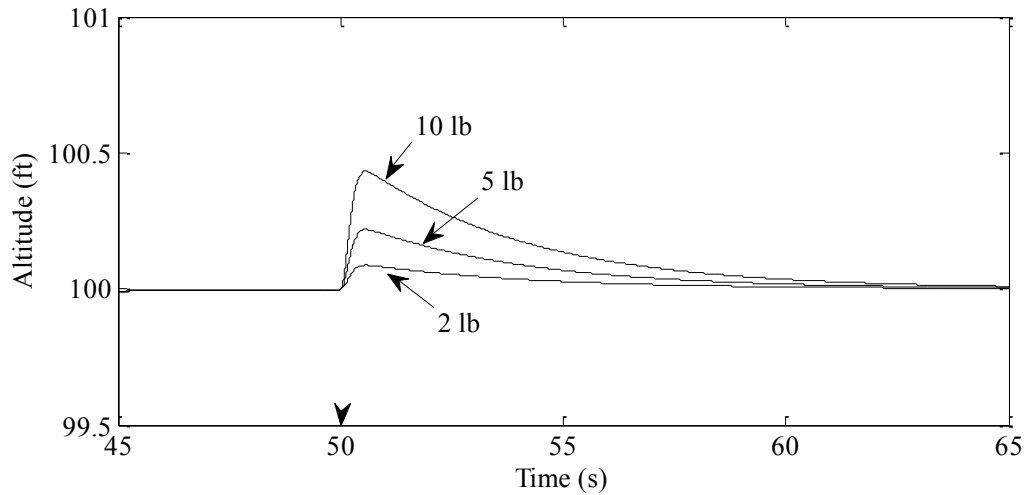
Figure 4-59: Change in altitude with motor time constant 0.25 s (Controller III); payloads (10 lb , 5 lb, 2 lb)

Figure 4-60 shows the effect of changing the motor time constant to the altitude after payload drop. As the motor time constant increases, the amount of change in altitude also increases, as the controller is slow to response to the change.
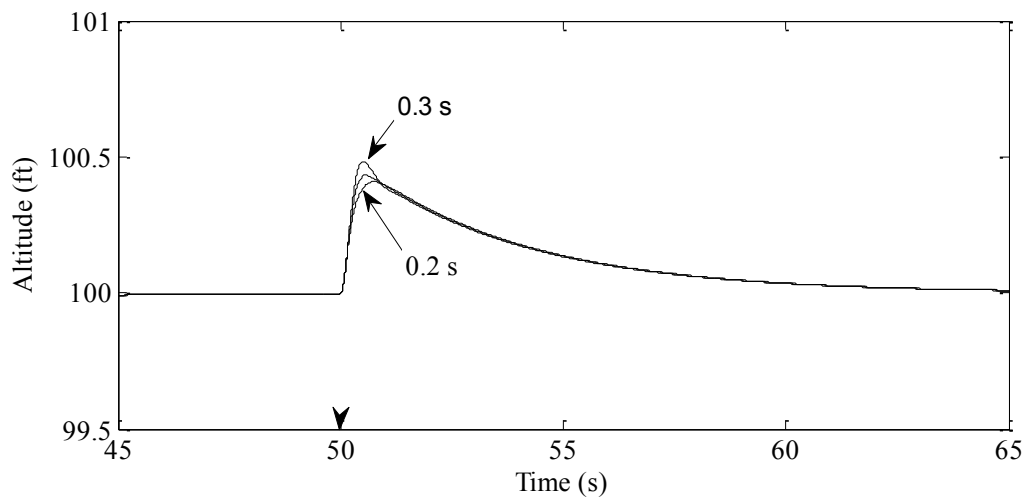
Figure 4-60: Altitude change after 10 lb payload drop (Controller III); motor time constant (0.3 s, 0.25 s, 0.2 s)

The results of the Controller III with 10 lb payload and the value of τ_m set to 0.25 s are summarized in Table 4-7.

Table 4-7: Controller III results with 10 lb payload; motor time constant 0.25 s

Performance index	Value
Time taken after takeoff to reach 100 ft	34.31 s
Maximum change in altitude after payload drop	0.43 ft
Maximum change in velocity after payload drop	1.53 ft/s
Time to recover within 2% of change in altitude after payload drop	15.21 s

By placing the zero, the controller I designed can be implemented with modifications for a motor with time constant of 0.25 s. This controller gives good result while keeping the helicopter stable throughout flight, however does not work with motor time constant of zero.

4.5 Incorporating Actuator Dynamics into QFT Controller Design

In this section, a controller will be designed assuming that the actuator dynamics is unknown and will be included in the design process. Two methods can be used to design the controller. The first method combines the actuator dynamics plant with the first-order vertical helicopter plant while uncertainties in both plants are quantified. In the second method, a new first-order plant replaces the combined actuator dynamics and vertical channel plant.

4.5.1 Design using Second-Order Transfer Function (Controller IV)

A QFT controller was developed by incorporating the motor transfer function as a part of the plant model. Using the same uncertainties in the plant as Equation (4-11) while adding small uncertainties in the motor time constant, τ_m. The uncertainties in the motor dynamics are approximated to represent the current helicopter system and the changed plant model is shown in Equation (4-26):

$$P(s) = \left(\frac{1}{\tau_m s + 1}\right)\left(\frac{k_h}{\tau_h s + 1}\right) \qquad (4\text{-}26)$$

$$7.5 \leq k_h \leq 9.5$$

$$1.3 \leq \tau_h \leq 2.3 \qquad (4\text{-}27)$$

$$0.2 \leq \tau_m \leq 0.3$$

Figure 4-61 displays the new templates with updated plant model.
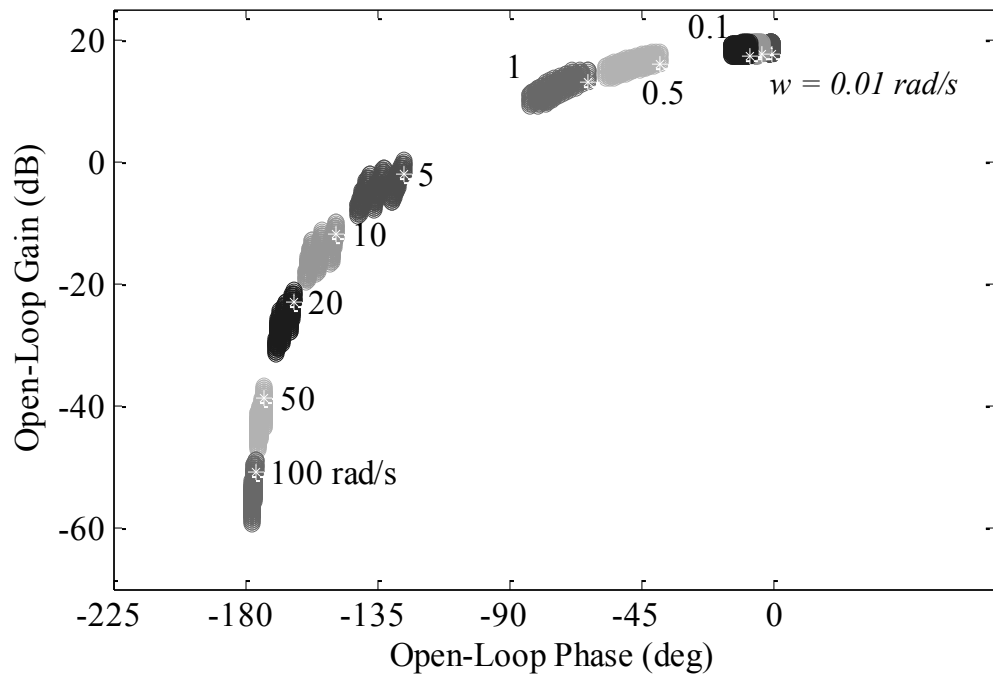
Figure 4-61: Plant templates (Controller IV)

The performance criterions for the controller design were kept the same as the QFT controller designed in section 4.3. The nominal loop function without the controller is shown in Figure 4-62.
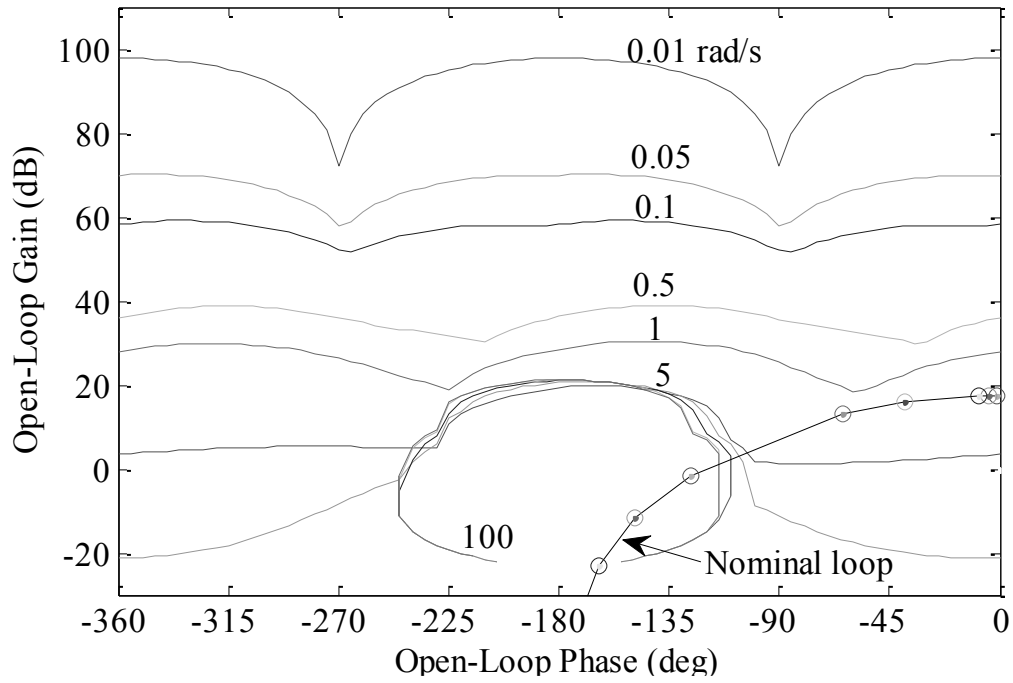
Figure 4-62: Nominal loop (Controller IV)

The controller shown in Equation (4-28) is needed to shape the loop function to satisfy the performance criterion. The tuned loop with the controller is displayed in Figure 4-63.

$$G(s) = \frac{6\left(\frac{s}{7}+1\right)\left(\frac{s}{1.65}+1\right)}{s} \qquad (4\text{-}28)$$
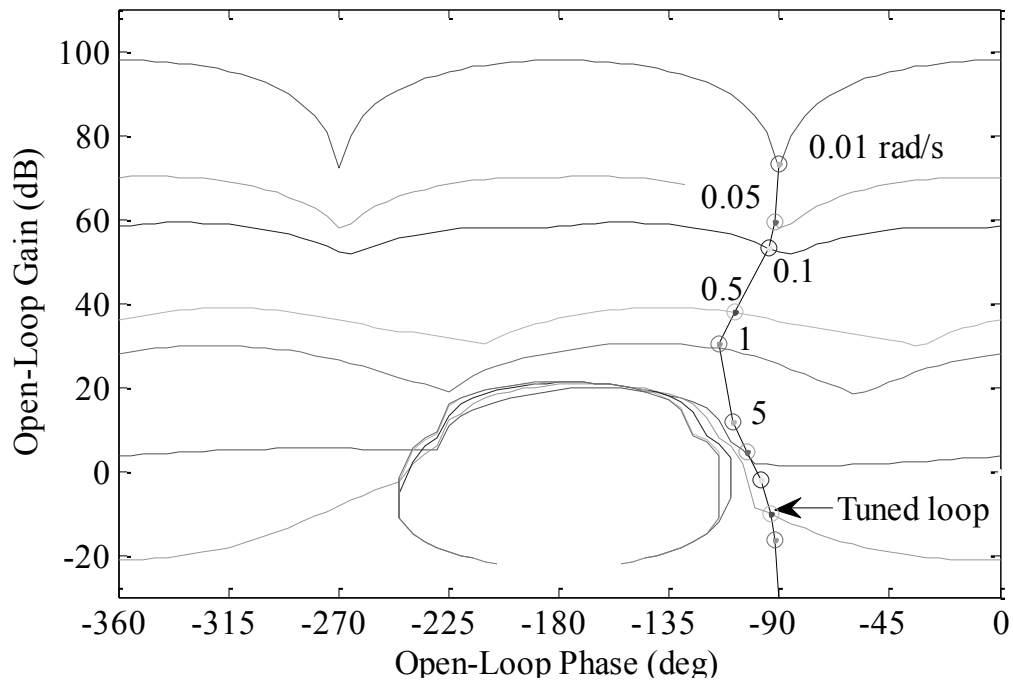
Figure 4-63: Tuned loop (Controller IV)

The next step is to design a prefilter to push the plant response below the upper bounds of the tracking criterion. The prefilter designed is shown below while the response of the plant with the prefilter is shown in Figure 4-64.

$$F(s) = \frac{1}{\left(\frac{s}{3.3} + 1\right)} \tag{4-29}$$
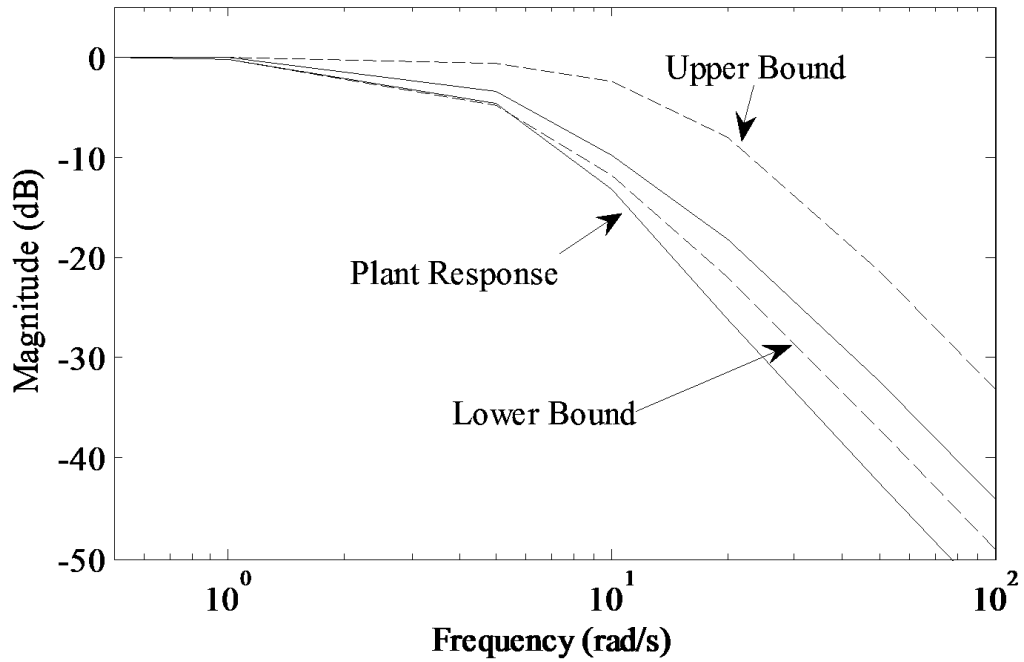
Figure 4-64: Plant response with prefilter (Controller IV)

The controller (4-28) and prefilter (4-29) were than implemented in the simulation and the altitude response of the helicopter can be seen in Figure 4-65.
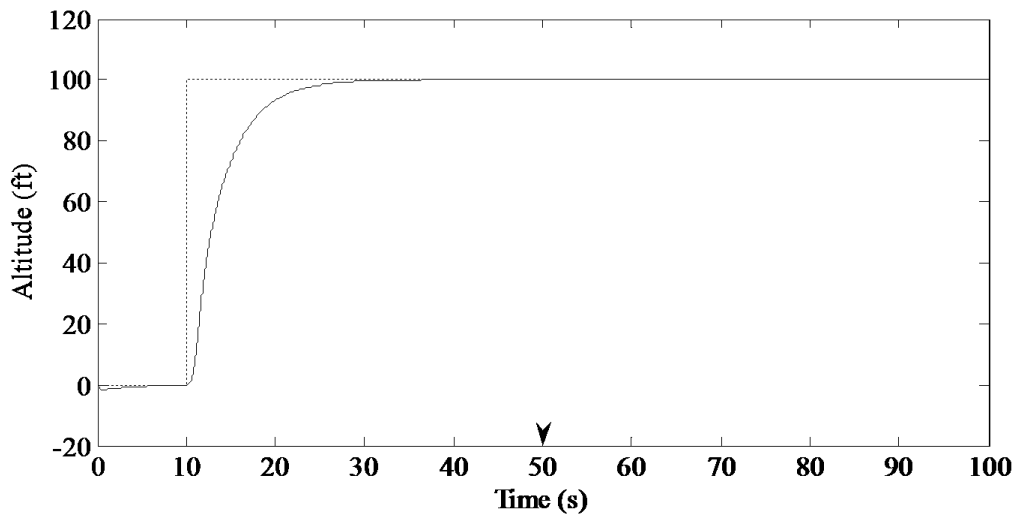
Figure 4-65: Altitude response with 10 lb payload (Controller IV); motor time constant 0.25 s

Figure 4-66 displays the vertical velocity response of the helicopter with 10 lb payload and motor time constant of 0.25 s. The vertical velocity attained to reach 100 ft is 30.72 ft/s.
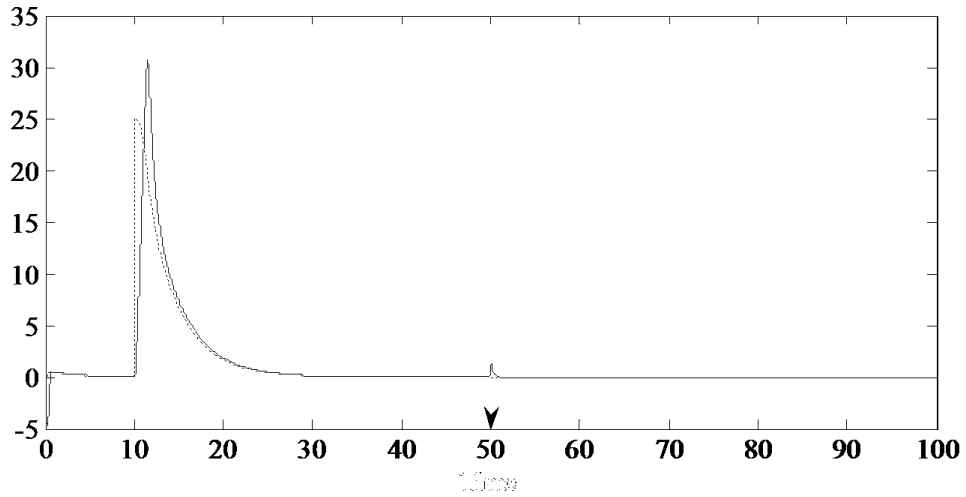
Figure 4-66: Vertical velocity with 10 lb payload (Controller IV); motor time constant 0.25 s

Figure 4-67 shows the vertical velocity change after the 10 lb payload and motor time constant of 0.25 s. After the payload drop, the velocity changes to 1.36 ft/s compared to 1.15 ft/s seen in Figure 4-28.
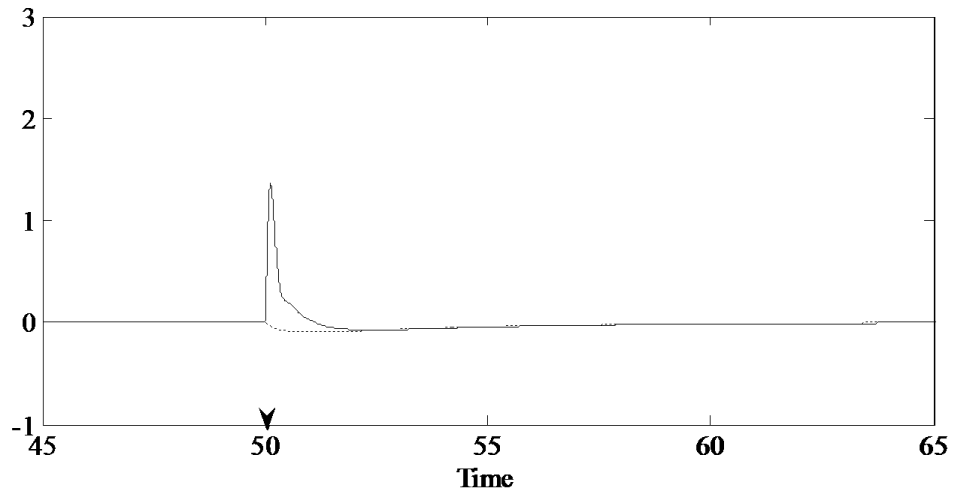
Figure 4-67: Vertical velocity after 10 lb payload drop (Controller IV); motor time constant 0.25 s

The collective pitch command as generated is shown in Figure 4-68 where the collective pitch command settles to 12 deg after reaching 100ft.
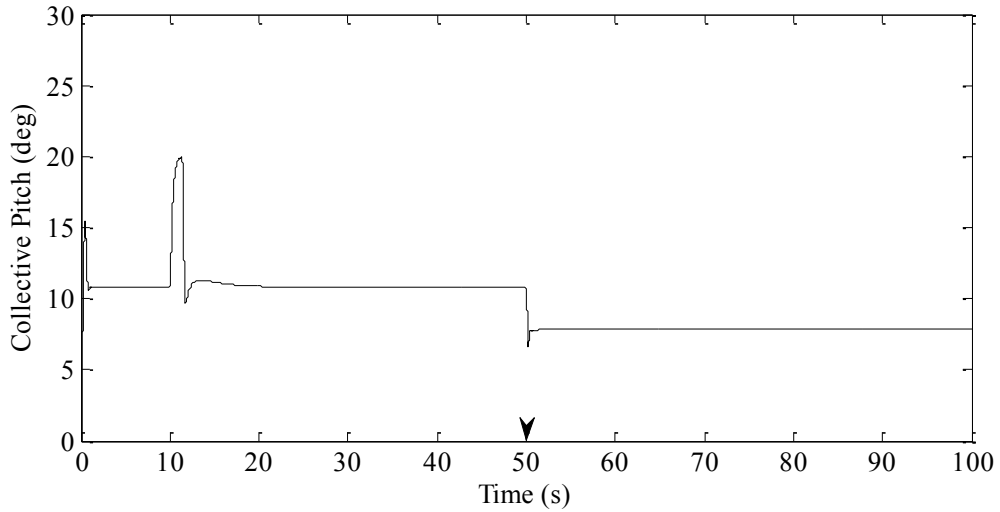
Figure 4-68: Collective pitch with 10 lb payload (Controller IV); motor time constant 0.25 s

Figure 4-69 shows the change in collective pitch after the drop of 10 lb payload with motor time constant of 0.25 s. The collective pitch command settles to 7.8 deg as seen with controller I.
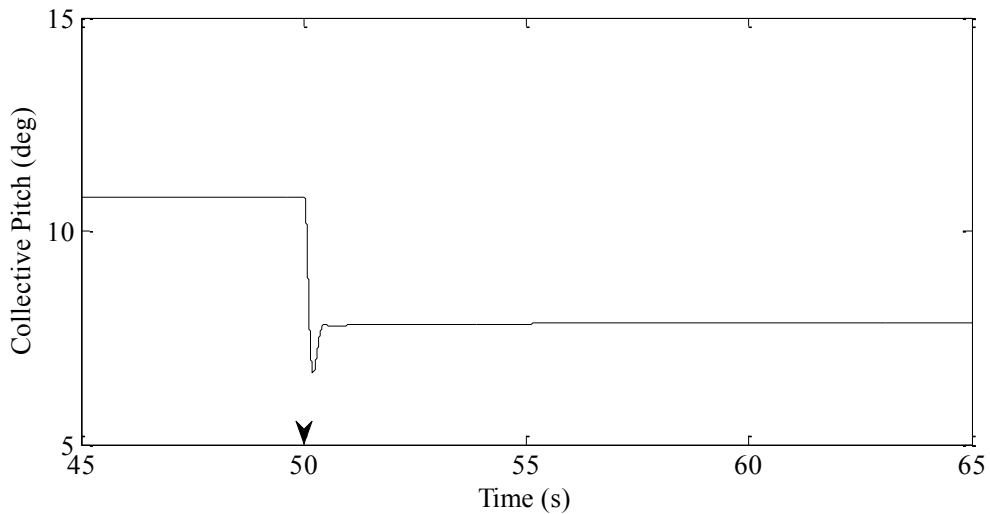
Figure 4-69: Collective pitch change after 10 lb payload drop (Controller IV); motor time constant 0.25 s

Figure 4-70 shows the change in altitude with payloads (10 lb, 5 lb, 2 lb) while keeping the motor time constant at 0.25 s. The change in altitude increases with increase in payload. For 10 lb payload, the change in altitude is 0.39 ft while the time to recover within 2 % of change in altitude after payload drop is 16.05 s.
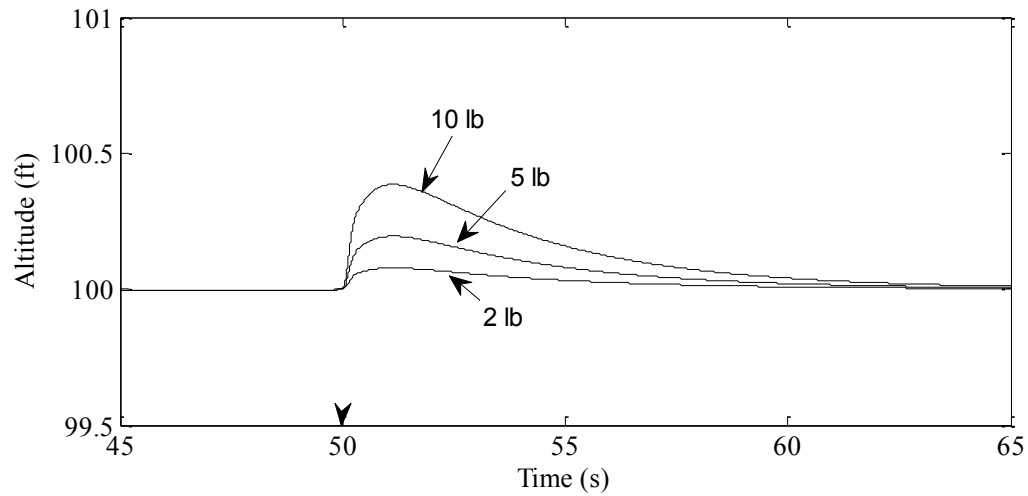
Figure 4-70: Altitude change with payloads (10 lb, 5 lb, 2 lb) (Controller IV); motor time constant 0.25 s

Figure 4-71 shows the change in altitude with motor time constants (0. 3 s, 0.25 s, 0.2 s) and 10 lb payload. With the increase in motor time constant, the change in altitude after the payload drop increases that is for motor time constant of 0.3 s, the altitude changed by 0.39 ft whereas for motor time constant of 0.2 s, the altitude changed by 0.38 ft.
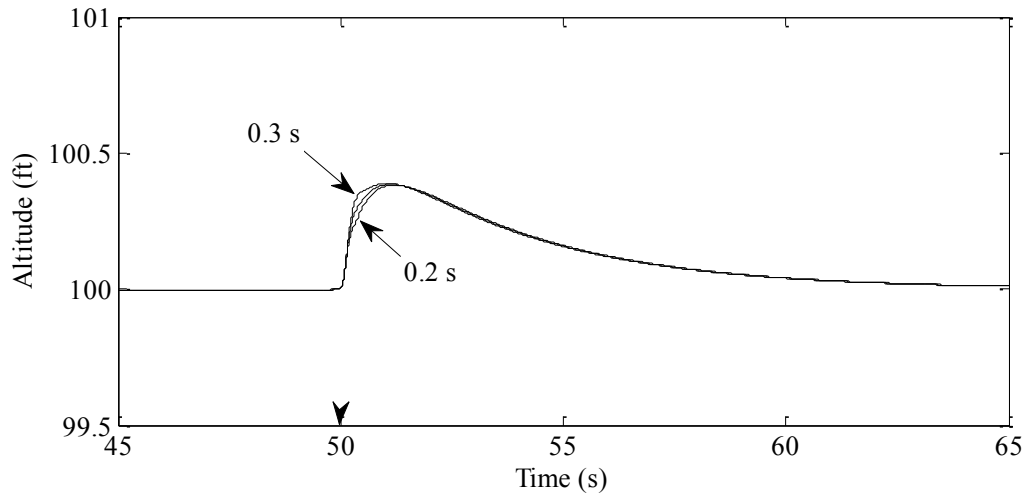
Figure 4-71: Altitude change after 10 lb payload drop with actuator dynamics (Controller IV); motor time constant (0.3 s, 0.25 s, 0.2 s)

The results for the Controller IV with 10 lb payload and motor time constant of 0.25s are summarized in Table 4-8.

Table 4-8: Controller IV results with 10 lb payload; motor time constant 0.25 s

Performance index	Value
Time taken after takeoff to reach 100 ft	33.88 s
Maximum change in altitude after payload drop	0.39 ft
Maximum change in velocity after payload drop	1.36 ft/s
Time to recover within 2% of change in altitude after payload drop	16.05 s

Compared to Controller I, it was observed that designing the controller with the actuator dynamics included in the design process gives better performance and works with motors with slower time constants.

4.5.2 Design using First-Order Estimation of Plant (Controller V)

Estimating the transfer functions of the helicopter and the actuator dynamics separately from the system is difficult. The solution is to estimate a single first-order plant that

combines the effects of both the helicopter and actuator dynamics as done in the industry. In order to estimate the transfer function, a step input is applied to the combined second-order transfer functions with all the uncertainties in the parameters of both transfer functions shown in Equations (4-32) and (4-33).

$$P(s) = \left(\frac{1}{\tau_m s + 1} \right) \left(\frac{k_h}{\tau_h s + 1} \right) \tag{4-30}$$

$$7.5 \leq k_h \leq 9.5$$

$$1.3 \leq \tau_h \leq 2.3 \tag{4-31}$$

$$0.2 \leq \tau_m \leq 0.3$$

The step input was applied to the second-order transfer function shown in Equation (4-30) and the first-order transfer function was estimated from the outputs as shown in Figure 4-72.
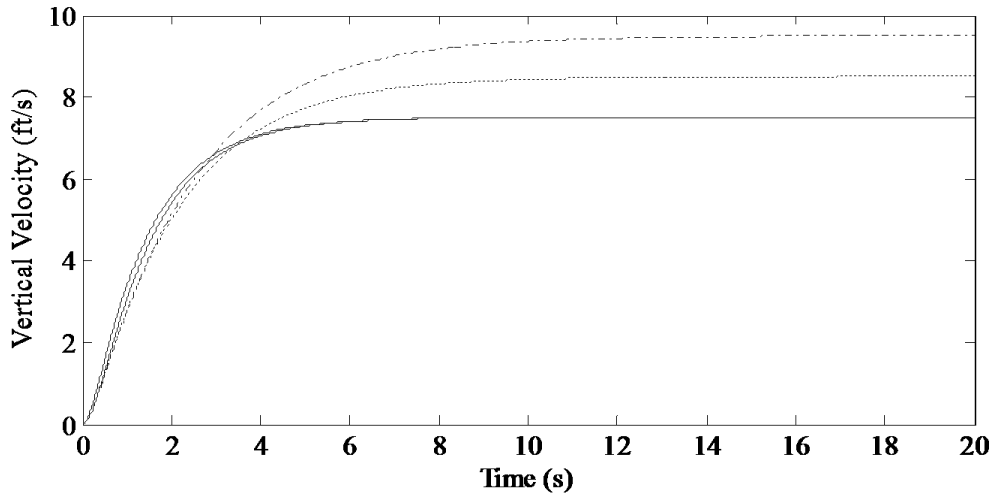
Figure 4-72: First-order estimation from second-order plant

$$P(s) = \frac{k_e}{\tau_e s + 1} \tag{4-32}$$

$$7.4 \leq k_e \leq 9.6$$

$$1.5 \leq \tau_e \leq 2.6 \tag{4-33}$$

To verify if the estimated first-order transfer function is accurate, step input was applied to the transfer function shown in Equation (4-32) and the output shown in Figure 4-73 was compared to Figure 4-72.
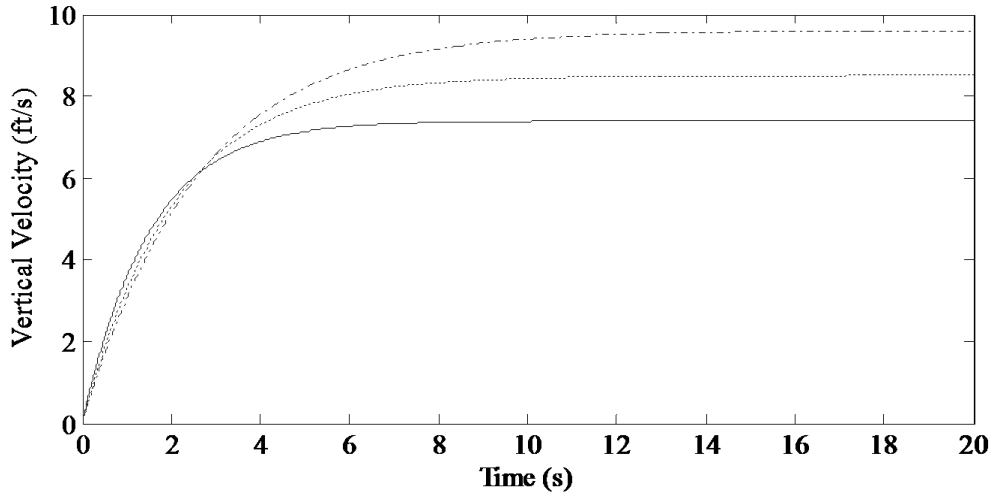
Figure 4-73: Vertical velocity response from the estimated transfer function

Similar to Section 4.3, the value for k_e is the estimated from the max output at which the vertical velocity settles. τ_e is estimated from the time taken for the vertical velocity after the step input to reach 63% of the max vertical velocity. The values of the transfer function have changed. Because of this new plant templates have to be generated and are shown in Figure 4-74.
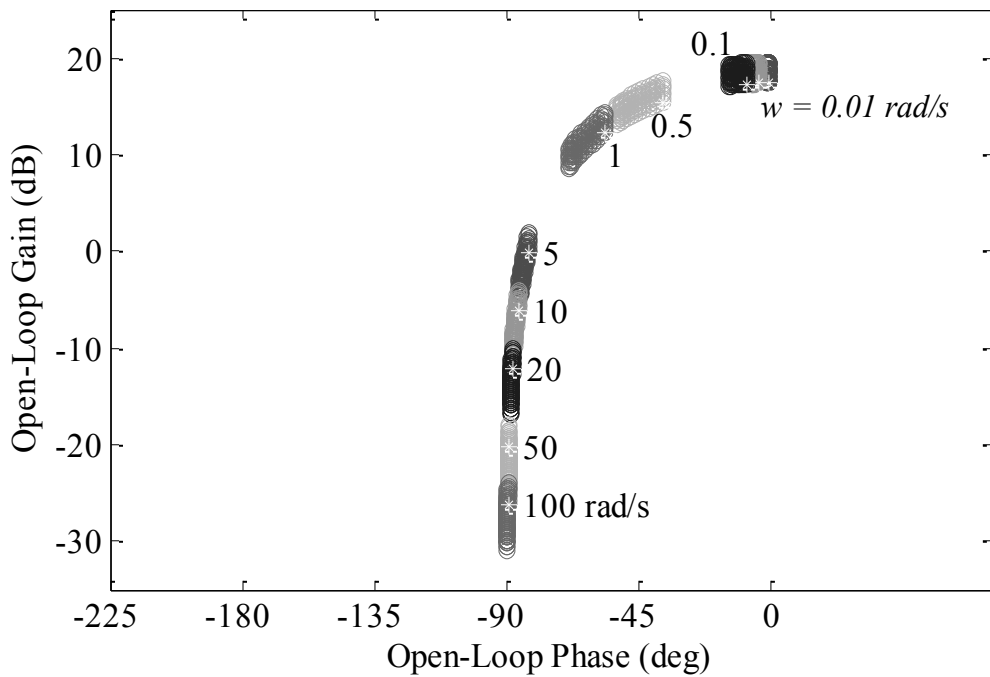
Figure 4-74: Plant templates (Controller V)

The stability, tracking and disturbance rejection bounds for the new first-order estimated plant remain the same as that used to design Controller I. Figure 4-75 displays the nominal loop with the bounds.
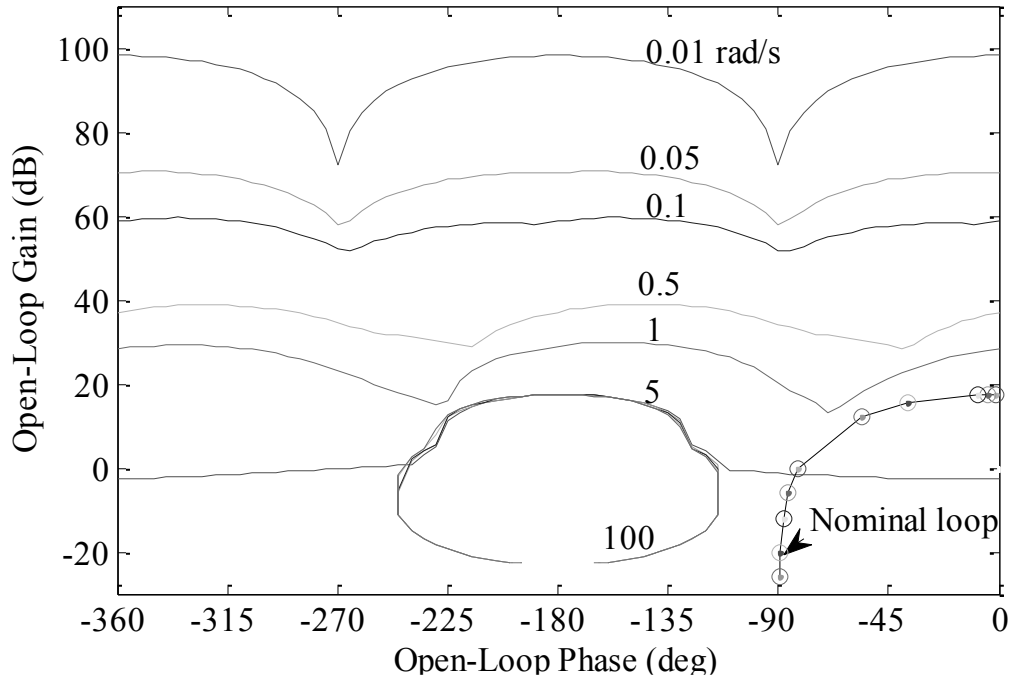
Figure 4-75: Nominal loop (Controller V)

Similar to the previous controller designs, the loop gain does not meet the performance criterion. Figure 4-76 shows the tuned loop with the controller designed shown in Equation (4-34).

$$G(s) = \frac{7\left(\frac{s}{7}+1\right)\left(\frac{s}{2}+1\right)}{s\left(\frac{s}{25}+1\right)} \tag{4-34}$$
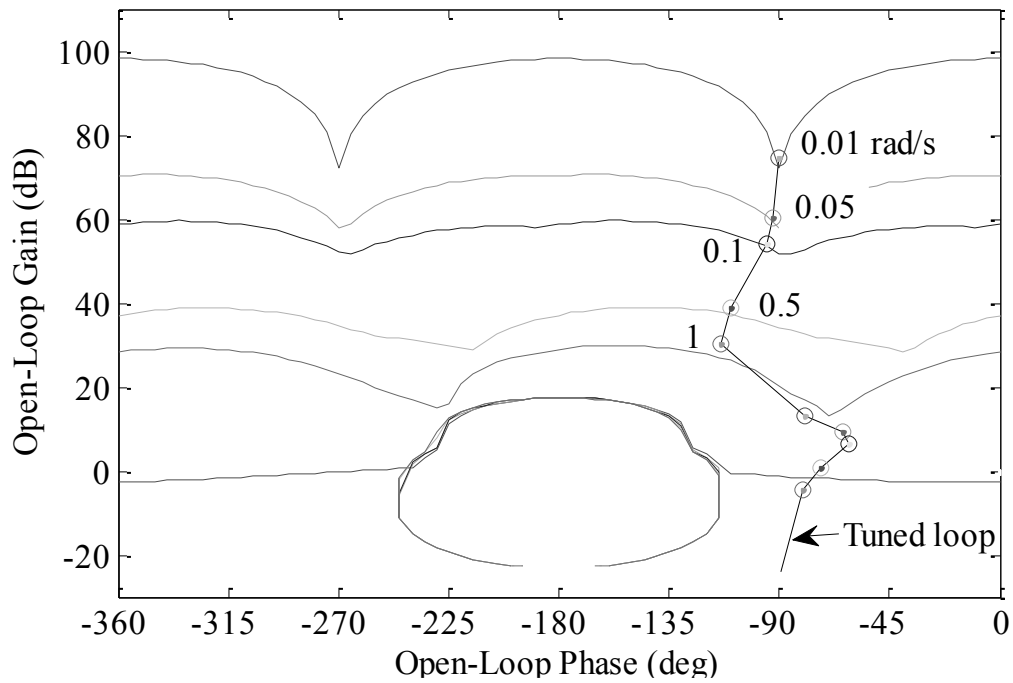
Figure 4-76: Tuned loop (Controller V)

Once the controller is designed, the next step is designing a prefilter to push the plant response below the upper bound limit. The prefilter as designed is shown below:

$$F(s) = \frac{1}{\left(\frac{s}{3.3} + 1\right)} \tag{4-35}$$

Figure 4-77 displays the response of the plant with the controller (4-34) and prefilter (4-35).
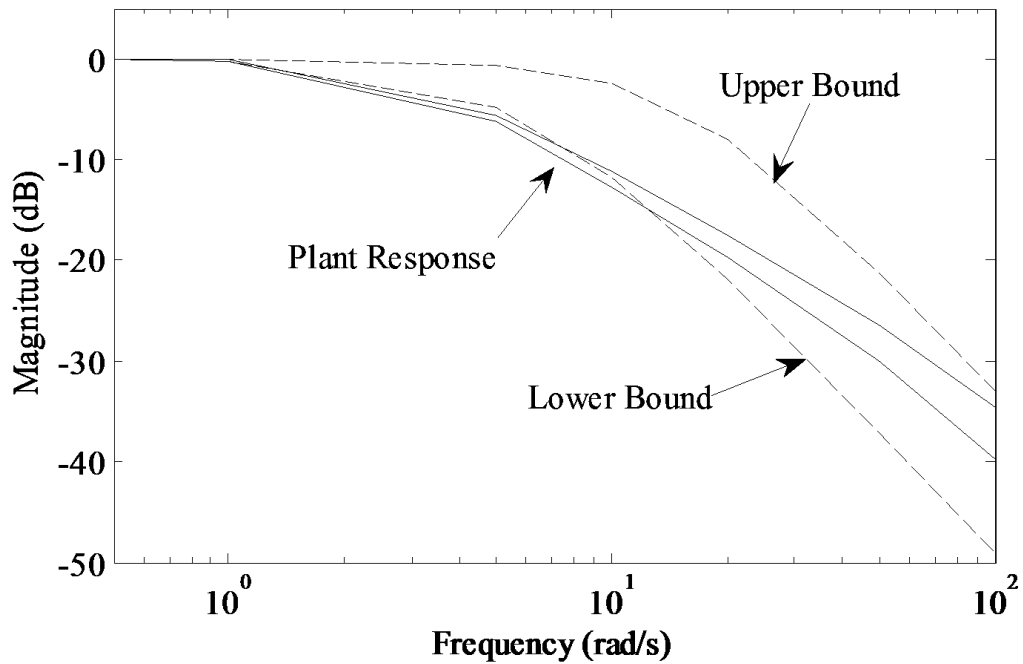
Figure 4-77: Plant response with prefilter (Controller V)

This controller and prefilter were than implemented in the simulation with the motor time constant, τ_m value of 0.25 s. Figure 4-78 displays the altitude response of the helicopter with the Controller V. The time taken to reach 100 ft is 33.91 s as compared to 34.44 s seen with Controller I.
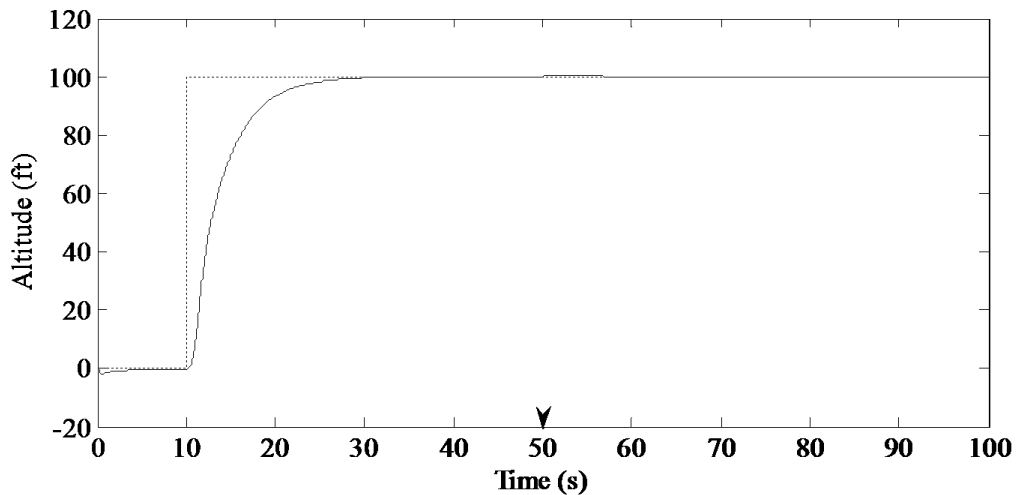
Figure 4-78: Altitude response with 10 lb payload (Controller V); motor time constant 0.25 s

Figure 4-79 displays the vertical velocity response of the helicopter with 10 lb payload and motor time constant of 0.25 s. The velocity attained to reach 100 ft is 33.91 ft/s.
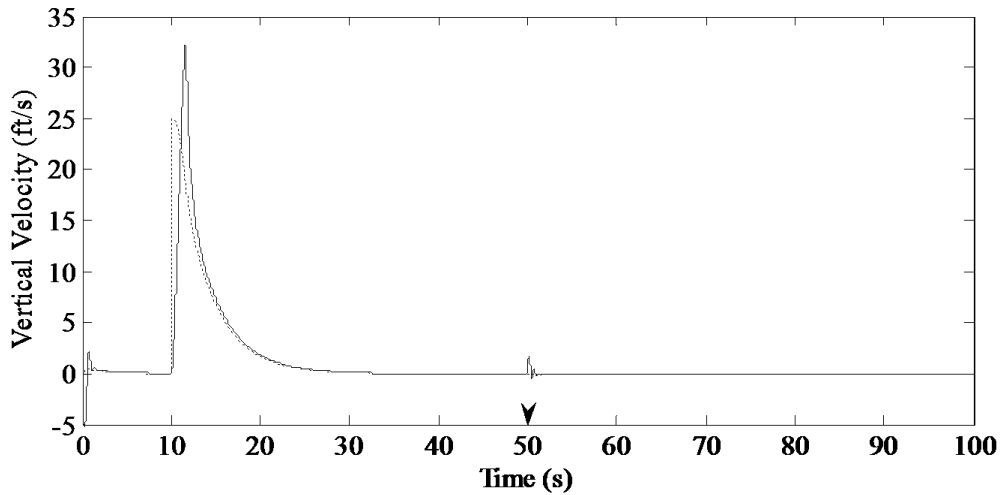
Figure 4-79: Vertical Velocity response with 10 lb payload (Controller V); motor time constant 0.25 s

Figure 4-80 shows the vertical velocity after the 10 lb payload is dropped with a motor time constant of 0.25 s. Some oscillations appear while the change in vertical velocity observed after the 10 lb payload drop is 1.78 ft/s.
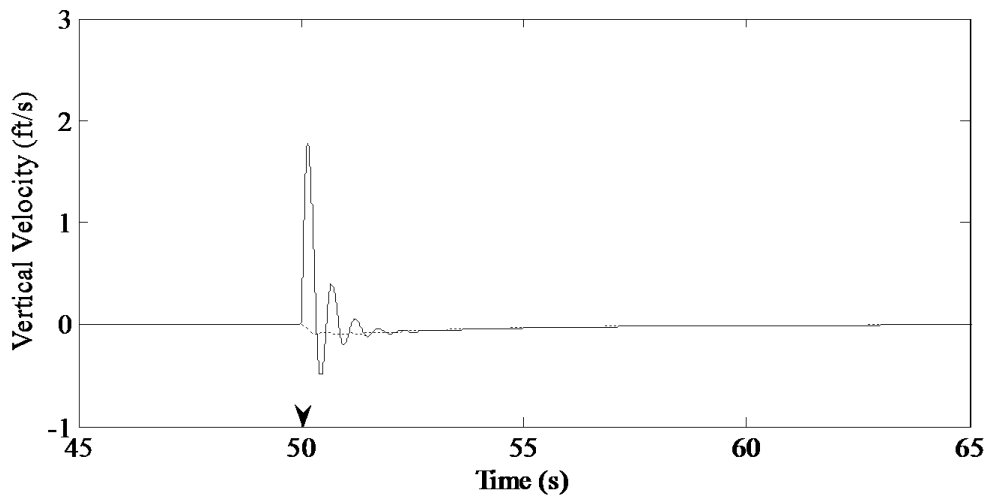
Figure 4-80: Vertical velocity change after 10 lb payload drop (Controller V); motor time constant 0.25 s

The collective pitch command as generated by the controller with 10 lb payload and motor time constant of 0.25 s is shown in Figure 4-81.
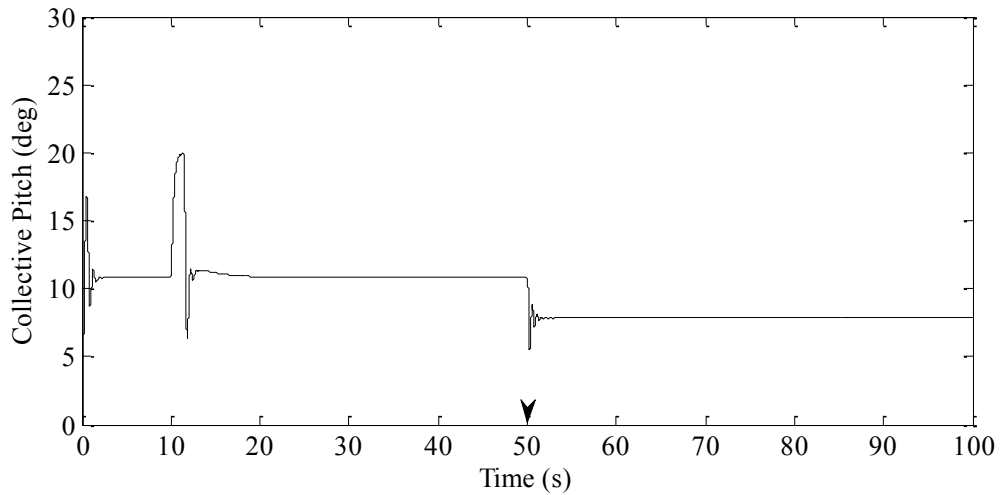
Figure 4-81: Collective pitch with 10 lb payload (Controller V); motor time constant 0.25 s

Figure 4-82 shows the change in collective pitch after the 10 lb payload is dropped with a motor time constant of 0.25 s.
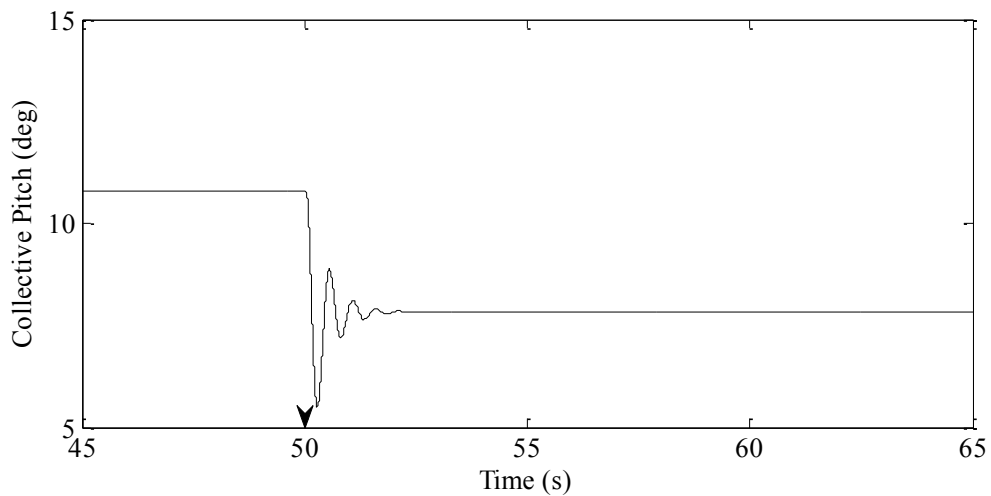
Figure 4-82: Collective pitch change after 10 lb payload (Controller V);motor time constant 0.25 s

Figure 4-83 shows the change in altitude with different payloads while keeping the motor time constant at 0.25 s. The change in altitude after the 10 lb payload drop is 0.37 ft. The time taken to recover within 2 % of change in altitude after 10 lb payload drop is 15.49 s.
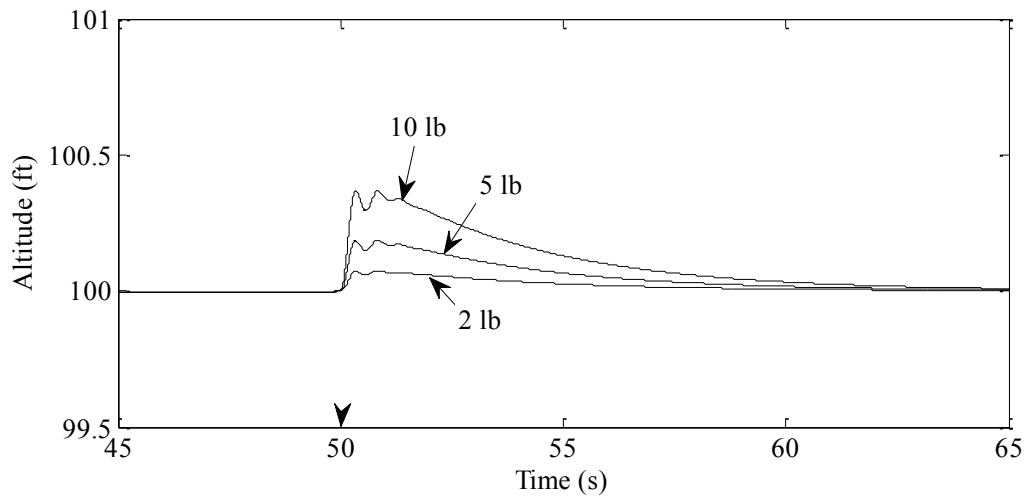
Figure 4-83: Altitude change with payloads (10 lb, 5 lb, 2 lb) (Controller V); motor time constant 0.25 s

Figure 4-84 shows the change in altitude with different motor time constants and 10 lb payload. With the increase in motor time constant, the change in altitude after the drop increases that is with a motor time constant of 0.3 s the change in altitude observed is 0.37 ft whereas with 0.2 s the change observed is 0.35 ft. The oscillations also increase with increase in motor time constant.
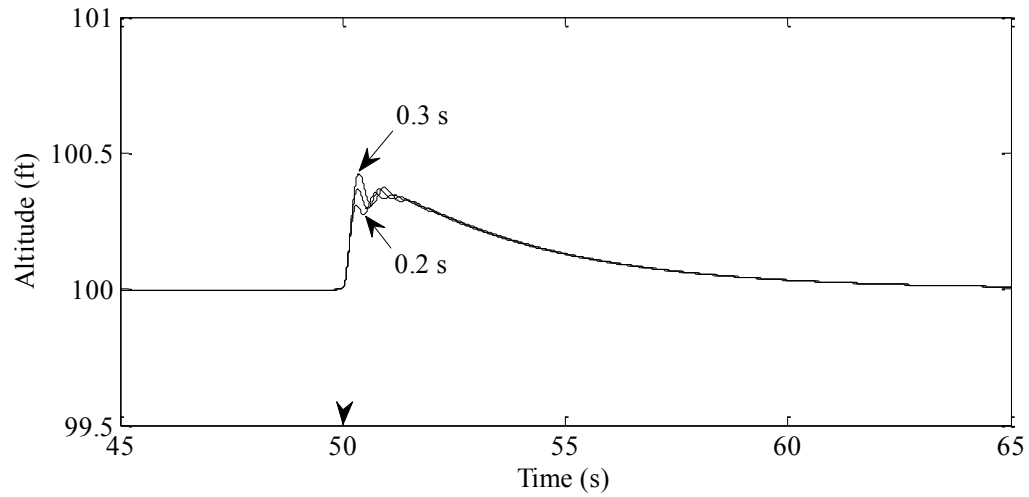
Figure 4-84: Altitude change after 10 lb payload drop (Controller V); motor time constants (0.3 s, 0.25 s, 0.2 s)

The results for the controller designed with first-order estimation motor dynamics with 10 lb payload and motor time constant of 0.25 s are summarized in Table 4-9.

Table 4-9: Controller V results with 10 lb payload; motor time constant 0.25 s

Performance index	Value
Time taken after takeoff to reach 100 ft	33.91 s
Maximum change in altitude after payload drop	0.37 ft
Maximum change in velocity after payload drop	1.78 ft/s
Time to recover within 2% of change in altitude after payload drop	15.49 s

Compared to the Controller IV, the Controller V gives better results. The change in altitude after payload drop is reduced to 0.37 ft, smaller than that observed before.

4.6 Comparison with PID Controller

The PID controller was than tuned for 10 lb payload and motor time constant of 0.25 s. The gains for the controller are shown in Equation (4-36).

$$K_P = 0.14 \left(\frac{rad}{\frac{ft}{s}} \right)$$

$$K_I = 0.06 \left(\frac{rad}{ft} \right)$$

(4-36)

The changes in altitude for payload range of 0 to 10 lb and motor time constant range of 0.2 to 0.3 s are shown in Figure 4-85.
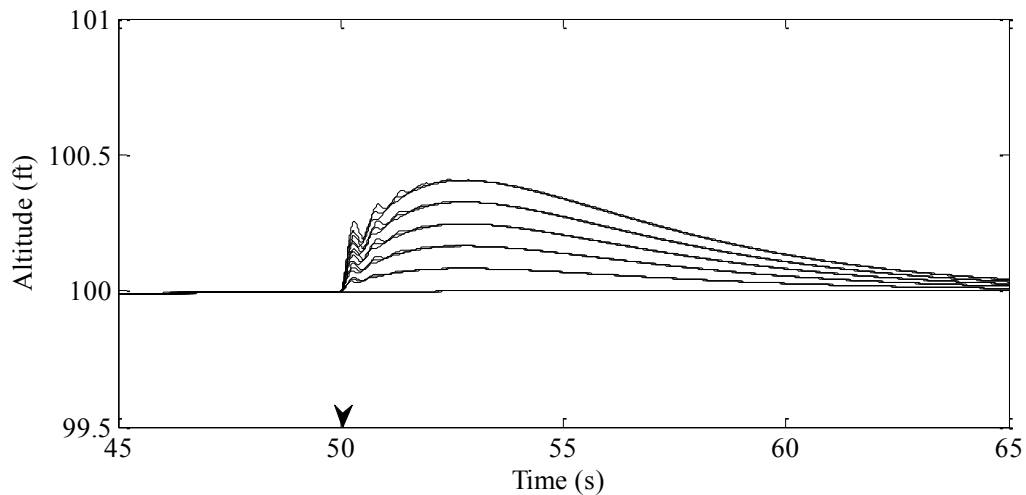
Figure 4-85: Altitude change after payload drop (PID Controller IV); payload range 0 to 10 lb and motor time constant range 0.2 to 0.3 s

Comparing this with the performance with Controller IV as seen in Figure 4-86, the change in altitude is similar for both controllers however the time to recover within 2 % of change in altitude is seen more with the PID controller. PID controller also showed some oscillations.
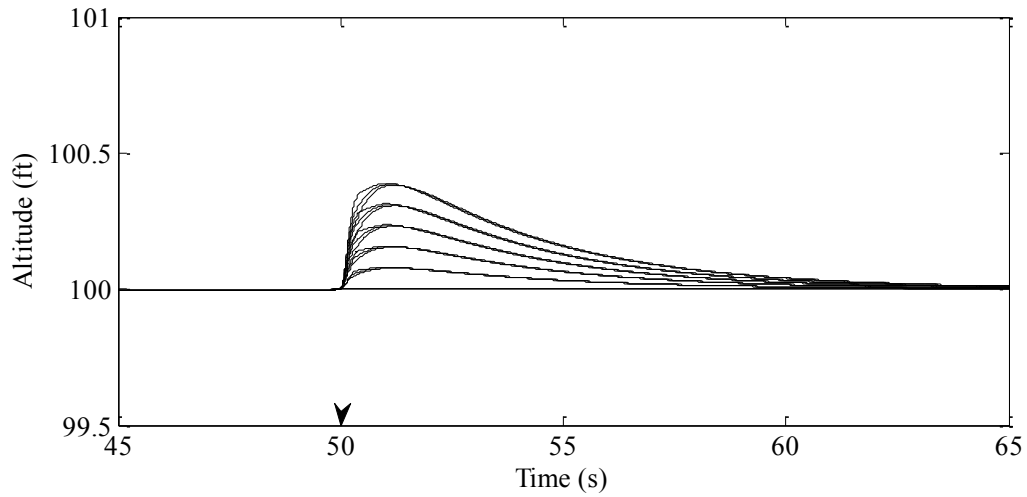
Figure 4-86: Altitude change after payload drop (Controller IV); payload range 0 to 10 lb and motor time constant range 0.2 to 0.3 s

However, compared to the performance with Controller V as seen in Figure 4-87, the change in altitude is similar for all three controller. Similar to PID controller, the Controller V also showed oscillations but still showed less time to recover within 2 % of change in altitude.
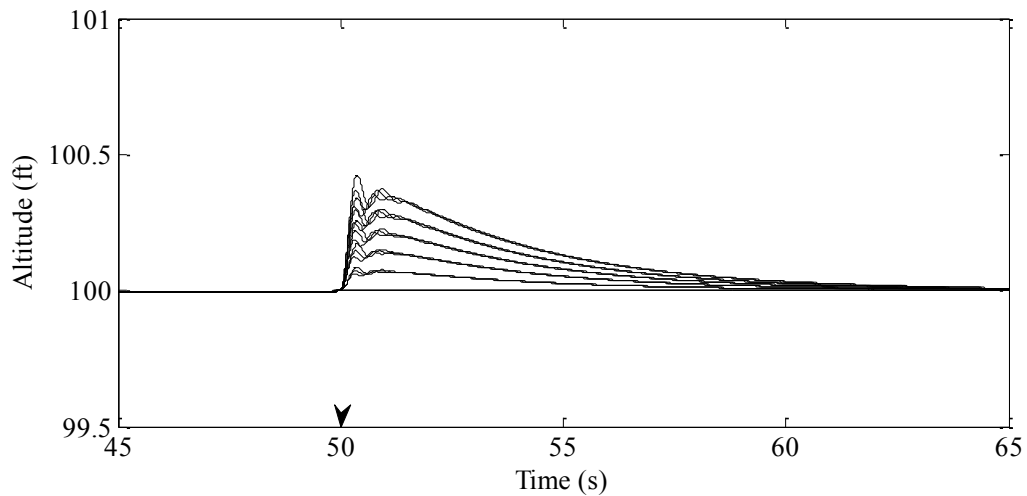
Figure 4-87: Altitude change after payload drop (Controller V); payload range 0 to 10 lb and motor time constant range 0.2 to 0.3 s

Thus, it is observed that the Controller IV shows the best response without any oscillations.

4.7 Summary

Several QFT controllers were designed for the inner loop of the vertical channel of the helicopter. The performance of the controllers were evaluated while flying the helicopter to 100 ft. Different payloads were dropped after 50 s and the change in altitude after the payload drop was compared. Controller I was effective throughout the flight plan and was able to reduce the change in altitude to 0.43 ft after a 10 lb payload drop. It was noted that with the increase in payload the change in altitude also increased. However, it was observed that the collective pitch command crosses the hardware limit so a saturation limit was applied which increased the vertical velocity attained to fly the helicopter to 100 ft but did not affect the performance after the drop.

The performance of the controller was compared to a typical PID controller tuned using Ziegler Nichols tuning method. It was observed that this PID controller was not as effective as the QFT controller because the change in altitude after the payload drop was 2 ft as compared to 0.43 ft observed with QFT Controller. To improve the performance of the PID controller and match it with the performance of QFT controller, the gains were tuned. The gains were tuned to match the performance to QFT controller with 2 lb payload. The PID controller obtained showed similar change in altitude after the payload drop while the time to recover within 2% change in altitude after the payload drop increased. Alternately, the PID controller was tuned to match the performance with the QFT controller with 10 lb payload. It was observed that while the controller was effective in minimizing the change in altitude after the payload drop, it showed an increase in time to recover to 2 % of change in altitude after the payload drop.

Further, the effect of actuator dynamics on the controller performance was also evaluated. It was observed that the Controller I only works with motors of time constant less than 0.145. With the addition of the actuator dynamics, the performance deteriorated. The change in altitude after 10 lb payload drop increased to 0.58 ft from 0.43 ft.

New controllers were designed to make the simulation work with motor time constants higher than 0.145. The first controller designed was the Controller II using modified tracking criterion. This controller resulted in reduced performance; it allowed greater

change in altitude after 10 lb payload drop of 4.00 ft. Further, another controller (Controller III) was designed by cancelling the pole of the actuator dynamics by placing a zero with the controller designed earlier. The controller worked with motor with time constant of 0.25 s and performed better than the controller with modified tracking criterion. However, this would rely on the fact that the motor dynamics is known and so far, the actuator dynamics has not been included in the design process.

The next controller was designed by adding the actuator dynamics with the helicopter plant and incorporating it in the controller design process. This yielded a controller that showed improved performance, minimizing the change in altitude after payload drop to 0.39 ft, lower than the observed with Controller I. However, it is difficult to identify the transfer functions from the system directly. Subsequently, a new controller was designed by replacing the second-order transfer function by a single first-order estimated transfer function. This also resulted in a performance similar to that of Controller IV but showed slightly less change in altitude after the payload drop of 0.37 ft. However, this controller also resulted in oscillations in both altitude and velocity but this method most likely represents the one followed in the industry where the plant order is unknown and obtained by first-order estimation. The results of all the controllers designed with 10 lb payload are summarized in the Table 4-10.

Table 4-10: Results of all controllers with 10 lb payload

Controllers	Time taken after takeoff to reach 100 ft (s)	Maximum change in altitude after payload drop (ft)	Maximum change in velocity after payload drop (ft/s)	Time to recover within 2% of change in altitude after payload drop (s)
Controller I	34.44	0.43	1.15	15.20
PID Controller I	26.25	2.19	1.26	26.90
PID Controller II	36.43	0.46	1.18	16.43
PID Controller III	36.62	0.43	1.03	16.70
Controller I (motor time constant 0.125 s)	34.44	0.58	2.00	14.07
Controller II (motor time constant 0.25 s)	14.34	4.00	4.97	10.00
Controller III (motor time constant 0.25 s)	34.31	0.43	1.53	15.21
Controller IV (motor time constant 0.25 s)	33.88	0.39	1.36	16.05
Controller V (motor time constant 0.25 s)	33.91	0.37	1.78	15.49
PID Controller IV (motor time constant 0.25 s)	17.12	0.41	1.25	21.72

5. Conclusions

5.1 Contributions of this Thesis

In this thesis, the following research was conducted:

(i)   A mathematical nonlinear model for unmanned helicopter was implemented.

(ii)   A full open loop simulation for an unmanned helicopter Xcell 60 was developed.

(iii)   Controllers were developed for the vertical channel of the helicopter.

First, a nonlinear six degree of freedom (6 DOF) mathematical model was implemented. The equations of motion were calculated using the Newton-Euler equations, while the forces and torques of the helicopter were calculated from the rotor dynamics using the Blade Element Theory.

The mathematical model was than implemented in Simulink software for X-Cell 60 helicopter. The simulation used fourth order Runga-Kutta integration method. The open loop simulation was verified in simulation for all three channels: vertical, longitudinal and lateral.

Controllers were designed for the vertical channel of the helicopter. The transfer function for the vertical channel was estimated from the simulation and then used in the QFT controller design process. The controllers were then designed and implemented in the simulation while the performance was evaluated while carrying and dropping of different payloads. It was observed that as the payload weight increased the change in altitude after the payload drop increased. Further, actuator dynamics was implemented in simulation and it was observed that the controller performance was affected. It was also observed that the first controller designed only worked for motors with time constants less than 0.145 s.

A new controller was then designed with modified tracking criterion of QFT design process to make the simulation work for motors with time constants more than 0.145 s. However, this controller showed reduced performance. Further, assuming the actuator dynamics is known the first QFT controller designed was modified by adding the pole of

the actuator dynamics as a zero in the controller transfer function. This controller showed promising results. However, it is not always possible to model the actuator dynamics accurately.

Hence, a new QFT controller was developed by including the uncertainties in the actuator dynamics in the QFT design process. The performance of this controller showed lower change in altitude after the payload drop. However, it is not always possible to identify the transfer functions of both the helicopter and actuator dynamics separately from the actual system. Thus, the second-order transfer function was replaced by a single first-order transfer function and was then used to design a QFT controller. This controller showed the best performance of all the controllers designed but showed some oscillations in altitude and velocity.

In conclusion, the QFT control design has proven to be an effective method of designing a controller for the vertical channel of an unmanned helicopter to get the desired performance. The controller designed with QFT gives better performance than a typical PID controller and is robust enough to reject any uncertainties in the system.

5.2 Future Work

For future work, the following issues need to be addressed. First the simulation developed in Simulink needs to be quantitatively verified using real flight test data. Secondly, the controllers developed in this thesis need to be implemented on real helicopter and the performance has to be evaluated. Finally, the simulation can be improved by developing controllers for the longitudinal and lateral channel of the helicopter.

References

[1] M. W. Weilenmann and H. P. Geering, "A Test Bench for the Rotorcraft Hover Control," *Jounal of Guidance, Control, and Dynamics*, vol. 17, no. 4, pp. 729-736, July-August 1994.

[2] R. W. Prouty, *Helicopter Performance, Stability and Control*. Malabar, Florida, USA: Krieger Publishing Company, 2005.

[3] J. Seddon and S. Newman, *Basic Helicopter Aerodynamics*. West Sussex, England: John Wiley & Sons, 2011.

[4] G. D. Padfield, *Helicopter Flight Dynamics: The Theory and Applicaiton of Flying Qualities and Simulation Modelling*. Washington DC, USA: Blackwell Publishing, 2007.

[5] E. A. Wan and A. A. Bogdanov, "Model predictive neural control with applicaiton to a 6 DOF helicopter model," in *American Conrol Conference, IEEE*, Arlington,VA, 2001, pp. 488 - 493.

[6] T. J. Koo and S. Sastry, "Output tracking control design of a helicopter model based on approximation linearization," in *Conference on Decision and Control, IEEE*, Tempa, Florida, 1998, pp. 3635-3640.

[7] Y-R. Tang and Y. Li, "Design of an Optimal Flight Control System with Integral Augmented Compensator for a Nonlinear UAV Helicopter," in *10th World Congress on Intelligent Control and Automation*, Beijing, China, 2012, pp. 3927-3932.

[8] Z. Bai, P. Liu, J. Wang, X. Hu, and X. Zhao, "Control system design of a small-scale unmanned helicopter," in *Control and Automation (ICCA), 8th IEEE International Conference*, Xiamen, China, 2010, pp. 1414-1417.

[9] C. S. Yoo, Y. S. Kang, and B. J. Park, "Hardware-In-the-Loop simulation test for actuator control system of Smart UAV," in *Control Automation and Systems (ICCAS), International Conference*, Gyeonggi-do, South Korea, 2010, pp. 1729-1732.

[10] I. A. Raptis and K. P. Valavanis, *Linear and Nonlinear Control of Small-Scale Unmanned Helicopters*.: Springer Science+Business Media B.V., 2011.

[11] C. P. Sanders, P. A. DeBitetto, E. Feron, H. F. Vuong, and N. Leveson, "Hierarchial control of small autonomous helicopters," *37th IEEE, Conference in Decision and

Control, vol. 4, pp. 3629-3634, 1998.

[12] G. Lai, K. Fregene, and D. Wang, "A control structure for autonomous model helicopter," in *Canadian Conference on Electrical and Computer Engineering, IEEE*, Halifax, Nova Scotia, Canada, 2000, pp. 103-107.

[13] R. Mahony, T. Hamel, and A. Dzul, "Hover control via lyapunov control for an autonomous model helicopter," in *Conference on Decision and Control*, Phoenix, Arizona, USA, 1999, pp. 3490-3495.

[14] H. Shim, T. J. Koo, F. Hoffmann, and S. Sastry, "A comprehensive study of control design for an autonomous helicopter," in *37th Conference on Decisio and control, IEEE*, Tampa, Florida, 1998, pp. 3653-3658.

[15] R. A. Hess and P. J. Gorder, "Quantitative Feedback Theory Applied to the Design of a Rotorcraft FLight Control System," *Journal of Guidance, Control, and Dynamics*, vol. 16, no. 4, pp. 748-753, July-August 1993.

[16] A. M. Dollar, D. R. Bersak, and P. E. I. Pounds, "Stability of small-scale UAV helicopters and quadrotors with added payload mass under PID control," *Autonomous Robots*, vol. 33, pp. 129-142, 2012.

[17] S. K. Agrawal, S-R. Oh, and J-C. Ryu, "Dynamics and Control of a Helicopter Carrying a Paload Using a Cable-Suspended Robot," *Mechanical Design*, vol. 128, pp. 1113-1121, 2006.

[18] I. A. Raptis and K. P. Valavanis, *Linear and Nonlinear Control of Small-Scale Unmaned Helicopters*. London, UK: Inteligent Systems, Control and Automation:Science and Engineering 45, Springer Science+Business Media B.V., 2011.

[19] I. Horowitz, *Synthesis of Feedback Systems*. New York, USA: Academic Press, 1963.

[20] C. H. Houpis, S. J. Rasmussen, and M. Garcia-Sanz, *Quantitative Feedback Theory Funadamentals and Applications*. Boca Raton, Florida, USA: CRC Press., 2005.

[21] O. Yaniv, *Quantitative Feedback Design of Linear and Nonlinear Control Systems*. Norwell, Massachusetts, USA: Kluwer Academic Publishers, 1999.

[22] M. B. Tishcler, B. Mettler, and T. Kanade, *System Identification Modeling of a Model-scale Helicopter*. Pittsburgh, Pennsylvania, USA: Carnegie Mellon University, The Robotics Institute, 2000.

[23] Flight Control: CIFER. [Online]. http://uarc.ucsc.edu/flight-control/cifer/overview.shtml

[24] C. Borghesani, Y. Chait, and O. Yaniv, The QFT Frequency Domain Control Design Toolbox User's Guide, 2003.

[25] S. B. Deshpande, R. M. Mohril, and D. M. Sajnekar, "Comparison of Pole Placement & Pole Zero Cancellation Method for Tuning PID controller of A Digital Excitation Control System," *International Journal of Scientific and Research Publications*, vol. 3, no. 4, p. 358, April 2013.

[26] Transfer Fcn. [Online]. http://www.mathworks.com/help/simulink/slref/transferfcn.html

[27] Horizon. [Online]. http://www.micropilot.com/products-horizonmp.htm

Appendix A: Implementation on Horizon Simulation

Horizon is a commercially available simulation and ground control software for unmanned helicopters developed by Micropilot Inc. [27]. This software uses model of X-Cell 60 helicopter. However, the sample time is much slower 0.033 s as compared to the one used in this thesis (0.001 s). The first controller as developed in Section 4.2 was implemented using the Horizon simulation and its performance was compared to the existing PID controller.

A.1 PID Controller

The current controller as implemented in the Horizon simulation is a typical PID controller. To evaluate the performance of the controller the helicopter with a payload of 10 lb was flown to an altitude of 100 ft over 25 s. The payload was dropped after 55 s. The altitude response of the helicopter can be seen in Figure Appendix A 1. The time to reach the altitude of 100 ft was 28.1 s.
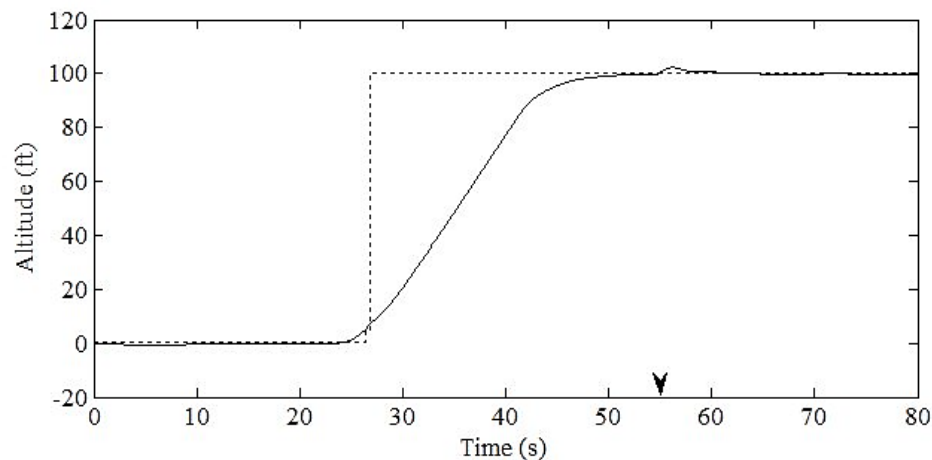
Figure Appendix A 1: Altitude response (Horizon PID controller)

Figure Appendix A 2 shows the change in altitude after 10 lb payload drop. As seen the change in altitude after the payload drop was 2.25 ft while the time to recover within 2 % of change in altitude after payload drop is 7.7 s.
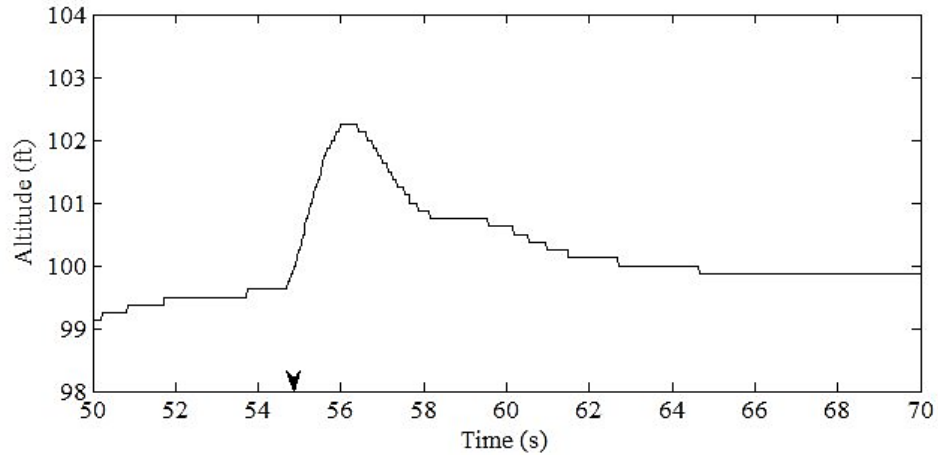
Figure Appendix A 2: Altitude change after 10 lb payload drop (Horizon PID Controller)

The vertical velocity response of the helicopter is shown in Figure Appendix A 3. There are some differences between the Simulink simulation and the Horizon simulation. The velocity is negative when flying up as it is seen in body fixed frame while in the simulation it was seen in inertial frame relative to earth surface. The max vertical velocity of the helicopter in Horizon is restricted to -5 ft/s by putting a saturation limit while the velocity in the Simulink simulation reaches 30 ft/s when flying to 100 ft. The change in velocity after the payload drop was seen to be -2.25 ft/s.
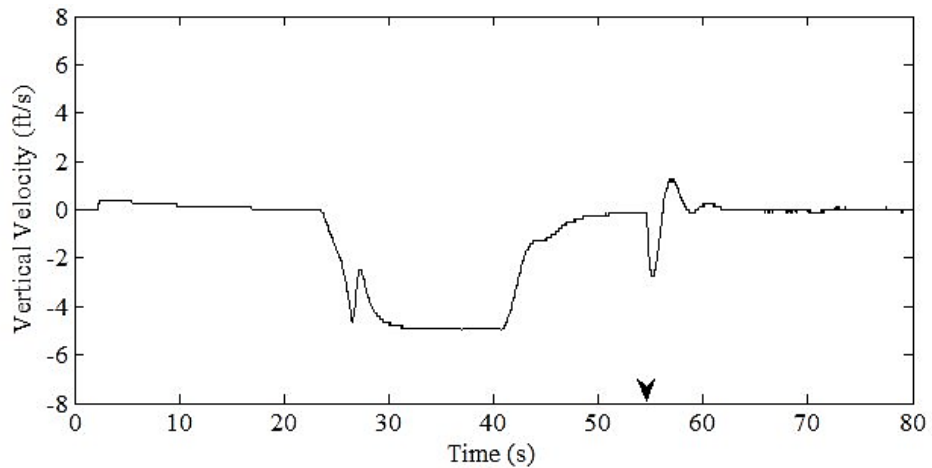
Figure Appendix A 3: Velocity response (Horizon PID Controller)

The collective pitch input command in Horizon simulation is calculated as percent of servo as shown in Figure Appendix A 4. The overall pattern as seen was similar to that observed using the Simulink simulation.
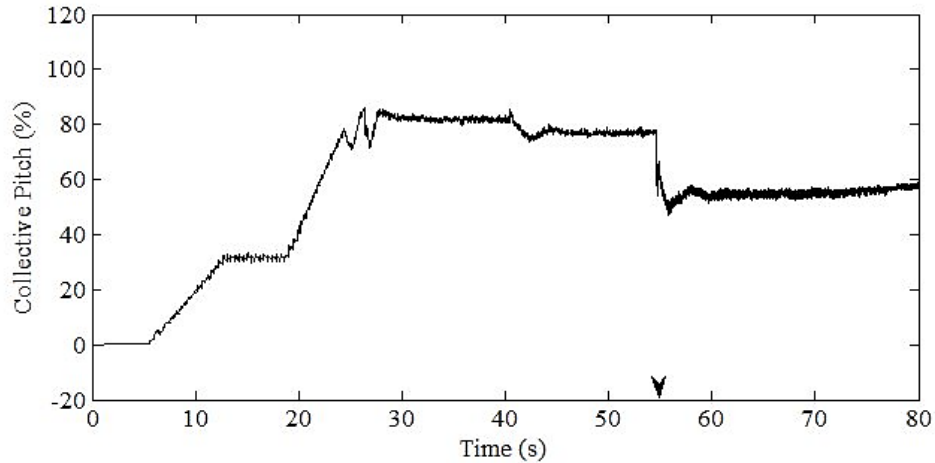
Figure Appendix A 4: Collective pitch (Horizon PID Controller)

The results of the Horizon PID Controller with 10 lb payload are summarized in Table A 1.

Table A 1: Horizon PID controller results

Performance index	Value
Time taken after takeoff to reach 100 ft	28.1 s
Maximum change in altitude after payload drop	2.25 ft
Maximum change in velocity after payload drop	-2.75 ft/s
Time to recover within 2% of change in altitude after payload drop	7.7 s

A.2 QFT Controller

Figure Appendix A 5 shows the altitude response of the helicopter. The time to reach to altitude 100 ft is 26.9 s. slightly faster than that observed in Figure Appendix A 1. After the payload drop, the change in altitude is 0.38 ft as shown in Figure Appendix A 6, which is much less than that observed in Figure Appendix A 2. The time taken to recover within 2% if change in altitude after the payload drop is 3.4 s much faster than that observed with the PID controller.
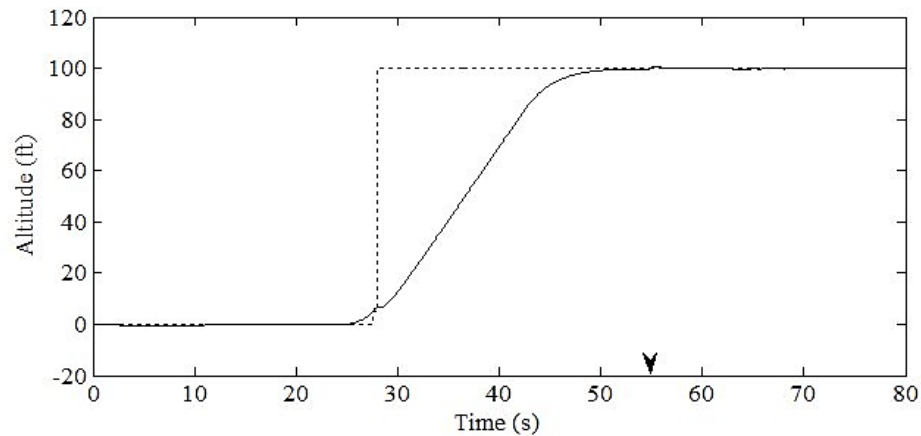
Figure Appendix A 5: Altitude response (QFT Controller I)
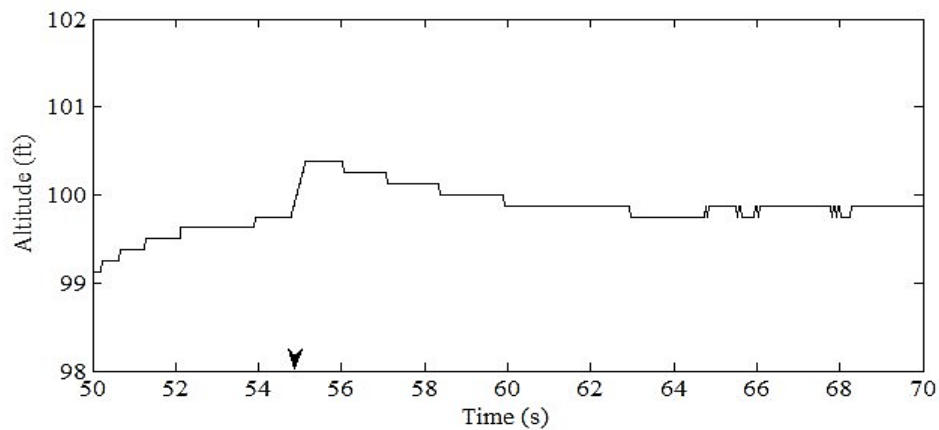
Figure Appendix A 6: Altitude change after 10 lb payload drop (QFT Controller I)

After the payload drop, the change in velocity is -2.38 ft/s, which is lower than that observed before with PID controller as seen in Figure Appendix A 7.
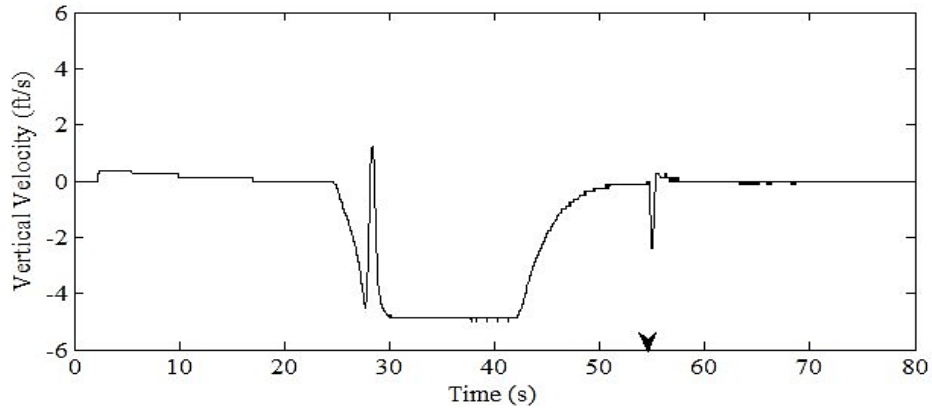
Figure Appendix A 7: Velocity response (QFT Controller I)

The collective pitch command as generated by the QFT controller looks similar to that observed in Figure Appendix A 4.
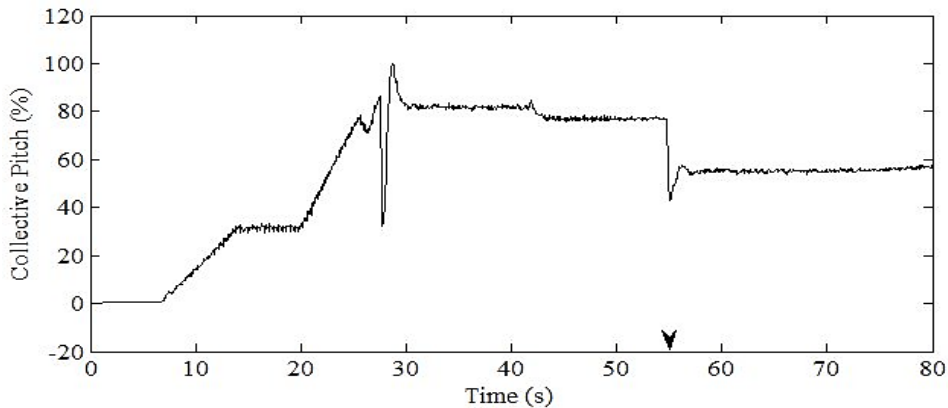
Figure Appendix A 8: Collective pitch (QFT controller I)

The results of the QFT controller implemented in Horizon with 10 lb payload are summarized in Table A 2.

Table A 2: Results of the QFT controller I implemented in Horizon

Performance index	Value
Time taken after takeoff to reach 100 ft	26.9 s
Maximum change in altitude after payload drop	0.38 ft
Maximum change in velocity after payload drop	-2.38 ft/s
Time to recover within 2% of change in altitude after payload drop	3.4 s

A.3 Summary

QFT controller I designed in section 4.2 was implemented in the commercially available software; Horizon made by Micropilot Inc. Performance of both the existing PID controller and the QFT controller was compared. As compared to the PID controller, the QFT controller was fast to response. While the change in altitude after the payload drop for QFT controller was 0.38 ft, almost six times less than that observed with the PID controller. Similarly, the QFT controller also showed less change in vertical velocity after the payload drop and was faster to recover to 100 ft. Hence, the QFT controller shows better performance than the existing PID controller. The results of the two controllers in Horizon are summarized in Table A 3.

Table A 3: Summary of the results of controllers implemented in Horizon

Controllers	Time take to reach 100 ft (s)	Change in altitude after payload drop (ft)	Change in velocity after payload drop (ft/s)	Time to recover within 2% of change in altitude after payload drop (s)
PID controller	28.1	2.25	-2.75	7.7
QFT controller	26.9	0.38	-2.38	3.4

Appendix B: System Identification (CIFER)

CIFER [23] (Comprehensive Identification from Frequency Response) is a software developed by U.S. Army and University of California, Santa Cruz. It was designed to tackle difficulties associated with system identification using a flight test data to identify parameters for aircraft. Over the years, CIFER has been used on a wide range of rotary wing and fixed wing aircraft flights such as XV-15, Bell-214ST, AV-8 Harrier, etc. and has proved exceptionally reliable and accurate [23].

CIFER converts the time domain data into frequency domain responses. It performs multiple identification techniques and identifies transfer functions by providing important information such as bandwidth and crossover characteristics. CIFER also checks for offsets and biases in the data by performing fully automated weighting function based on frequency response accuracy.

In order to identify the transfer function of the vertical channel of the helicopter, a step input was applied to the collective pitch channel of the helicopter with 10 lb payload and without carrying any payload. The input and output from the simulation was stored in excel worksheet with the sample time of 0.001 s. The program creates frequency domain analysis on the data and outputs Figure 4-4 and Figure 4-5. Using the NAVFIT function in CIFER, the first-order transfer function shown in Equations (4-8) and (4-9) are obtained including the cost of the fit where fit cost below 50 is considered excellent.